

**DESIGN OF INNOVATIVE SOFT WEARABLE ROBOTS
FOR INDUSTRIAL OVERHEAD TASKS**

A Dissertation
Presented to
The Academic Faculty

By

Dario Panariello

In Partial Fulfillment
of the Requirements for the Degree of
Doctor of Philosophy in Technology Innovation and Management



Università degli studi di Napoli Federico II
Department of Industrial Engineering
September 2021

Supervisors:
Prof. Antonio Lanzotti
Prof. Giuseppe Di Gironimo
Dr. Stanislao Grazioso

The Chair of the Doctoral Programme:
Prof. Renato Redondi

Copyright © 2021 by Dario Panariello

Abstract

The recently growing interest in health at work aims at prolonging employees' working lives, by reducing the risks associated to work-related musculoskeletal disorders. The current devices used in industrial environment to reduce the biomechanical overloads are rigid wearable robots (or exoskeletons), which includes passive and active systems. The rigid exoskeletons have a kinematic structure similar to the human kinematic structure and use rigid links to transfer forces from the exoskeleton to the worker. In particular, the rigid wearable robots use preloaded springers or electric motors to generate the forces. However, the motion of the rigid exoskeleton is perceived as non-natural for the users since there are joint alignment problems between the human joint axes and the exoskeleton joint axes when the user performs a task. To avoid the problem, soft exoskeletons have been introduced in the literature. They do not use rigid structure to transfer the forces but they are related directly to human anatomy using a soft suit. Moreover, the soft wearable robots are mainly for rehabilitation applications and for supporting the daily living tasks. The recent design and developments of new solutions of wearable robots, which include actuators able to generate even higher forces, could allow to implement this technology in industrial environments where higher forces are required. In the present thesis, the design of two wearable robots for industrial overhead tasks are presented. To do that, a biomechanical analysis, which includes the assessment of the joint angles, joint torques and muscle activations, of the industrial overhead tasks performed at two working heights is carried out in laboratory setting. The results show that for a specific working configuration the torques and muscle activations of the back decrease and the worker's effort are concentrated in a specific limb, i.e. upper limb. Ultimately, the analysis conducted allows to define this specific configuration combined with a wearable robot for supporting the upper-limb movements as the best solution for the workers to reduce the biomechanical overloads. Then, the functional requirements of the soft wearable robot are defined using the results of the biomechanical analysis and a two degrees-of-freedom model of the upper limb. Based on the functional requirements, two concepts, which includes the soft suits, are presented: (i) tendon-driven wearable robot, an under-actuated system which use a single electric motor combined with a gear system to support the shoulder and elbow flexion; (ii) pneumatic wearable robot, it uses four McKibben artificial muscles to support the joint movements; two McKibben to support the shoulder flexion and two McKibben to support the elbow flexion. A detailed design is carried out in order to define the dimensional and geometric characteristics of the actuation and power transmission systems of the proposed two wearable robots. Finally, a comparison between the two wearable robots for industrial overhead tasks is proposed using multi-criteria decision making.

Contents

Introduction	1
1 Soft wearable robots: state of the art	4
1.1 Taxonomy of wearable robots	4
1.2 A brief overview of industrial wearable robots	5
1.3 A detailed analysis of the most promising soft wearable robots for upper-limb	7
1.3.1 Classification of the main soft wearable robots for upper-limb assistance	7
1.3.2 Discussion	16
1.3.3 Research and technology limitations	16
2 Biomechanical analysis of industrial overhead tasks	19
2.1 Methods	20
2.1.1 Multiple performance metrics	20
2.1.2 Biomechanical analysis of workers	21
2.2 Experiments	22
2.2.1 Participants	23
2.2.2 Laboratory task and description	23
2.2.3 Instrumentations	25
2.2.4 Protocols	26
2.2.5 Data processing and analysis	28
2.3 Results	31
2.3.1 Ergonomic assessment – RULA score	31
2.3.2 Task performance	35
2.3.3 Kinematic movements	35
2.3.4 Dynamic loads	39
2.3.5 Muscle activities	41
2.4 Discussion	41
2.4.1 Overall discussion of the results	43
2.4.2 Comparison comparing works	44
2.4.3 Possible exploitation of the results	45

3	Functional requirements of soft wearable robot	46
3.1	Summary of the biomechanical results	46
3.2	Functional requirements	47
4	Concept design of the two soft wearable robots	53
4.1	Soft suit	53
4.2	Concept 1: Tendon-driven wearable robot	55
4.2.1	Transmission system	56
4.2.2	Actuation system	57
4.2.3	Working principle	59
4.3	Concept 2: Pneumatic wearable robot	60
4.3.1	Transmission system and actuators	61
4.3.2	Control board system	62
4.3.3	Working principle	62
4.4	Contributions of the proposed soft wearable robots	63
5	Technological insights in concept development	65
5.1	Tendon-driven wearable robot	65
5.1.1	Modeling of transmission and actuation systems	65
5.1.2	Choice of the components	69
5.2	Pneumatic wearable robot	69
5.2.1	Modeling of McKibben artificial muscle	69
5.2.2	Definition of McKibben requirements	75
5.2.3	Pneumatic control board	76
6	Comparison of the two concepts based on group decision making	79
6.1	Multi-criteria decision making	79
6.2	Results	81
6.3	Discussion	82
	Conclusion	85
A	Modeling	87
A.1	Inverse kinematics	87
A.2	Inverse dynamics	87
B	Biomechanical analysis results	91
B.1	Joint angle and torque results	91
B.2	Muscle activation results	91
C	ELIGERE questionnaire	95
C.1	Description of the alternatives	95
C.2	Questionnaires	96

List of Figures

1.1	Classification of the wearable robots in: (i) rigid exoskeletons; (ii) semi-rigid exoskeletons; (iii) soft exoskeletons.	5
1.2	Rigid exoskeletons for industrial application. (a) full powered exoskeleton, Guardian XO from Sarcos; (b) upper-limb exoskeleton for overhead tasks, Mate from Comau; (c) back exoskeleton for lifting tasks, Laevo V2 from Laevo; (d) lower-limb exoskeleton for sedentary tasks, Chairless Chair from noonee.	7
1.3	Main soft wearable robots for assisting the shoulder joint. (a) passive tendon-driven wearable robot from Seoul National University [1]; (b) fabric-based wearable robot from National University of Singapore [2]; (c) fabric-based wearable robot from Stanford University [3]; (d) textile wearable robots from Harvard University at the Wyss Institute for Biologically Inspired Engineering [4]; concept of hybrid soft wearable robot from University of Illinois [5].	11
1.4	Main soft wearable robots for assisting the elbow joint. (a) tendon-driven wearable robot from School of Mechanical and Aerospace Engineering at Robotics Research Center in Singapore [6]; (b) tendon-driven wearable robot from University of Aeronautics and Astronautics in China [7]; (c) fabric-based wearable robot from National University of Singapore [8]; (d) fabric-based wearable robot from Arizona State University [9]; (e) hybrid soft wearable robot from Korea Institute of Machinery and Materials [10].	11
1.5	Main fabric-based wearable robots for assisting the wrist joint, from Soft Robotics Research Center at Seoul National University [11] (a) and from University of Southern California [12] (b).	11
1.6	Main soft wearable robots for multi-joint. (a) tendon-driven wearable robots from Shenyang Institute of Automation [13]; (b) tendon-driven systems from University of California [14]; (c) tendon-driven wearable robot from Nanyang Technological University in Singapore [15,16]; (d) textile wearable robot from Politecnico di Torino [17]; (e) soft wearable robot with pneumatic gel muscles from Hiroshima University [18].	12

1.7	(a): bones in the upper limb; (b): shoulder complex is comprised of three bones: the clavicle, humerus and scapula. The shoulder complex is composed by four junctures: sternoclavicular (sc joint), acromioclavicular (ac joint), glenohumeral (sh joint) and scapulothoracic (st joint) joints. The elbow complex is composed by three junctures: humeroulnar (hr), humeroradial (hu) and proximal radioulnar (pr) joints. The wrist complex is composed by distal radioulnar (dru) joint.	13
1.8	(a): schematization of the upper limb; sh joint: shoulder joint; el joint: elbow joint; wr joint: wrist joint; ha CoM: CoM of the hand. (b) upper limb movement.	14
2.1	Biomechanical analysis of the industrial task to reduce the risks associated to WMSD.	20
2.2	Front view of the experimental setup comprising four poles as based and overhead platform to perform drilling, leveraging and cabling tasks.	24
2.3	Posture of the subject during the execution of drilling task (a), leveraging task (b) and cabling task (c).	24
2.4	Side view of the two anthropometric characteristics selected to evaluate the working height configurations defined in [19].	25
2.5	Marker set on the human body, where: LTR/RTR: Left/Right Temporal Regions; LMC/RMC: Left/Right Medial end of the Clavicle; C7: Cervical vertebra; LA/RA: Left/Right Acromion; RLHE/RMHE: Right Lateral/Medial Humeral Epicondyle; RRS/RUS: Right Radial/Ulnar Styloid; R2MC/R5MC: Right 2 nd /5 th Metacarpal; S: Sacrum; LT/RT: Left/Right Greater Trochanter; LK/RK: Left/Right Lateral Femoral Epicondyle; LM/RM: Left/Right Malleolus; LMe/RMe: 5 th Metatarsal of the Left/Right Foot.	27
2.6	Marker and EMG sensors on the subject's body. (a - c) front view; (b) side view.	29
2.7	Average values of execution time for the four subjects (subj. a; subj. b; subj. c and subj. d) in the two working height configurations: <i>low configuration</i> and <i>middle configuration</i>	35
2.8	The evolution over time of joint angles presented as mean \pm standard deviation for each configuration (<i>low configuration</i> and <i>middle configuration</i>). The joint angles represented in the figure are: α : shoulder flexion-extension; β : shoulder abduction-adduction; γ : shoulder rotation; δ : elbow flexion-extension; ϵ : pronation and supination; ζ : wrist flexion-extension; η : wrist radial-ulnar deviation; θ : trunk flexion-extension; ι : trunk lateral bending; κ : trunk axial rotation.	36

2.9	Average values, for each work cycle, of upper arm joint angles for the two configurations referred to as <i>low configuration</i> and <i>middle configuration</i> . The mean joint angles represented in the figure are: α : shoulder flexion-extension; β : shoulder abduction-adduction; γ : shoulder rotation; δ : elbow flexion-extension. R^2 : linear determination coefficient. For a correct view of these plots, the readers are invited to see the image with colors.	37
2.10	Average, for each work cycle, of trunk joint angles for the two configurations referred to as <i>low configuration</i> and <i>middle configuration</i> . The mean joint angles represented in the figure are: θ : trunk flexion-extension; ι : trunk lateral bending; κ : trunk axial rotation. R^2 : linear determination coefficient. For a correct view of these plots, the readers are invited to see the image with colors.	37
2.11	Average values of the joint torques for the four subjects (subj. a; subj. b; subj. c and subj. d) in two different configurations.	40
2.12	Root Mean Square (RMS) of the normalized muscle activation (NMA) values for the four subjects (subj. a; subj. b; subj. c and subj. d) in two different configurations.	42
3.1	The proposed biomechanical-based process to derive the functional requirements of a soft industrial exoskeleton.	47
3.2	Kinematic model with two DoF, shoulder and elbow movement in the sagittal plane, of the human arm.	49
3.3	Evolution of the joint angles, torques, required lengths and forces for drilling overhead tasks. α and τ_1 : shoulder flexion-extension angle and torque; δ and τ_2 : elbow flexion-extension angle and torque; l_{sh} and l_{el} : shoulder and elbow required lengths; f_{sh} and f_{el} : shoulder and elbow required forces.	51
4.1	Main components of soft suit: shoulder brace (t1), two arm braces (t2) and (t3); wrist brace (t4), bands (n) and elastic band (n2)	54
4.2	Soft suit of the soft wearable robot worn by the user. Shoulder brace (t1), two arm braces (t2) and (t3); wrist brace (t4), bands (n) and elastic band (n2)	54
4.3	CAD model of tendon-driven exoskeleton under-actuated for assisting shoulder and elbow flexion.	56
4.4	Actuation system of the tendon-driven exoskeleton. The main components of the wearable robot are: absolute encoder (a); electric motor (b); planetary reducer (c); principal transmission shaft (d); two principal gear wheels (f) and (e), solenoid (h); mechanical pin (g); two secondary transmission shafts (o) and (l), two secondary gear wheels (i) and (n); two coils (m) and (p).	58
4.5	CAD model of pneumatic exoskeleton for assisting shoulder and elbow flexion.	61
4.6	Architecture of pneumatic control board.	62

5.1	Elbow model in the sagittal plane [20]	67
5.2	Forces, torque and power required by the electric motor to support the elbow flexion. f_{el} : cable force before transmission; $f_{el,real}$ cable force after transmission; τ_{em} torque required by the electric motor; $power$ the power required by the electric motor.	68
5.3	Virtual work theorem applied to ideal cylindrical artificial muscle [21].	71
5.4	Geometrical characterization of the planar jointed identical pantographs of McKibben muscle [21].	72
5.5	Plot of the static force of the ideal McKibben muscle.	73
5.6	Analysis of the forces in the real McKibben artificial muscle [21].	74
5.7	Plot of the static force of the real McKibben muscle.	75
5.8	Plot of static force of ideal and real McKibben artificial muscle. The imposed values are: $\alpha_{PAM} = 20$ deg and $h_0 = 0.15$.	76
5.9	Pneumatic control board. (a) Arduino Mega; (b) potentiometer; (c) switch module with 4 Mosfet channels; (d) solenoid valves; (e) power supply; (f) air compressor.	78
6.1	Eligere questionnaire results of the workers:(top-left) the score of the criteria; (top-right) the final ranking of the configurations; (bottom-left) the score of the tendon-driven configuration w.r.t criteria separately; (bottom-right) the score of the pneumatic configuration w.r.t. criteria separately. W: weight; I: invasiveness; OS: operating space.	82
6.2	Eligere questionnaire results of the managers: (top-left) the score of the criteria; (top-right) the final ranking of the configurations; (bottom-left) the score of the tendon-driven configuration w.r.t criteria separately; (bottom-right) the score of the pneumatic configuration w.r.t. criteria separately. IN: innovativeness; S: safety; R: robustness.	83
6.3	Eligere questionnaire results of the researchers: (top-left) the score of the criteria; (top-right) the final ranking of the configurations; (bottom-left) the score of the tendon-driven configuration w.r.t criteria separately; (bottom-right) the score of the pneumatic configuration w.r.t. criteria separately. RS: response speed; FA: full-assisted; M: maintainability.	83
A.1	Schematic model of the generic body segment between two human joints.	88
A.2	Graphical model of the inverse dynamics calculation of joint forces and torques for each segment	89

B.1	The evolution of joint angles, during the execution of drilling task, presented as mean \pm standard deviation for <i>middle configuration</i> . The joint angles represented in the figure are: α : shoulder flexion-extension; β : shoulder abduction-adduction; γ : shoulder rotation; δ : elbow flexion-extension.	92
B.2	The evolution of joint angles, during the execution of leveraging task, presented as mean \pm standard deviation for <i>middle configuration</i> . The joint angles represented in the figure are: α : shoulder flexion-extension; β : shoulder abduction-adduction; γ : shoulder rotation; δ : elbow flexion-extension.	92
B.3	The evolution of joint torques, during the execution of drilling task, presented as mean \pm standard deviation for <i>middle configuration</i> . The joint torques represented in the figure are: τ_1 : shoulder flexion-extension torque; τ_2 : shoulder abduction-adduction torque; τ_3 : shoulder rotation torque; τ_4 : elbow flexion-extension torque.	93
B.4	The evolution of normalized muscle activations (NMA), during the execution of drilling task, presented as mean \pm standard deviation for <i>middle configuration</i> . The muscles represented in the figure are: <i>AD</i> : anterior deltoid; <i>MD</i> : medial deltoid; <i>UT</i> : upper trapezium; <i>BB</i> : biceps brachii; <i>TB</i> : triceps brachii.	93
B.5	The evolution of normalized muscle activations (NMA), during the execution of leveraging task, presented as mean \pm standard deviation for <i>middle configuration</i> . The muscles represented in the figure are: <i>AD</i> : anterior deltoid; <i>MD</i> : medial deltoid; <i>UT</i> : upper trapezium; <i>BB</i> : biceps brachii; <i>TB</i> : triceps brachii.	94
B.6	The evolution over time of normalized muscle activations (NMA), during the execution of cabling task, presented as mean \pm standard deviation for <i>middle configuration</i> . The muscles represented in the figure are: <i>AD</i> : anterior deltoid; <i>MD</i> : medial deltoid; <i>UT</i> : upper trapezium; <i>BB</i> : biceps brachii; <i>TB</i> : triceps brachii.	94
C.1	Comparison of the worker's criteria.	97
C.2	Comparison of the alternatives based on the worker's criteria.	98
C.3	Comparison of the manager's criteria.	98
C.4	Comparison of the alternatives based on the manager's criteria.	99
C.5	Comparison of the researcher's criteria.	99
C.6	Comparison of the alternatives based on the researcher's criteria.	100

List of Tables

1.1	List of the most promising soft wearable robots for upper-limb, presented in the literature from 2016 to 2020.	9
2.1	Anthropometric characteristics: Height, Weight, Uarm (upper arm), Larm (lower arm) and personal detail (i.e. age) of the subjects involved for the experiments. S.D.: standard deviation; Min.: minimum value; Max.: maximum value.	23
2.2	Positions of EMG sensors on the human muscles.	29
2.3	The table shows the RULA local and final score for drilling overhead task. The letters a, b, c and d represent the four subjects and WC represents work cycle of the trial.	32
2.4	The table shows the RULA local and final score for leveraging overhead task. The letters a, b, c and d represent the four subjects and WC represents work cycle of the trial.	33
2.5	The table shows the RULA local and final score for cabling overhead task. The letters a, b, c and d represent the four subjects and WC represents work cycle of the trial.	34
3.1	Mean values \pm standard deviation of joint angles and torques for the selected tasks. DT: drilling task; LT: leveraging task; CT: cabling task.	48
3.2	Mean values \pm standard deviation of root mean square (RMS) of the normalized muscle activation (NMA) for the selected tasks. DT: drilling task; LT: leveraging task; CT: cabling task.	48
3.3	Anthropometric data and measures for the involved subjects in the experiments, as obtained by using the model in [16]	50
5.1	Main components of fabric-based artificial muscle.	77
5.2	Components of control board system	77
C.1	Fuzzy conversion scale used in Eligere platform.	95

Introduction

The thesis presents the design of two soft wearable robots based on the biomechanical analysis of the industrial overhead tasks. The design includes the soft suit and power system of the two proposed exoskeletons: (i) tendon-driven wearable robot; (ii) pneumatic wearable robot.

Problem The overhead tasks are very common in assembly lines of automotive and aerospace industries and in daily tasks for construction workers. In industrial settings, they are complex and usually involve the production of multiple variants of the same product; being difficult to automate, overhead tasks are mostly performed by workers. In these scenarios, the manipulation abilities and cognitive skills of the worker are essential to successfully complete the task. The industrial overhead tasks have been defined as the most demanding industrial tasks for the workers and they are one of the main causes of the onset of work-related musculoskeletal disorders (WMSD). As a matter of fact, in Europe, the registered occupational diseases affect almost 50% of industrial workers (70–80 million) ¹. The 45% of the WMSD cases afflict the upper limbs, the 38% afflict the back, and 17% afflict lower limbs. In the USA, the U.S. Bureau of Labor Statistics ² reports around 650,000 work-related WMSD, resulting in costs to employers of over 20 billion dollars (including worker compensation and medical expenses). Frequent repetition of the same task, excessive forces induced on the joints, and awkward postures are cited as the most important ergonomic risk factors; indeed, they are listed as a major causes of WMSD in industrial workplace [22].

Background In industry, the recent technologies used to reduce the risk associated to WMSD are: (i) wearable sensors to monitor worker activities in order to reduce the WMSD related to incorrect posture; (ii) wearable robots (or exoskeletons) to support the worker movements during the execution the industrial tasks in order to reduce the WMSD related to biomechanical overloads. In the last decade, wearable robots for upper limbs have been implemented in industrial practice to reduce the biomechanical overloading and fatigue of the worker during daily work. The most adopted technologies in industry are rigid exoskeletons, which include passive and active systems [23].

¹<https://osha.europa.eu/>

²<https://www.bls.gov/>

Limits of the existing solutions The rigid exoskeletons are usually designed schematizing the shoulder as a 3 degrees of freedom (DOF) spherical joint, reproducing the behaviour of glenohumeral joint and neglecting the others articulations, i.e. scapulothoracic, sternoclavicular and acromioclavicular joints [24]. In the same way, the elbow joint is usually modeled as fixed joint; however, the natural elbow axis is not fixed but moves along the surface of a double conic frustum [25]. These hypotheses cause joint alignment problems [26]: it is recognized that the motion of rigid exoskeletons is perceived as non-natural for humans. Furthermore, rigid exoskeletons are invasive for the users and, being bulky, in most of cases, they require a modification of workplaces. Advancements in soft materials and bioinspired design have led to promising solutions for wearable robots. Soft exoskeletons have revolutionized the concept of motion assistance to human beings, in terms of invasiveness and natural human-robot interaction, as they are not related to a rigid structure but directly to human anatomy. The development of commercially available solutions of soft exoskeletons in the future might encouraging the widespread adoption of assistance devices in industry. However, most of soft exoskeletons that have been designed and developed in the last years are intended to be used in assistive daily living tasks and rehabilitative applications, since they require lower forces than industrial applications.

Proposal The recent developments of actuators, i.e. electric motors, pneumatic artificial muscles (PAM) and textiles, able to generate ever higher forces could allow the use of soft wearable robots also in industrial settings [27]. The thesis presents the design of soft wearable robots starting from biomechanical analysis of industrial overhead tasks. To do that, the following steps are followed: (i) definition of the functional requirements of soft wearable robot based on biomechanical analysis of industrial overhead tasks performed at laboratory environment; (ii) definition of soft suit and two possible concepts of soft wearable robots for industrial tasks, i.e. tendon-driven wearable robot and pneumatic wearable robot. The proposed soft suit and tendon-driven wearable robot are an Italian patent pending technology [28]; (iii) definition of the dimensional characteristics of the actuators and transmission systems; (iv) comparison of the systems using subjective opinions of the workers, they allow to compare the solutions from the user's point of view; managers, they allow to compare the solution from the customer's point of view; researchers, they allow to compare the solutions from a technical point of view.

Outline

The manuscript is outlined as follows

- Chapter 1: State of the art of rigid exoskeletons for industrial applications and soft wearable robots are reported.
- Chapter 2: The biomechanical analysis of the industrial overhead tasks, i.e. drilling, leveraging and cabling tasks, performed at laboratory environment is presented.
- Chapter 3: A two degrees of freedom human upper-limb model is used to define the design requirements of soft wearable robot based on the results obtained by the biomechanical results of industrial overhead tasks.
- Chapter 4: Soft suit and two concepts of soft wearable robots are presented, i.e. tendon-driven and pneumatic wearable robots.
- Chapter 5: Detailed design of the proposed wearable robots, i.e. geometric and operating characteristics of the actuators, is carried out.
- Chapter 6: A multi-criteria decision making is used to compare the two concepts of wearable robots.

Chapter 1

Soft wearable robots: state of the art

In the present chapter a taxonomy of the wearable robots are presented in Sec. 1.1, an overview of the most used wearable robots for industrial applications are reported in Sec. 1.2, then a detailed analysis of the most promising soft wearable robots are illustrated in Sec. 1.3.

1.1 Taxonomy of wearable robots

The wearable robots, or exoskeletons, are wearable devices which can be used to assist the human performance in different fields, i.e. rehabilitation, assistive daily living tasks and industry. In the literature, two different classifications of the wearable robots are proposed: (i) based on the body part supported; (ii) based on actuation and transmission systems.

In particular, the first classifies exoskeletons in:

- wearable robots for upper-limb: devices which assist the movements of shoulder, elbow, wrist and hand;
- wearable robots for lower-limb: devices which assist the movements of hip, knee and ankle;
- wearable robots for back and neck: devices which assist the movements of back and neck.

The second classification, instead, divides the exoskeletons in rigid, semi-rigid and soft systems as reported in Fig. 1.1. In particular:

- passive rigid wearable robots: the exoskeletons are composed by rigid links which allow the transmission of the forces generated by a passive system, i.e. preloaded springs (see Sec. 1.2);



Figure 1.1: Classification of the wearable robots in: (i) rigid exoskeletons; (ii) semi-rigid exoskeletons; (iii) soft exoskeletons.

- active rigid wearable robots: the exoskeletons are composed by rigid links which allow the transmission of the forces generated by motors, i.e. electric motors (see Sec. 1.2);
- passive soft wearable robots: the exoskeletons are composed by flexible (soft) tissue, they do not assist the user using forces; i.e. wrist brace (see Sec. 1.3);
- active soft wearable robots: the exoskeletons are composed by flexible (soft) tissue which allow the transmission of the forces generated by cable or fluid systems, i.e. pneumatic actuators (see Sec. 1.3).
- semi-rigid wearable robots: the exoskeletons are composed by rigid and soft links.

1.2 A brief overview of industrial wearable robots

Rigid exoskeletons have been the first exoskeletons introduced in the literature and real environments. In particular, the main application area are: (i) military applications to support or improve military performance in hostile environments; (ii) rehabilitation to support the patient during the performance of a wide range of motions to partially or totally recover motor functions; (iii) assistive in order to support the patient during daily living tasks; (iv) industrial applications to support the workers during the execution of manufacturing tasks.

An exhaustive list of the industrial exoskeletons presented in the literature is reported in [23]. The authors include a list of rigid exoskeletons for upper-limb, back and hip, lower limb presented from 1995 to 2014. They also describe the systems and their potential effects in terms of physical load reduction on the wearer.

In this section, the exoskeletons already on the market and implemented in real industrial contexts are presented. In particular, the existing exoskeletons

can be divided as: (i) full powered exoskeletons (active exoskeletons); (ii) passive exoskeletons.

Usually, the full powered exoskeletons are active devices and they use motors, i.e. electric motors, to transmit the forces from robot to user. Active exoskeletons provide full support/power of the movements, follow body kinematics, actuate all or most of the human joints and require high energy. They are implemented to increase the user's performance. A classic example in construction environments is Guardian XO ¹ (Sarcos, USA), see Fig. 1.2a. The advantages of the full powered exoskeletons are: high level of assistance and adaptable; the disadvantages, instead, are: they require high energy, they are heavy and bulky.

The passive exoskeletons, instead, are used as a preventive tool for workplace injuries and they use passive actuations, i.e. preloaded springers. Moreover, passive exoskeletons provide only partial support of movements, actuate only a few joints based on task to be supported. For this reason they are task specific and can be divided in:

Overhead tasks Usually, the overhead tasks are industrial tasks employed in manufacturing industries, i.e. assembly lines, aeronautical and war industries. The most exoskeletons adopted in real industrial scenario to support the upper-limb, i.e. shoulder and elbow movements, are: EksoEVO ² (Ekso Bionics, USA); ShoulderX ³ (Suitx, USA); SkelEx ⁴ (Skel-Ex, NL); Airframe ⁵ (Levitare Technologies, USA); H-VEX ⁶ (Hyundai, KR); Paexo ⁷ (Ottobock, GE); Mate ⁸ (Comau, IT), see Fig. 1.2b. They are passive and rigid exoskeletons; in particular, the wearable robots use preloaded springers to generate forces transmitted to the worker using rigid links anchored to the worker's biceps. The exoskeletons for overhead tasks are also defined as exoskeletons zero gravity since they compensate the gravity force of the upper limb and tool.

Lifting tasks Usually, the lifting tasks are carried out in industrial and logistic environments. The most exoskeletons adopted in real industrial and logistic scenarios to support back and hip are: Laevo V2 ⁹ (Laevo, NL), see Fig. 1.2c; BackX ¹⁰ (SuitX, USA). They are passive and rigid exoskeletons; in particular, the wearable robots use preloaded springers to generate forces transmitted to the worker using rigid links anchored to the worker's quadriceps.

¹<https://www.sarcos.com/products/guardian-xo-powered-exoskeleton/>

²<https://eksobionics.com/ekso-evo/>

³<https://www.suitx.com/shoulderx>

⁴<https://www.skelex.com/>

⁵<https://www.levitatetech.com/>

⁶<https://www.hyundai.com/>

⁷<https://paexo.com/>

⁸<https://mate.comau.com/>

⁹<https://www.laevo-exoskeletons.com/en/laevo-v2>

¹⁰<https://www.suitx.com/backx>

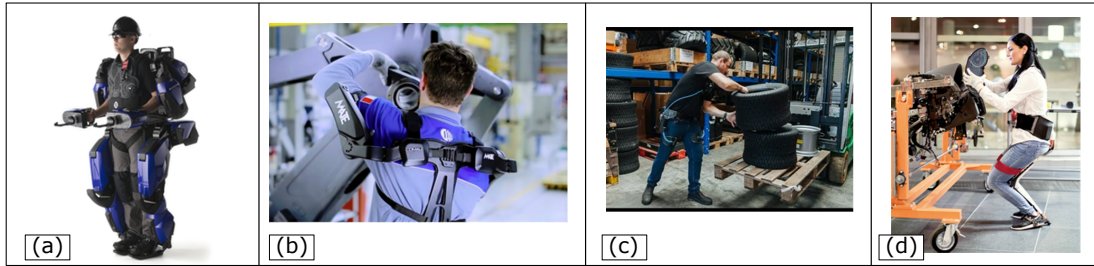


Figure 1.2: Rigid exoskeletons for industrial application. (a) full powered exoskeleton, Guardian XO from Sarcos; (b) upper-limb exoskeleton for overhead tasks, Mate from Comau; (c) back exoskeleton for lifting tasks, Laevo V2 from Laevo; (d) lower-limb exoskeleton for sedentary tasks, Chairless Chair from noonee.

Sedentary tasks Usually, sedentary tasks involve the worker in a specific configuration and position. One of the most exoskeletons used in real automotive industries is Chairless Chair ¹¹ (Noonee, DE), see Fig. 1.2d. It is a rigid exoskeleton; in particular, it allows the worker to sit anywhere in order to perform the required task in an ergonomic way and without overloading the joints of the lower-limbs.

1.3 A detailed analysis of the most promising soft wearable robots for upper-limb

An exhaustive list of soft wearable robots is presented in many recent works [27, 29, 30]. Here, the authors have illustrated the soft wearable robots for upper body (i.e. neck, upper limb and trunk) and lower body (i.e. hip, knee and ankle), describing in detail the different types of actuators and power transmissions. A detailed analysis of the most promising soft wearable robot for upper-limb assistance is proposed in Sec. 1.3.1 [31], excluding hand wearable robots. In particular, compared to studies already presented in the literature [27, 29], the main features of a soft exoskeleton are analysed, by taking into consideration design concept, i.e. degrees of freedom, supported movements, range of motions and mass; actuation, i.e. actuation methods, actuators and power transmissions; sensing system; control strategy and application. Finally, advantages, disadvantages and current limitations of the soft wearable robots are discussed in Sec. 1.3.3.

1.3.1 Classification of the main soft wearable robots for upper-limb assistance

The most promising soft wearable robots presented in the literature are reported in Tab. 1.1. The table classifies wearable robots based on supported joint an-

¹¹<https://www.noonee.com/>

gles, i.e. shoulder, elbow, wrist and multi-joint. Moreover, it reports, for each wearable robot: supported movements (SM), range of motion (RoM), mass, actuator and power transmission, sensing system, control strategy and application. The pictures of the analysed soft wearable robots are reported in the following figures: Fig. 1.3 for shoulder joint exoskeletons, Fig. 1.4 for elbow joint exoskeletons, Fig. 1.5 for wrist joint exoskeletons and Fig. 1.6 for multi-joint exoskeletons.

Table 1.1: List of the most promising soft wearable robots for upper-limb, presented in the literature from 2016 to 2020.

	Design concept		Actuation		Sensing system	Control strategy	Appl.
	SM	RoM [deg]	Mass [g]	Actuation method			
Shoulder joint							
[1]	α, β	100	-	passive systems	tendon-driven	-	assistive
[2]	β	90	35	pneumatic	textile/fabric	IMU pressure sensor	rehab., assistive
[3]	β	90	350	pneumatic	textile/fabric	-	rehab.
[4]	α, β	90	480	pneumatic	textile/fabric	-	assistive
[5]	α	120	-	pneumatic	tendon-driven	-	-
Elbow joint							
[6]	δ	180	1200	electric	tendon-driven	encoder, load cell	assistive
[7]	δ	-	-	electric	tendon-driven	EMG, IMU, encoder	rehab., assistive
[8]	δ	75	-	pneumatic	textile/fabric	EMG, pressure sensor	rehab.

[9]	δ	-	-	pneumatic	textile/ fabric	-	pressure control	lifting activity
[10]	δ	-	1000	pneumatic	tendon- driven	encoders	position control	assistive
Wrist joint								
[11]	ϵ	160	-	pneumatic	PAM	force sensor, encoder	position control	rehab.
[12]	ϵ	95	200	pneumatic	textile/ fabric	pressure sensor	pressure control	rehab.
Multi-joint								
[13]	$\alpha, \beta, \gamma,$ $\delta, \epsilon, \zeta, \eta$	-	-	electric	tendon- driven	mocap, load cell	position control	rehab.
[14]	α, β, γ δ, ϵ	-	1300	electric	tendon- driven	IMU	mimetic control	rehab.
[16]	α, δ	-	7500	electric	tendon- driven	encoders	voice control	industry
[17]	$\alpha, \delta,$ ϵ	-	-	pneumatic	textile/ fabric	-	-	-
[18]	$\alpha, \delta,$ ϵ, ζ	-	2100	pneumatic	PAM	pressure sensor	static control	rehab.

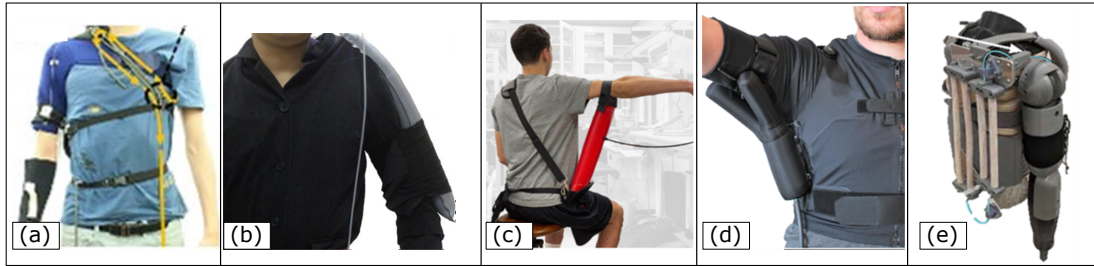


Figure 1.3: Main soft wearable robots for assisting the shoulder joint. (a) passive tendon-driven wearable robot from Seoul National University [1]; (b) fabric-based wearable robot from National University of Singapore [2]; (c) fabric-based wearable robot from Stanford University [3]; (d) textile wearable robots from Harvard University at the Wyss Institute for Biologically Inspired Engineering [4]; concept of hybrid soft wearable robot from University of Illinois [5].

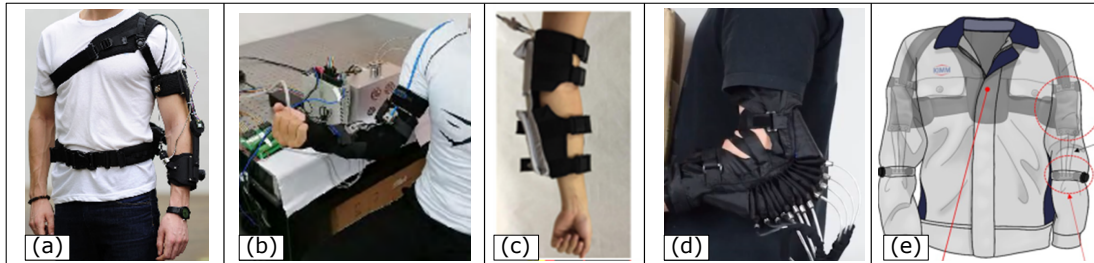


Figure 1.4: Main soft wearable robots for assisting the elbow joint. (a) tendon-driven wearable robot from School of Mechanical and Aerospace Engineering at Robotics Research Center in Singapore [6]; (b) tendon-driven wearable robot from University of Aeronautics and Astronautics in China [7]; (c) fabric-based wearable robot from National University of Singapore [8]; (d) fabric-based wearable robot from Arizona State University [9]; (e) hybrid soft wearable robot from Korea Institute of Machinery and Materials [10].

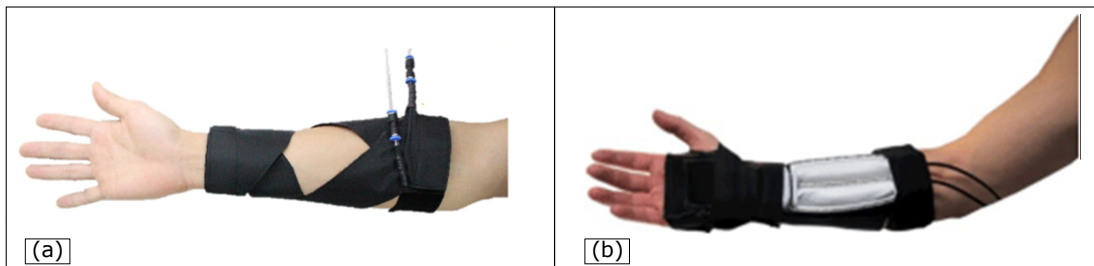


Figure 1.5: Main fabric-based wearable robots for assisting the wrist joint, from Soft Robotics Research Center at Seoul National University [11] (a) and from University of Southern California [12] (b).

Upper-limb kinematics The upper limb is composed by three main articulations [25]: shoulder, elbow and wrist joints, see Fig. 1.7. The shoulder articulation is the most complex joint and it connects the humerus with the shoulder. The

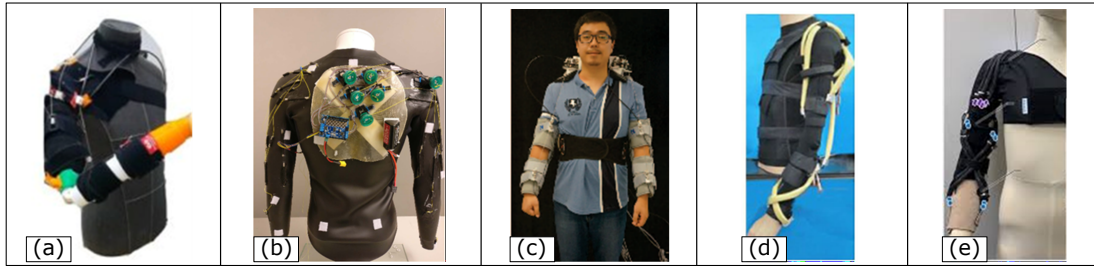


Figure 1.6: Main soft wearable robots for multi-joint. (a) tendon-driven wearable robots from Shenyang Institute of Automation [13]; (b) tendon-driven systems from University of California [14]; (c) tendon-driven wearable robot from Nanyang Technological University in Singapore [15,16]; (d) textile wearable robot from Politecnico di Torino [17]; (e) soft wearable robot with pneumatic gel muscles from Hiroshima University [18].

shoulder joint is modelled as a 3 degrees of freedom (DOF) joint, i.e. a spherical joint, simulating the movements of the glenohumeral. The three movements are defined as: shoulder flexion–extension α , shoulder abduction–adduction β and shoulder rotation γ , see Fig. 1.8. The elbow is a synovial joint between the humerus, in the upper arm, and the radio and ulna, in the forearm. For a first approximation, the elbow joint is modelled as a 1 DOF joint, i.e. a simple hinge joint as reported in Fig. 1.8. The movement is defined as elbow flexion–extension δ . The wrist joint connects the radius with the ulna and the radius with the hand. It is schematised as a 3 DOF joint and the movements are defined as: pronation and supination ϵ , wrist flexion–extension ζ and wrist radial–ulnar deviation η , see Fig. 1.8. Table 1.1 reports the supported movements (SM) by the wearable robots: α , β and γ for wearable robots supporting the shoulder; δ for wearable robots supporting the elbow; ϵ , ζ and η for wearable robots supporting the wrist; for the wearable robots supporting multiple joints, we have a combination of all the angles.

Design concept Apart from the actuation sources and systems, soft exoskeletons are also characterized by: (i) anchor points, that guarantee the execution of correct movement to be supported; (ii) suits, that guarantee the correct position of the anchor points, actuators and power transmissions. In particular, the correct execution of the required movements is guaranteed by the correct positioning of the anchor points of the pneumatic actuators or power transmission, i.e. tendons, on the subjects’ body. The positions of the anchor points are not standard and change in each configuration presented in Tab. 1.1. However, some common features are: (i) the shoulder movements are carried out placing the anchor points on trunk/upper back/shoulder and upper arm, see Fig. 1.3; (ii) the elbow movement is assisted placing the anchor points on the upper arm and forearm, see Fig. 1.4; (iii) the wrist movements are assisted placing the anchor points on forearm and hand, see Fig. 1.5. In most of the cases reported in Tab. 1.1, two anchor points

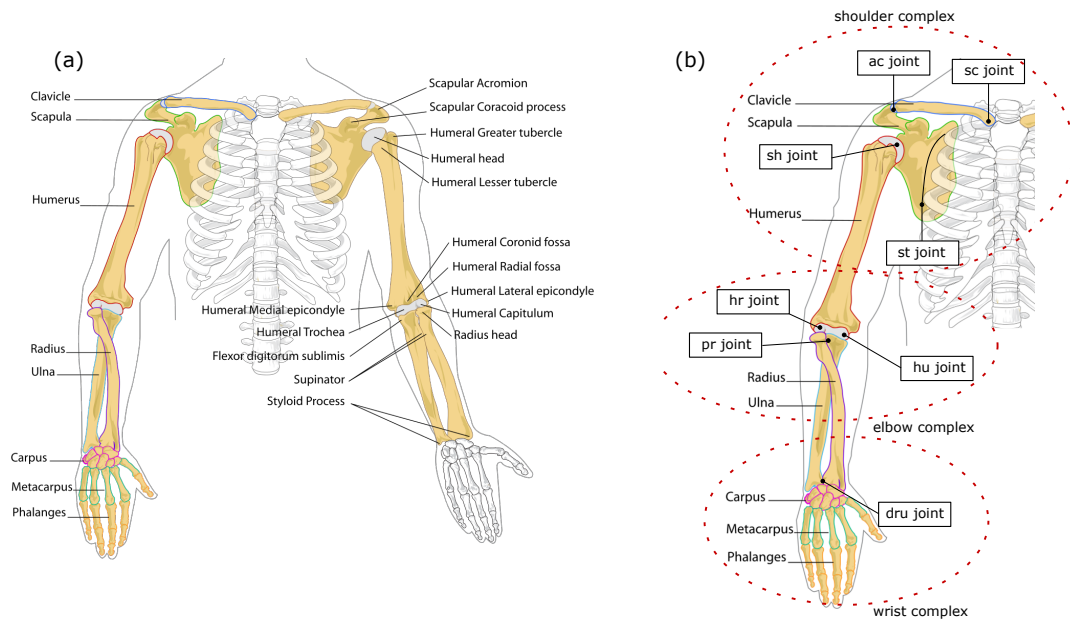


Figure 1.7: (a): bones in the upper limb; (b): shoulder complex is comprised of three bones: the clavicle, humerus and scapula. The shoulder complex is composed by four junctures: sternoclavicular (sc joint), acromioclavicular (ac joint), glenohumeral (sh joint) and scapulothoracic (st joint) joints. The elbow complex is composed by three junctures: humeroulnar (hr), humeroradial (hu) and proximal radioulnar (pr) joints. The wrist complex is composed by distal radioulnar (dru) joint.

allow to perform the movement in one direction, i.e. 1 DOF; these exoskeletons are defined full-actuated since for each DOF they use an actuator. The wearable robots proposed in [1,4,16], instead, are defined under-actuated since an actuator can assist more than 1 DOF. In particular, a specific configuration of the anchor points allow to perform shoulder flexion-extension α and shoulder abduction-adduction β using a free-to-move anchor point from anterior part to the medial part and soft cruciate linkage, respectively. A mechanical solution, instead, is proposed in [16] to carry out shoulder and elbow flexion-extension (α and δ). In this exoskeleton the anchor points, located on the upper arm and forearm, allow to flex the elbow joint (δ) until 90 degrees, when δ reaches 90 degrees the elbow angle is locked and the same cable, using a different position of anchor point (i.e. shoulder and upper arm), assists the shoulder joint (α). The suits, as mentioned above, are used to fix the anchor points on the human and for adjustment the wearable robot to individual users using strap, Velcro, hook-and-loop or by reinforcing the anchor areas with flexible plate [4]. Most of the proposed suits use shoulder, elbow, wrist braces and in some cases jackets [4, 10, 14, 17]. Finally, as reported in Tab. 1.1, the soft exoskeletons are generally lightweight; the mass of the systems is lower than 500 g, except for wearable robots where the power

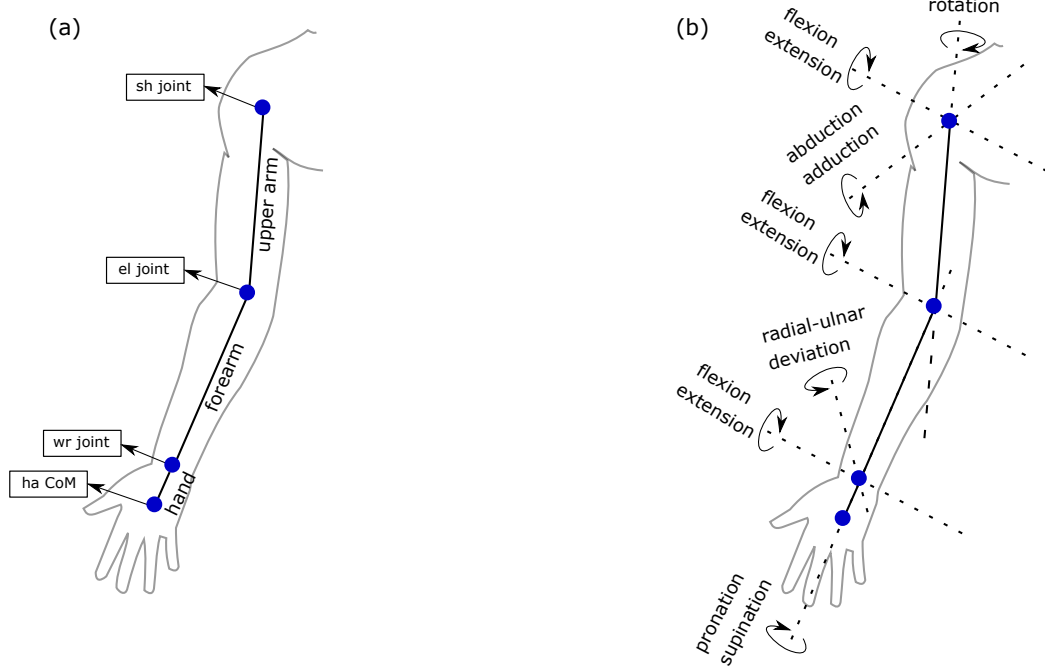


Figure 1.8: (a): schematization of the upper limb; sh joint: shoulder joint; el joint: elbow joint; wr joint: wrist joint; ha CoM: CoM of the hand. (b) upper limb movement.

system is worn [6, 14, 16, 18].

Actuation The actuators and power transmission systems reported in Tab. 1.1 can be classified in: (i) cable-driven systems, which use Bowden cables (or tendons) to generate the required movements; (ii) fluid-driven soft actuators (or pneumatic actuators), which use specific cavities and geometries to generate force when pressurised. In particular, the latter can be divided in: pneumatic artificial muscles (PAM), fabric-based inflatables and textiles (textile/fabric). The PAM are historically the first pneumatic actuators that have been used for soft wearable robots [27]; then, they have been improved by making actuators capable of generating higher forces, such as flat pneumatic actuators (FPA) [11] and pneumatic gel muscles (PGM) [18]. In the last decade, soft actuators made from fabric or a combination of material properties, i.e. textiles, have started having great impact on the design and fabrication of soft wearable robots. The common methods of fabrications include the combination of the following materials: polyurethane (PU) [2, 3]; thermoplastic polyurethane (TPU) [8, 9, 12] and inextensible textile [4]; Twaron with a latex tube (M.T.D13.L1) [17]. The actuation method is electric for cable-driven systems, i.e. based on electric motors, and pneumatic for fluid-driven soft actuators. Hybrid solutions are also proposed: passive (i.e. springs) and pneumatic systems are used to generate the contraction of the tendons in [1] and in [5, 10].

Sensing system The sensors used and reported in Tab. 1.1 can be divided in: (i) sensors to monitor human activities, i.e. encoders, motion capture (mocap), inertial measurements units (IMU) and electromyography (EMG); (ii) sensors to monitor the state of the actuators and power transmissions, i.e. pressure sensors and load cells. In particular, encoders are usually used for measuring elbow movement (δ) [6, 7, 10, 32] or for measuring elbow and shoulder movements (α and δ) [16]; motion capture systems are used to estimate shoulder, elbow and wrist movements ($\alpha, \beta, \gamma, \delta, \epsilon, \zeta$ and η) [13]; IMUs, placed on the upper arm and forearm, are used to estimate attitude (i.e. roll, pitch and yaw) [14] and measuring elbow movement (δ) [7] through the extraction of quaternions; EMG, usually placed on biceps brachii (BB) and triceps brachii (TB), are used to estimate the maximum voluntary contractions (MVC) in [8] and, placed on BB, to estimate the elbow joint torque using a sequence of filters including the Kalman filter [7]; encoder and EMG together, placed on BB, TB and brachioradialis, are used to estimate the elbow joint torque using the Hill-type muscle model [32]. Finally, load cells can be integrated in cable-driven systems to measure the tension of the cable [6, 13]; pressure sensors, instead, are usually adopted by pneumatic-based systems to monitor air pressure [2, 8, 12, 18].

Control strategy The main control strategies reported in Tab. 1.1 can be divided in: (i) position control; (ii) pressure control; (iii) intention-detection control; (iv) torque estimation control. The position control (i) and pressure control (ii) are easy-to-use control strategies, but they do not guarantee a perfect symbiosis between human and robot. In particular, in position control strategies (i) the pneumatic actuator pressure or cable length is varied in order to follow a predetermined trajectory, dependent on the task to be performed. Position control is usually performed in closed-loop and encoders, mocap and IMU are implemented in the feedback branch [2, 10, 11, 13]. Pressure control strategies (ii), instead, are usually used for pneumatic actuators where predefined trajectories of the arm define a reference pressure to be applied in input. With this regards, two strategies are proposed: an open-loop control [3, 4, 9] and closed-loop control where pressure sensors are usually implemented in the feedback branch [12, 18]. Intention-detection (iii) and torque estimation control (iv) strategies try to follow the human movements, in order to get closer to a symbiosis between human and robot. Intention-detection controls (iii) are proposed in [16] as open-loop using voice command control and in [8, 14] as closed-loop control. In particular, intention-based motions using EMG signals is proposed in [8] and mimetic control using IMU is illustrated in [14] where the actuated arm, i.e. the right arm, follows the movement of the non-actuated arm, i.e. the left arm. The torque estimation control (iv) is proposed in [7] as EMG-based torque estimation control strategy. In this work the authors propose to estimate the elbow joint torque using EMG signals and a Kalman filter; then, an incremental angle is estimated and compared to feedback branch composed by elbow joint (δ) measured using encoder. Finally, a promising control strategy is proposed in [6, 32] as gravity

compensation torque. In particular, the authors estimate the elbow joint torque required using single-joint model and the assistive torque generated by the soft exoskeleton is evaluated measuring the tension of the cable, using load cell; then the difference between gravity compensation and assistive torque, defined as interaction force, is converted to a reference velocity for the motor in order to have an interaction force equal to zero. In this way the assistive torque is equal to gravity compensation torque of the elbow joint (δ). An improvement of the control strategy is proposed in [32] where the elbow torque is evaluated through Hill-type muscle model using the EMG and encoder signals.

Application The fields of applications can be divided in: (i) rehabilitation for medical use; (ii) assistive for daily living (ADL) tasks; (iii) industry for industrial tasks. The main applications of examined soft wearable robots, as Tab. 1.1 underlines, are rehabilitation and assistive.

1.3.2 Discussion

The analysis of the soft wearable robots for upper limb illustrated in Sec. 1.3.1 underlines that tendon-driven, fabric-based inflatables and textile are the actuation systems mostly adopted in the last decade. As indicated in [27], the first are controllable and can generate high forces; however, during use, the cables could generate high friction forces and the anchor points could slip. The second, instead, are simple and fast to fabricate, lightweight and can generate high forces; however, during use, delamination of the layers could be generated.

The illustrated advantages of the soft wearable robots are still linked to experiments performed in a laboratory setting. In particular, unlike rigid exoskeletons that have been widely implemented and validated in application contexts, as in industry [23], most of the examined soft wearable robots have been only tested in laboratory settings, as for instance, validation through reduction of muscle activations and fatigue of the subject during the execution of specific tasks. The authors in [4], instead, propose to validate the soft wearable robots across five stroke survivors. However, the involvement of five subjects is still not statistically relevant as underlined in [23], where the authors suggest that eight is the minimum number of subjects to consider the study as statistically significant [23].

1.3.3 Research and technology limitations

To improve design and fabrication and to observe a complete involvement of soft wearable robots in all fields of application the following limitations should be overcome:

Tools for design and simulation Currently the behaviour of soft actuators, i.e. forces generated and displacements, are studied using (i) finite element method (FEM) [33,34]; (ii) experimental simulations [17]. Then, the joint torques

generated by the actuators are evaluated through static or dynamic considerations using kinematic model of the arm. In other cases, i.e. rigid exoskeletons, the systems are modeled and simulated using musculoskeletal models as reported in [35], using Anybody Modeling System¹², and in [36], using OpenSim simulator¹³. Software applications for design and simulation of soft wearable robots integrated with musculoskeletal models have not yet been explored in depth; a recent example of application is proposed in [37]. They could lead to significant improvement in soft wearable robotics, since they would allow to compare different design concepts, materials and geometries of wearable robots before the physical prototyping.

Transportability of soft wearable robots Tendon-driven systems are defined transportable systems since they wear, usually on the back, the power systems composed of electric motors, gears and batteries. The pneumatic exoskeletons, instead, are not transportable since there are still technological limitations that prevent the wearing of the power system, i.e. air compressor. In this directions, different works have been presented solutions that aim to miniaturize the pumps for soft pneumatic actuators [38]. To date, we can conclude that the system transportability is fundamental for daily living tasks in which the wearable robot assists the subject throughout the day. In other applications, where the subject's position is within predefined areas such as medical and industrial tasks, the portability of the system plays a less relevant role. For these reasons, today tendon-driven systems are preferred for assistive applications and pneumatic systems are more suitable for rehabilitation and industrial contexts.

Wearability of soft wearable robots The wearability of the systems depend on the size of the exoskeleton. In this regard, one of the main advantages of pneumatic actuators is the possibility to wear them under clothing in order to create a more comfortable and less invasive wearable systems [10]. This feature could bring enormous benefits in industrial sector, where it will no longer be necessary to adapt workstations to workers who wear wearable robots; it will be enough to wear a simple actuated suit to reduce the risks associated to musculoskeletal disorders related to biomechanical overload [39, 40]. To enhance the wearability, design approaches where the suits and anchor points are based on the real 3D models and anthropometric characteristics of the human [41] can be explored, as already done in different fields as orthopaedics [42, 43]. Another important trend that can be observed in the direction of enhanced wearability is the implementation of flexible sensors (or soft sensors) in order to eliminate bulky components of exoskeletons, i.e. IMU and encoders. Moreover, two different approaches could be used: (i) flexible sensors on the human that evaluate the movements, i.e. joint angles, based on voltage of the soft sensor resistance [44]; (ii) flexible sensors in the actuators that measure the position and behaviour of the actuators [27].

¹²<https://www.anybodytech.com/>

¹³<https://simtk.org/projects/opensim/>

Control of soft wearable robots The control strategies of tendon-driven wearable robots, i.e. EMG-based torque estimation and admittance control strategies [6, 7], have been investigated more thoroughly than control strategies for pneumatic soft wearable robots. Control strategies for soft pneumatic actuators are required to successfully implement soft wearable robots in real environments. In particular, control strategies must be able to follow and adapt to joint movement in a natural and accurate way. To do that, two main approaches could be followed: (i) kinematics-based approach [45]; (ii) synergy-based approach [46–48].

Chapter 2

Biomechanical analysis of industrial overhead tasks

The chapter presents the biomechanical analysis of the whole upper body during the execution of the most demanding overhead tasks, i.e. drilling, leveraging and cabling tasks. Initially, the tasks were performed at laboratory environment at two different working heights defined as: *low configuration* and *middle configuration*. Before to perform biomechanical analysis, an ergonomic assessment of the worker was conducted in order to define the most demanding task and any correlations between the selected tasks. In particular, rapid upper limb assessment (RULA) method was used to define the worker ergonomic and risks associated to WMSD. Then, a biomechanical analysis of the most demanding task was carried out in order to define a better working configuration for the workers. In particular, multiple performance metrics are derived to have a complete view of the worker biomechanical behaviour of upper body, i.e. upper-limb, neck and trunk, during the execution of the task, with the objective to understand the real sources of WMSD. In particular, the performance metrics include: average timing values of the task execution, temporal profiles and average of joint angles, average of joint torques, root mean square of the normalized muscle activations. The evolution over time of the joint angles and joint torques are evaluated reproducing the movement of the worker in virtual scenario using digital human models (DHM), i.e. OpenSim [49]; the muscle activations, instead, are computed from the electromyographic (EMG) signals. The analysis is also compared with comparing works. The results suggest that only an integrated approach can be effectively used to define the biomechanical behaviour of the worker, and thus provide guidelines for ergonomic design of industrial workstations and, rational selection or development of assistance aids (i.e. robotic exoskeletons), if needed for the task.

2.1 Methods

In the biomechanical analysis four different aspect is considered: (1) task performance; (2) kinematic movements; (3) dynamic loads; (4) muscle activities. For each aspect, a performance measure is derived. The biomechanical analysis is based on the reconstruction of joint angles and torques from motion capture and ground reaction forces data using biomechanical modelling, and estimation of muscle activation from surface electromyography. The overall methodology used in this chapter is illustrated in Fig. 2.1.

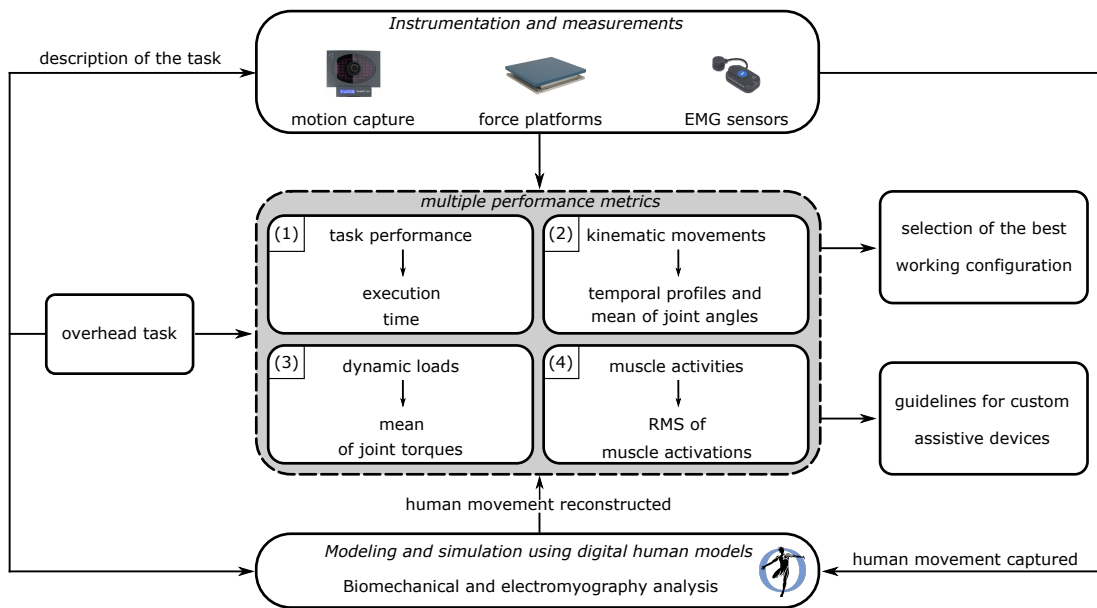


Figure 2.1: Biomechanical analysis of the industrial task to reduce the risks associated to WMSD.

2.1.1 Multiple performance metrics

Task performance

Classic metrics used to evaluate the task performance are: (i) number of repetitions during a time period [50]; (ii) time to reach a specific target which represents the work position [51]; (iii) execution time of the task [19, 52–54]. In real factory scenarios, workers are usually instructed to perform a task in the shortest possible time, to enhance productivity. Therefore, task performance metric selected is the execution time of the task.

Kinematic movements

With movements we refer to kinematics and posture of the worker during the execution of an industrial task. Common metrics used to measure workers movement

are: (i) range of motion (RoM) of workers during the execution of a task [53, 54]; (ii) maximal or average value [51]; (ii) temporal profiles, i.e. evolution over time of the joint angles of the workers [51]. In this work, average values of joint angles is used as performance metric since the task can be considered static task. Moreover, pairwise comparison of joint angles is used, as proposed in [55], to evaluate the the influence of each joint on the specific industrial task. Finally, the temporal profiles of joint angles is reported to validate the results obtained for the selected task and to take into account the variation of the joints not visible through the selected metrics. The joint angles are reconstructed using inverse kinematics (see, e.g. App. A.1).

Dynamic loads

The loading of each joints during the execution of an industrial task can be evaluated in static and dynamic conditions: (i) static joint loads using average values [53] and static joint torques using temporal profile [56, 57]; (ii) dynamic torques using average values [54]. Since industrial tasks often involve the use of tools which generate vibrations (e.g. drilling tasks), in this work, the average values of joint torques is selected as dynamic performance metric. Dynamic analysis are therefore useful to establish the configuration of the workstation which minimize the joint torques on the workers. The joint torques are reconstructed using inverse dynamics (see, e.g. App. A.2).

Muscle activities

The muscle activities are usually quantified with a direct measure of muscle activations [19, 51, 58, 59]. The EMG signals can be studied in: (i) time domain, using the average or root mean square (RMS) values of the signal [58, 59]; (ii) frequency domain, using mean power frequency (MPF) or median power frequency (MDF) [19]. In this work, the time domain is used to have a perfect correlation between muscle activation and kinematic/dynamic results. In particular, root mean square (RMS) values of muscle activations is selected to characterize the muscle activities of the worker and to define the part of the body subject to the largest physiological demand during the activity. The calculation of this metric requires specific protocol (see Sec. 2.2.4) for treatment and processing of EMG signals.

2.1.2 Biomechanical analysis of workers

Human movements capturing

Classic technologies used for human movements capturing include: (i) optical cameras with markers and without markers [53, 60, 61]; (ii) wearable motion sensing suits with e.g. inertial measurements units (IMU) [62] and/or soft sensors [44].

For dynamic analysis, instead, the most adopted technologies are: (i) force platforms; (ii) wearable force sensors, e.g. wearable force plates [63]. In industrial settings, wearable motion capture systems and wearable force sensors would be preferable, as the inertial suit Xsens MVN [64] and wearable force sensors as Xsens shoes [65]. However, they present a low accuracy [66] in evaluating human joint angles and torques if compared to laboratory equipment (optical cameras and force platforms), which currently are the most accurate systems for tracking human motions. In this work, the optical cameras with markers and force platforms is used in order to obtain results as accurate as possible. Finally, muscle activations are measured using surface EMG (sEMG) sensors as proposed in the literature [19, 51, 58, 59].

Human movements reconstruction

Digital human models (DHM) are used to describe the behaviour of the subject from the human motion data, and they are used to replicate the human activity in virtual environment. Classic software used in this context can be divided in: (i) static DHM software (as Simens Tecnomatix Jack [67]) (ii) biomechanical-based DHM software which implements biomechanical models of the human body with an accurate dynamic analysis (as AnyBody [68] and OpenSim [49]). For a comprehensive overview of DHM and associated software tools, the reader can refer to [69]. One of the most used biomechanical-based DHM environments is OpenSim, an open source software. Here, simulations are generated by experimentally measured kinematic, kinetic and EMG patterns. This software, initially devoted mainly to medical and sports applications, has recently demonstrated interesting capabilities in risk-assessment of WMSD [39, 70]. Therefore, OpenSim is used also in this work. The basic advantages of OpenSim are: (i) scaling of the digital human model (DHM) based on real anthropometric characteristics; (ii) generating a muscle-driven simulation of human movements; (iii) computing of DHM joint angles, torques and muscle activations. The detailed procedures for inverse kinematics and inverse dynamics starting from motion capture and ground reaction forces data are reported in App. A. However, in this study the muscle activation is computed directly by the EMG signals, in order to obtain a more manageable and accurate analysis of the human muscle activities.

2.2 Experiments

A laboratory study on drilling, leveraging and cabling overhead tasks performed at different working heights were conducted according to literature indications [19, 50, 52]. The objective of the experiments is to define the best working configuration for the workers through ergonomic and biomechanical analysis. The experiments were performed at ErgoS Lab, the Laboratory of Advanced Measures on Ergonomics and Shapes at CeSMA, University of Naples Federico II.

Table 2.1: Anthropometric characteristics: Height, Weight, Uarm (upper arm), Larm (lower arm) and personal detail (i.e. age) of the subjects involved for the experiments. S.D.: standard deviation; Min.: minimum value; Max.: maximum value.

	Age [yr]	Height [cm]	Weight [kg]	Uarm [cm]	Larm [cm]
Mean	27.0	182.1	84.9	36.6	26.9
S.D.	5.0	6.8	8.5	0.8	2.7
Min.	24.0	176.0	77.0	36	23.5
Max.	34.0	189.0	95.4	37.5	29.0

2.2.1 Participants

Four right-hand Italian males, volunteer subjects, were selected from the local population to participate for the experiments. The subjects do not have or have limited experience with industrial work. All participants did not report any musculoskeletal disorders or problems over the past twelve months. Participants gave written informed consent, according to the Statement of Ethics Committee of University of Naples Federico II – Ref. Protocol 335/20, before starting the experiments. After an initial briefing, a physician collected their anthropometric characteristics and personal details: these are reported in Tab. 2.1. According to the Italian population stature distribution [71], two subjects belong to the 97th percentile (in the following referred to with the letters *a* and *b*), while two subjects belong to the 50th percentile (in the following referred to with the letters *c* and *d*) as proposed in [72].

2.2.2 Laboratory task and description

Task setup An experimental platform for performing overhead tasks with different working heights was designed (see, e.g. Fig. 2.2): it is composed of four circular section poles (height-adjustable), which support an overhead platform composed by a rectangular structure (square section).

Tasks description Drilling task (DT): the subjects were asked to stay with the right hand below the head for about 7 seconds (reset position) and to drill a wooden beam (dimension: 70x70 mm) with a drill having a wood tip of diameter 10 mm (working posture). The weight of the drill is 1850 g. Each trial consisted in three repetitions of the operations (work cycles). An example of the execution of drilling overhead task is reported in Fig. 2.3a. Leveraging task (LT): the subjects were asked to clamp 3 bolts with 2 wrenches (weight: 70 g). The bolts were fixed on aluminium profile (dimension: 36x36x2 mm), as shown in Fig. 2.3b; each trial consisted in three work cycles. Cabling task (CT): the subjects were asked to insert the cable inside a hole and finally to perform a knot with both hands, as illustrated in Fig. 2.3c; this task represents a simulated light assembly tasks



Figure 2.2: Front view of the experimental setup comprising four poles as based and overhead platform to perform drilling, leveraging and cabling tasks.

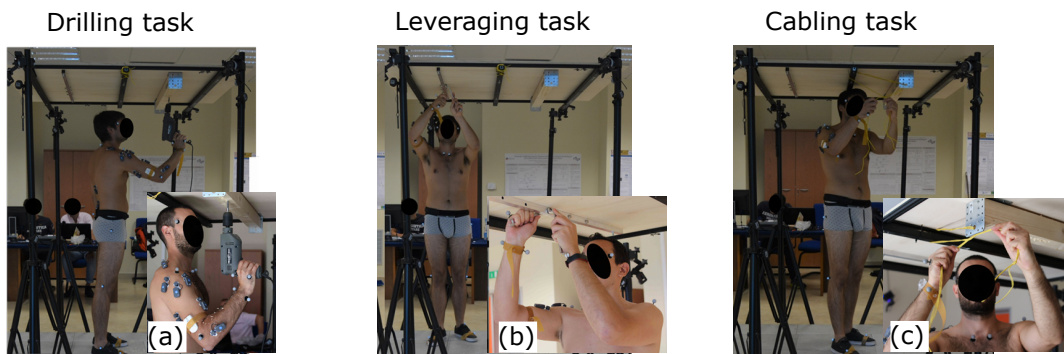


Figure 2.3: Posture of the subject during the execution of drilling task (a), leveraging task (b) and cabling task (c).

where the subjects do not use a tool. For each trial the subjects carried out one work cycle. For all the tasks, two trials were conducted and the recovery time between two consecutive tests was chosen equal to 50% of the duration of the test.

Independent variable The independent variable of the experiment was the height of the platform for drilling task. In particular, the task was replicated at two different working heights, called in the following *low configuration* and *middle configuration*. The working height h depends on the anthropometric characteristics of the subjects, and is defined as:

$$h = A + n(B - A) \quad (2.1)$$

where:

- A : lowest possible working height for the selected task (see Fig. 2.4) and

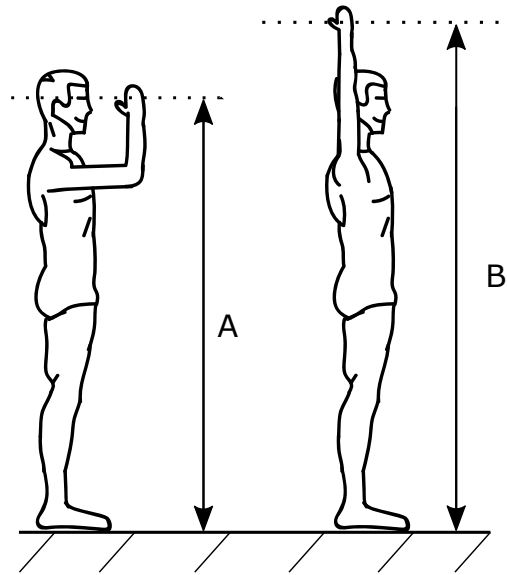


Figure 2.4: Side view of the two anthropometric characteristics selected to evaluate the working height configurations defined in [19].

defined in [19] as: "hand height with the shoulder and elbow fixed to 90 degrees in neutral upper arm rotation";

- B : highest possible working height for the selected task (see Fig. 2.4) and defined in [19] as "hand height with the upper arm in full flexion (maximum overhead reach) with shoulders parallel to ground";
- n : weight coefficient, it can assume values between 0 and 1.

In present experiments, two working heights are used: h_1 , using $n = 0$ (low configuration) and h_2 , using $n = 0.4$ (middle configuration), as proposed in [19]. For each working height, two trials were performed; the recovery time between two consecutive tests was chosen equal to 50% of the duration of the test. Since four subjects were involved for two trials of three work cycles each, a total of 116 experiments have been performed.

2.2.3 Instrumentations

This section describes the sensors and equipment used to measure human parameters related to the ergonomic and biomechanical measures described in Sec. 2.1.

Motion capture system The system used in the experiments to track the kinematics is a motion capture system composed by ten infrared digital cameras (SMART DX 6000, BTS Bioengineering). The sampling frequency of the cameras is 340 Hz, at their maximum resolution of 2048 x 1088 pixel.

Ground reaction forces Eight integrated force platforms (P-600, BTS Bioengineering) with sample frequency of 680 Hz are used for ground reaction forces measurements.

Surface electromyography Muscle activities are measured by using eight EMG sensors (FREEEMG 1000 and 300, BTS Bioengineering).

2.2.4 Protocols

Two different protocols were defined to track human joint angles and to measure the human muscle activations. One physician was involved in this study to guarantee the correct placement of the markers and EMG sensors on the human body.

Marker protocol

For the overhead task, we used an ad-hoc measurement protocol composed of twenty-two markers. The protocol includes twelve markers placed on the upper body according to the work in [73] and, additionally, two markers on the hand according to [74]. The latter two markers have been added in the marker protocol as they allow to define and calculate the wrist angles during the execution of the industrial task. With respect to [73], the two additional markers on the anterior superior iliac spine and four markers placed on the left arm were excluded since the subjects involved in the current experiments are all right-handed, and thus these markers are not needed. The last eight markers were placed on the lower body of the subject according to palpable anatomical landmarks on the lower extremity used in [75]. The full marker set is illustrated in Fig. 2.5.

The defined marker protocol allows to reconstruct the following joint angles and the relative joint torques:

- Upper-limb angles/torques which includes shoulder flexion–extension (α/τ_1) and abduction–adduction (β/τ_2);
- Lower limb angles/torques which includes shoulder rotation (γ/τ_3) and elbow flexion–extension (δ/τ_4);
- Wrist angles/torques which includes wrist flexion–extension (ϵ/τ_5), wrist radial–ulnar deviation (ζ/τ_6) and pronation–supination (η/τ_7);
- Trunk angles/torques which includes trunk flexion–extension (θ/τ_8), lateral bending (ι/τ_9) and axial rotation (κ/τ_{10});
- Neck angles/torques which includes neck flexion–extension (λ/τ_{11}), axial rotation (μ/τ_{12}) and lateral bending (ν/τ_{13}).

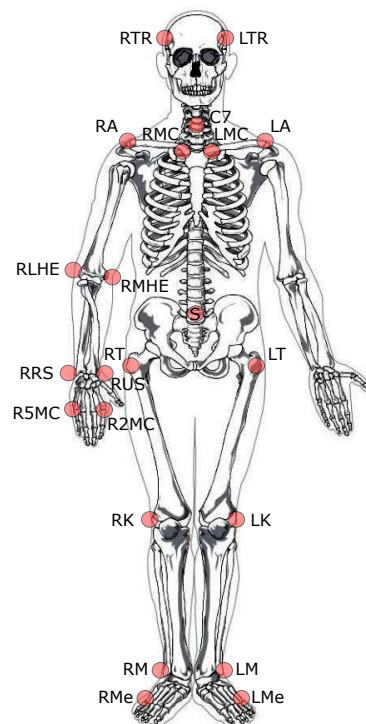


Figure 2.5: Marker set on the human body, where: LTR/RTR: Left/Right Temporal Regions; LMC/RMC: Left/Right Medial end of the Clavicle; C7: Cervical vertebra; LA/RA: Left/Right Acromion; RLHE/RMHE: Right Lateral/Medial Humeral Epicondyle; RRS/RUS: Right Radial/Ulnar Styloid; R2MC/R5MC: Right 2nd/5th Metacarpal; S: Sacrum; LT/RT: Left/Right Greater Trochanter; LK/RK: Left/Right Lateral Femoral Epicondyle; LM/RM: Left/Right Malleolus; LMe/RMe: 5th Metatarsal of the Left/Right Foot.

EMG protocol

The EMG sensors were placed on the upper body of the subjects according to [58, 76] and following to the indications given by the SENIAM project¹. The muscles included in the study are summarized in Tab. 2.2; the positions of the EMG sensors on real subject are shown in Fig. 2.6. In particular, the EMG sensors were positioned on the dominant side of the subject (right side for all subjects, see Sec. 2.2.1).

Before starting the experiments, the participants were asked to perform isometric maximal voluntary contractions (MVC) used to normalize the EMG signals (see Sec. 2.2.5). The manual muscle tests carried out for each muscle considered, according to SENIAM project, are:

- anterior deltoid (*AD*): the physician is positioned behind the subject and asks the subject to perform against resistance shoulder abduction in slight flexion, with the humerus in slight rotation;
- medial deltoid (*MD*): the physician is placed laterally to the subject and resists abduction of the arm to 90 degrees (without rotation);
- upper trapezium (*UT*): the physician stands behind the subject and unilateral action resists shoulder elevation and tilt of the head;
- biceps brachii (*BB*): the physician stands in front of the subject and resists elbow flexion (with the forearm in supination);
- long head of the triceps brachii (*TB*): the physician stands in front of the subject and resists elbow extension;
- extensor carpi radialis longus (*EC*): the physician stands in front of the subject and resists the wrist extension (with his hand closed in a fist);
- erector spinae at level L3 and T9 (*L3* and *T9*): the subject was asked to lift the trunk against resistance from a prone position.

2.2.5 Data processing and analysis

The marker positions, the ground reaction forces and muscle activations during the task execution were captured and processed using BTS SMART Capture and BTS SMART Analyzer software (BTS Bioengineering, Milan, Italy). Kinematics and dynamics were reconstructed using OpenSim. Then, the results of inverse kinematics, inverse dynamics as well as muscle activations were imported in MATLAB (MathWorks, Natick, USA) to identify the temporal events of the tasks and to perform the statistical analysis of the results.

¹<http://www.seniam.org>

Table 2.2: Positions of EMG sensors on the human muscles.

Body muscles	EMG sensor position
Shoulder or Neck	Anterior Deltoid (<i>AD</i>)
Shoulder or Neck	Medial Deltoid (<i>MD</i>)
Shoulder or Neck	Upper Trapezium (<i>UT</i>)
Arm or Hand	Biceps Brachii (<i>BB</i>)
Arm or Hand	Long Head of the Triceps Brachii (<i>TB</i>)
Arm or Hand	Extensor Carpi Radialis Longus (<i>EC</i>)
Trunk or Lower Back	Erector spinae at level L3 (<i>L3</i>)
Trunk or Lower Back	Erector spinae at level T9 (<i>T9</i>)

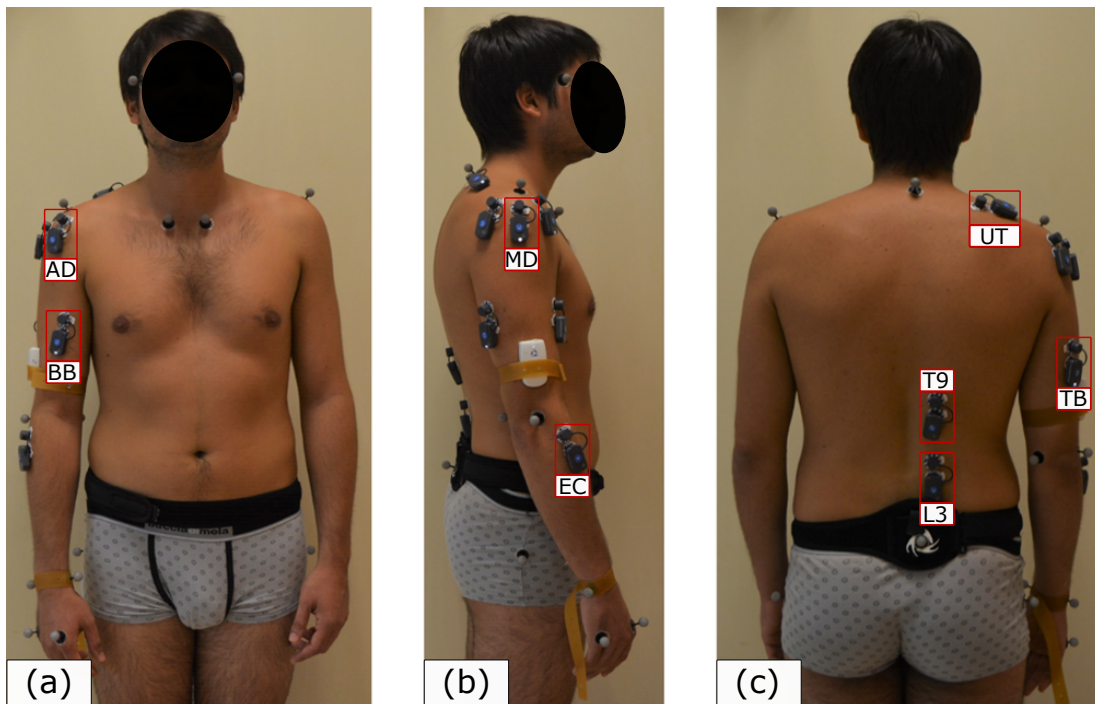


Figure 2.6: Marker and EMG sensors on the subject's body. (a - c) front view; (b) side view.

Kinematics and dynamics The evolution over time of the joint angles and torques specified in Sec. 2.2.4 were reconstructed using biomechanical musculoskeletal models available in OpenSim [49]. According our knowledge, a full model which considers all the joint angles and torques of our interest is not available in OpenSim. Therefore, we have used two different models: (i) *Full-Body Musculoskeletal Model* [77]; (ii) *Musculoskeletal Model of Head* [78]. The first model, usually used for full-body analysis, includes 37 degrees-of-freedom (DoF); among these, 7 DoF are available for each upper-limb. Through this model we were able to reconstruct the evolution over time of the angles and torques of: upper limbs, lower limbs and trunk. The second model, indeed, was used to reconstruct the angles and torques of the neck. Each OpenSim model, at the beginning, was scaled in accordance with the anthropometric characteristics of the subjects (as specified in Sec. 2.2.1). The details about the inverse kinematics and inverse dynamics computations are available in App. A.

Muscle activations The EMG signals were processed according to the following four steps [46]: (i) rectification; (ii) smoothing with a moving average filter (with time constant of 150 ms); (iii) filtering using a Butterworth low-pass filter with a cut off frequency of 2 Hz; (iv) normalization with respect to the maximum voluntary contractions.

Dependent variables The dependent variables evaluated in these experiments are the multiple performance metrics explained and illustrated in Sec. 2.1: i.e. task performance, temporal profile and mean of joint angles of the kinematic movements, mean of the joint torques and root mean square of muscle activations. The dependent variables were evaluated in the two different working heights specified in Sec. 2.2.2.

Statistical analysis The multiple performance metrics (see Sec. 2.1.1) are presented as mean \pm standard deviation, and the processing was performed using MATLAB. Initially, the data of *low configuration* and *middle configuration* are checked for normality with the Shapiro-Wilk test and then with the Levene's test for homogeneity of variances. The effect of the two working height configurations on mean of joint angles and torques as well as on root mean square of muscle activations, were tested with analysis of variance (ANOVA). The level of significance was set equal to 0.05. Finally, the effect size (ES) was calculated only for statistically significant results since the differences between the two working height configurations that depend on the sample fluctuation are not relevant. The ES values for each joint angle, torque and muscle activation at the low and middle working height configurations were calculated according to Cohen's d [79]. In accordance with [79, 80], we use the following scale for interpretation of the effect size results: small, for $ES \leq 0.2$; medium, for $0.2 < ES \leq 0.5$; large, for $0.5 < ES \leq 0.8$; very large, $0.8 < ES \leq 1.20$; huge, for $ES > 1.20$.

2.3 Results

In this section we present the results of the biomechanical analysis of the overhead drilling task, with regards to the metrics defined in Sec. 2.1.

2.3.1 Ergonomic assessment – RULA score

Before to carry out the biomechanical analysis, the joint angle results (indicated in Sec. 2.2.4) are used to assess the worker ergonomics. Over the last decade, the most adopted approaches for evaluating the risks associated to WMSD have been: Ovako Working Posture Analysing System (OWAS) [81], Rapid Upper Limb Assessment (RULA) [82] and Rapid Entire Body Assessment (REBA) [83]. These methods consider the working posture of the worker during the execution of the task, then assign a score for each part of the body and a final score which expresses the ergonomic condition of the worker. In particular, OWAS and REBA consider the human joints of the whole body; instead, RULA considers only the human joints of upper body. The RULA method is selected for the present work since the the tasks selected only concern the upper body and the RULA method is the standard approach used in current industries for evaluating the risks associated to WMSD.

For each subject and for each task considered, a table which describes the RULA local score and RULA final score is reported. The results are illustrated in the following:

Drilling task RULA local and final scores for drilling task are reported in Tab. 2.3. The table shows that, in most cases, the RULA final score is equal to seven (red zone) for the both working configurations selected defined as *low configuration* and *middle configuration*.

Leveraging task RULA local and final scores for leveraging task are reported in Tab. 2.4. Also in this case, the table shows that, in most cases, the RULA final score is equal to five or six (orange zone) for the both working configuration selected.

Cabling task RULA local and final scores for cabling task are reported in Tab. 2.5. The same considerations illustrated for the other two tasks can also be repeated for this task.

Table 2.3: The table shows the RULA local and final score for drilling overhead task. The letters a, b, c and d represent the four subjects and WC represents work cycle of the trial.

Drilling Task																								
RULA local score [-]																								
Upper arm				Lower arm				Wrist				Trunk				Neck				RULA final score [-]				
a	b	c	d	a	b	c	d	a	b	c	d	a	b	c	d	a	b	c	d	a	b	c	d	
<i>low configuration</i>																								
WC 1.1	3	3	3	3	2	2	2	4	4	4	5	5	2	2	1	2	1	1	1	1	7	7	6	7
WC 1.2	3	3	3	3	2	2	2	4	4	4	5	5	2	3	2	2	1	1	1	1	7	7	7	7
WC 1.3	3	3	3	3	2	2	2	4	4	4	5	5	2	3	2	2	1	1	1	1	7	7	7	7
WC 2.1	3	3	3	3	3	2	2	4	4	4	5	5	2	3	1	2	1	1	1	1	7	7	6	7
WC 2.2	3	3	3	3	3	2	2	4	4	4	5	5	2	3	1	2	1	1	1	1	7	7	6	7
WC 2.3	3	3	3	2	3	3	2	4	5	5	5	5	2	2	1	2	1	1	1	1	7	7	6	6
<i>middle configuration</i>																								
WC 1.1	4	4	3	4	1	2	2	1	4	5	5	4	2	2	2	2	1	1	1	1	7	7	7	7
WC 1.2	4	4	3	4	1	2	2	1	4	5	5	4	2	2	1	2	1	1	1	1	7	7	6	7
WC 1.3	4	4	3	4	1	2	2	1	4	5	5	3	2	2	1	2	1	1	1	1	7	7	6	7
WC 2.1	4	4	3	4	1	3	2	1	4	4	5	4	1	2	1	2	1	1	1	1	6	7	6	7
WC 2.2	4	4	3	3	1	3	2	1	4	4	5	4	1	2	2	2	1	1	1	1	6	7	7	7
WC 2.3	4	4	3	3	1	3	2	1	4	4	5	3	1	2	2	2	1	1	1	1	6	7	7	7

Table 2.4: The table shows the RULA local and final score for leveraging overhead task. The letters a, b, c and d represent the four subjects and WC represents work cycle of the trial.

Leveraging Task																									
RULA local score [-]																									
Upper arm				Lower arm				Wrist				Trunk				Neck				RULA final score [-]					
a	b	c	d	a	b	c	d	a	b	c	d	a	b	c	d	a	b	c	d	a	b	c	d		
<i>low configuration</i>																									
WC 1.1	4	3	3	3	2	2	3	3	1	1	1	1	1	3	2	1	1	1	1	1	1	5	6	5	5
WC 1.2	4	3	3	3	2	2	3	3	1	1	1	1	1	3	2	1	1	1	1	1	1	5	6	5	5
WC 1.3	4	4	3	3	2	2	3	3	1	1	1	1	1	3	2	1	1	1	1	1	1	5	6	5	5
WC 2.1	4	3	3	3	2	2	3	3	1	1	1	1	1	3	2	1	1	1	1	1	1	5	6	5	5
WC 2.1	4	3	3	3	2	2	3	3	1	1	1	1	1	3	2	1	1	1	1	1	1	5	6	5	5
WC 2.1	4	3	3	3	2	2	3	3	1	1	1	1	1	3	2	1	1	1	1	1	1	5	6	5	5
<i>middle configuration</i>																									
WC 1.1	4	3	3	3	2	2	3	3	1	1	1	1	1	3	2	1	1	1	1	1	1	5	6	4	5
WC 1.2	4	3	3	3	2	2	3	2	1	1	1	1	1	3	2	1	1	1	1	1	1	5	6	5	4
WC 1.3	4	3	3	3	2	2	3	3	1	1	1	1	1	3	2	1	1	1	1	1	1	5	6	5	5
WC 2.1	4	3	3	3	2	2	3	3	1	1	1	1	1	3	2	1	1	1	1	1	1	5	6	5	5
WC 2.2	4	3	3	3	2	2	3	3	1	1	1	1	1	3	2	1	1	1	1	1	1	5	6	5	5
WC 2.3	4	3	3	3	2	2	3	2	1	1	1	1	1	3	2	2	1	1	1	1	1	5	6	5	5

Table 2.5: The table shows the RULA local and final score for cabling overhead task. The letters a, b, c and d represent the four subjects and WC represents work cycle of the trial.

Cabling Task																							
RULA local score [-]															RULA final score [-]								
Upper arm				Lower arm				Wrist				Trunk			Neck				a	b	c	d	
a	b	c	d	a	b	c	d	a	b	c	d	a	b	c	d	a	b	c	d				
<i>low configuration</i>																							
WC 1	4	3	4	3	1	2	3	3	2	2	2	2	3	2	3	1	1	1	1	4	4	4	5
WC 2	4	4	4	3	2	2	3	3	2	2	2	2	1	2	2	1	1	1	1	4	4	4	4
<i>middle configuration</i>																							
WC 1	4	3	4	3	1	2	2	2	2	2	2	2	3	4	3	1	1	1	1	4	4	6	4
WC 2	4	3	4	3	2	2	2	2	2	2	2	2	1	3	4	3	1	1	3	4	4	6	4

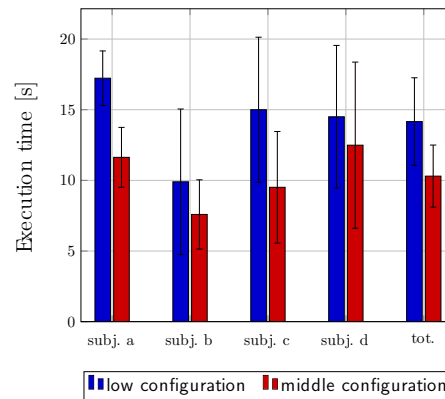


Figure 2.7: Average values of execution time for the four subjects (subj. a; subj. b; subj. c and subj. d) in the two working height configurations: *low configuration* and *middle configuration*.

The ergonomic assessment, i.e. RULA method, does not allow to define the best working configuration for the worker since this approach presents some limitations: (i) the methods can only be used for static works; (ii) they allow to make an overall ergonomic evaluation of the task, but they do not allow to identify the parts of the body (joints and muscles) which are mostly stressed by the task; (iii) they provide a rough final score, in the sense that only large angular variations of the human joints can cause a variation of final score. In summary, the empirical methods do not allow to have a complete analysis of the industrial task; this can be a problem mainly for complex tasks as the overhead tasks [39].

Finally, the biomechanical analysis is carried out only for drilling task since it is the most demanding task and all tasks, i.e. drilling leveraging and cabling, present the same correlations in terms of joint angles.

2.3.2 Task performance

The metric regarding task performance is the execution time of the task, which represents an estimate of productivity. The mean values of the execution time for the four subjects are reported in Fig. 2.7. Passing from *low configuration* to *middle configuration*, the figure shows a significant decrease, with a large effect, of the execution time of 3.86 s ($p = 0.006$; $ES = 0.800$) which corresponds to a relative decrease of 27.3% and thus, a potential increase of productivity.

2.3.3 Kinematic movements

We have selected two metrics regarding kinematic movements: temporal profiles of joint angles and average values of joint angles.

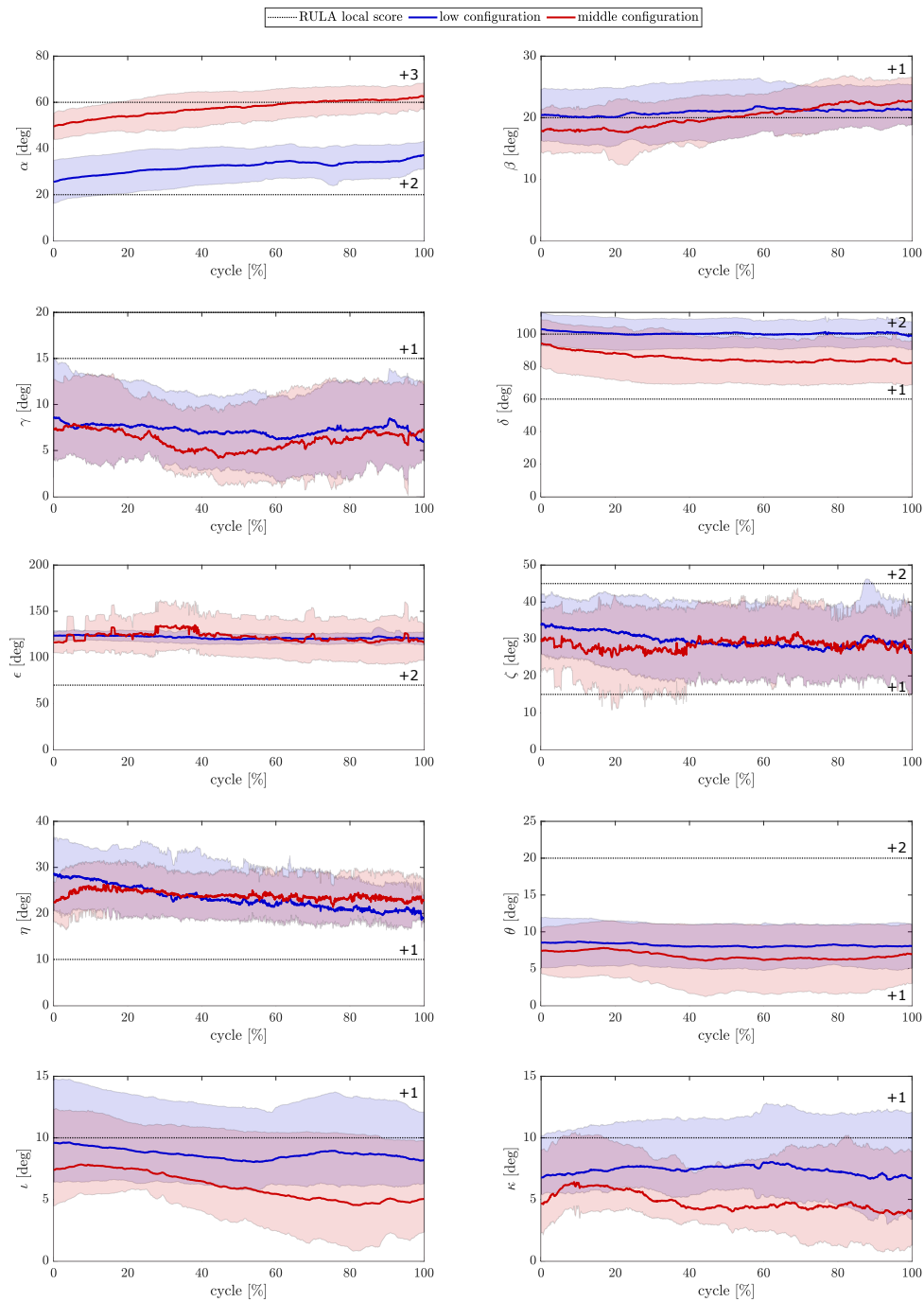


Figure 2.8: The evolution over time of joint angles presented as mean \pm standard deviation for each configuration (*low configuration* and *middle configuration*). The joint angles represented in the figure are: α : shoulder flexion-extension; β : shoulder abduction-adduction; γ : shoulder rotation; δ : elbow flexion-extension; ϵ : pronation and supination; ζ : wrist flexion-extension; η : wrist radial-ulnar deviation; θ : trunk flexion-extension; ι : trunk lateral bending; κ : trunk axial rotation.

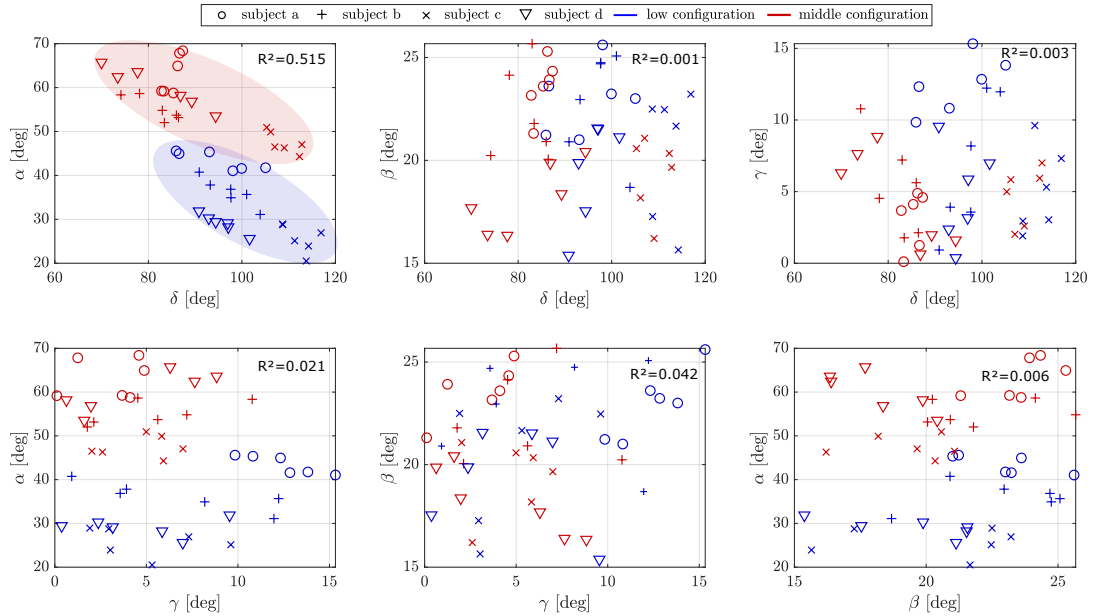


Figure 2.9: Average values, for each work cycle, of upper arm joint angles for the two configurations referred to as *low configuration* and *middle configuration*. The mean joint angles represented in the figure are: α : shoulder flexion-extension; β : shoulder abduction-adduction; γ : shoulder rotation; δ : elbow flexion-extension. R^2 : linear determination coefficient. For a correct view of these plots, the readers are invited to see the image with colors.

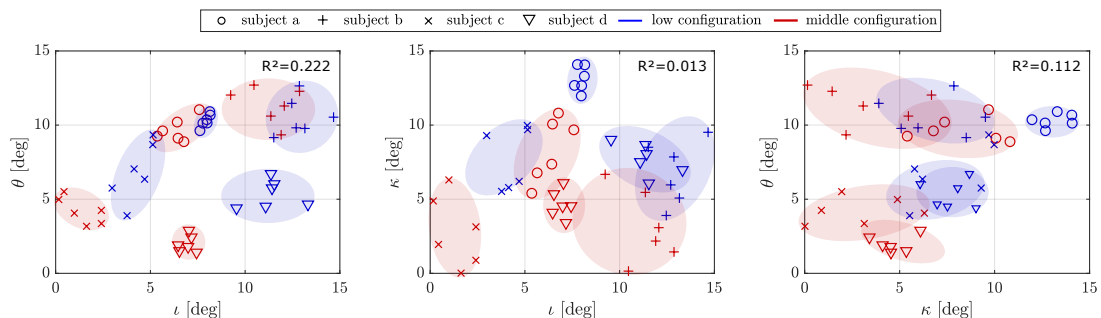


Figure 2.10: Average, for each work cycle, of trunk joint angles for the two configurations referred to as *low configuration* and *middle configuration*. The mean joint angles represented in the figure are: θ : trunk flexion-extension; ι : trunk lateral bending; κ : trunk axial rotation. R^2 : linear determination coefficient. For a correct view of these plots, the readers are invited to see the image with colors.

Temporal profile The inverse kinematic results in terms of mean \pm standard deviation, i.e. reconstruction of temporal profiles of human joint angles for the two configurations, are plotted in Fig 2.8. The plots in Fig 2.8 are in agreement with the selected task; for example, we can see from the first subplot (regarding joint angle α , i.e. shoulder flexion-extension) that the angle α increases passing from the *low configuration* to the *middle configuration*, as expected. We can also see that, during the execution of the task, for each work cycle, the same angle increases since the drilling of the drill bit inside the wooden beam increases. Notice that in these plots we do not include the neck angles (neck flexion-extension, axial rotation and lateral bending) since their variations for the drilling task are not relevant (indeed, these angle variations are around 1 degree). These plots also include the limit values of RULA local score, as these were used in Sec. 2.3.1 to evaluate the ergonomic assessment.

Average values of joint angles The evolution over time of the joint angles reported in Fig. 2.8 shows a constant trend of the pronation-supination and wrist angles. For this reason, we have compared only the joint angles of the upper arm (shoulder flexion-extension and abduction-adduction) and the joint angles of the lower arm (shoulder rotation and elbow flexion-extension), reported in Fig. 2.9, and trunk angles (trunk flexion-extension, axial rotation and lateral bending), reported in Fig. 2.10. In particular, we have represented the number of combinations, without repetitions, of k objects from n as following: $C_{n,k} = \frac{n!}{k!(n-k)!}$. For upper arm and lower arm angles the number of combinations are equal to 6 ($C_{4,2} = 6$, see Fig. 2.9) and for trunk angles the number of combinations are equal to 3 ($C_{3,1} = 3$, see Fig. 2.10). Observing Fig. 2.9 and Fig. 2.10, passing from *low configuration* to *middle configuration* we can notice the following results:

- a significant increase, with a huge effect, of the shoulder flexion-extension α of 22.42 degrees ($p < 0.001$; $ES = 2.922$);
- a significant decrease, with a medium effect, of the shoulder abduction-adduction β of 0.62 degrees ($p = 0.0015$; $ES = 0.223$);
- a significant decrease, with a large effect, of the shoulder rotation γ of 2.84 degrees ($p = 0.011$; $ES = 0.761$);
- a significant decrease, with a very large effect, of the elbow flexion-extension δ of 10.55 degrees ($p = 0.002$; $ES = 0.971$);
- a significant decrease, with a large effect, of the trunk lateral bending ι of 2.64 degrees ($p = 0.015$; $ES = 0.733$);
- a significant decrease, with a huge effect, of the trunk axial rotation κ of 4.09 degrees ($p < 0.001$; $ES = 1.375$).

The decrease of trunk flexion–extension θ is not significant ($p > 0.05$). The correlation between working heights for the shoulder flexion–extension α and elbow flexion–extension δ is visible in Fig. 2.9, where the points of *low configuration* tend to be positioned at bottom right, instead, the points of *middle configuration* tend to be positioned at top left. Moreover, the figure notices a small correlation between these angles ($R^2 = 0.515$). The other angles do not have correlations. The correlation between working heights for the trunk angles is indeed visible in Fig. 2.10, where the points of *low configuration* tend to be positioned at top right; indeed, the points of *middle configuration* tend to be positioned at bottom left, for each considered subject. In summary, we can conclude that the illustrated results show an increase trend of shoulder flexion–extension angle passing from *low configuration* to *middle configuration*; indeed, the other angles decrease.

2.3.4 Dynamic loads

The effects of loads during the execution of industrial task are taken into consideration through the evaluation of the temporal profiles and the average values of joint torques, as result of the inverse dynamic computation.

Average values of joint torques The average values of the torques of the most activated joints for the two configurations and for the four subjects are illustrated in Fig. 2.11. The figure does not include the trunk axial rotation torque (τ_{10}) since its variation is very small (less than 0.06 Nm). Moreover, the decrease of trunk flexion–extension θ is not statistically significant. The figure shows that the most loaded joints are trunk lateral bending (τ_9) and shoulder flexion–extension (τ_1). The first result (regarding τ_9) is in accordance with the execution mode of the task since the drilling task is carry out only with dominant hand. The second result (regarding τ_1), instead, is due to an increase in the working height and consequently an increase in the shoulder flexion–extension (α , see Fig 2.8). Moreover, passing from *low configuration* to *middle configuration*, Fig. 2.11 underlines:

- a significant increase, with a huge effect, of the shoulder flexion–extension torque τ_1 of 2.18 Nm ($p < 0.001$; $ES = 1.697$);
- a significant decrease, with a large effect, of the shoulder abduction–adduction torque τ_2 of 0.38 Nm ($p = 0.017$; $ES = 0.765$);
- a significant decrease, with a huge effect, of the shoulder rotation torque τ_3 of 0.28 Nm ($p < 0.001$; $ES = 1.311$);
- a significant decrease, with a very large effect, of the elbow flexion–extension torque τ_4 of 0.38 Nm ($p = 0.009$; $ES = 0.842$);
- a significant decrease, with a very large effect, of the trunk lateral bending torques τ_9 of 0.35 Nm ($p = 0.004$; $ES = 0.950$);

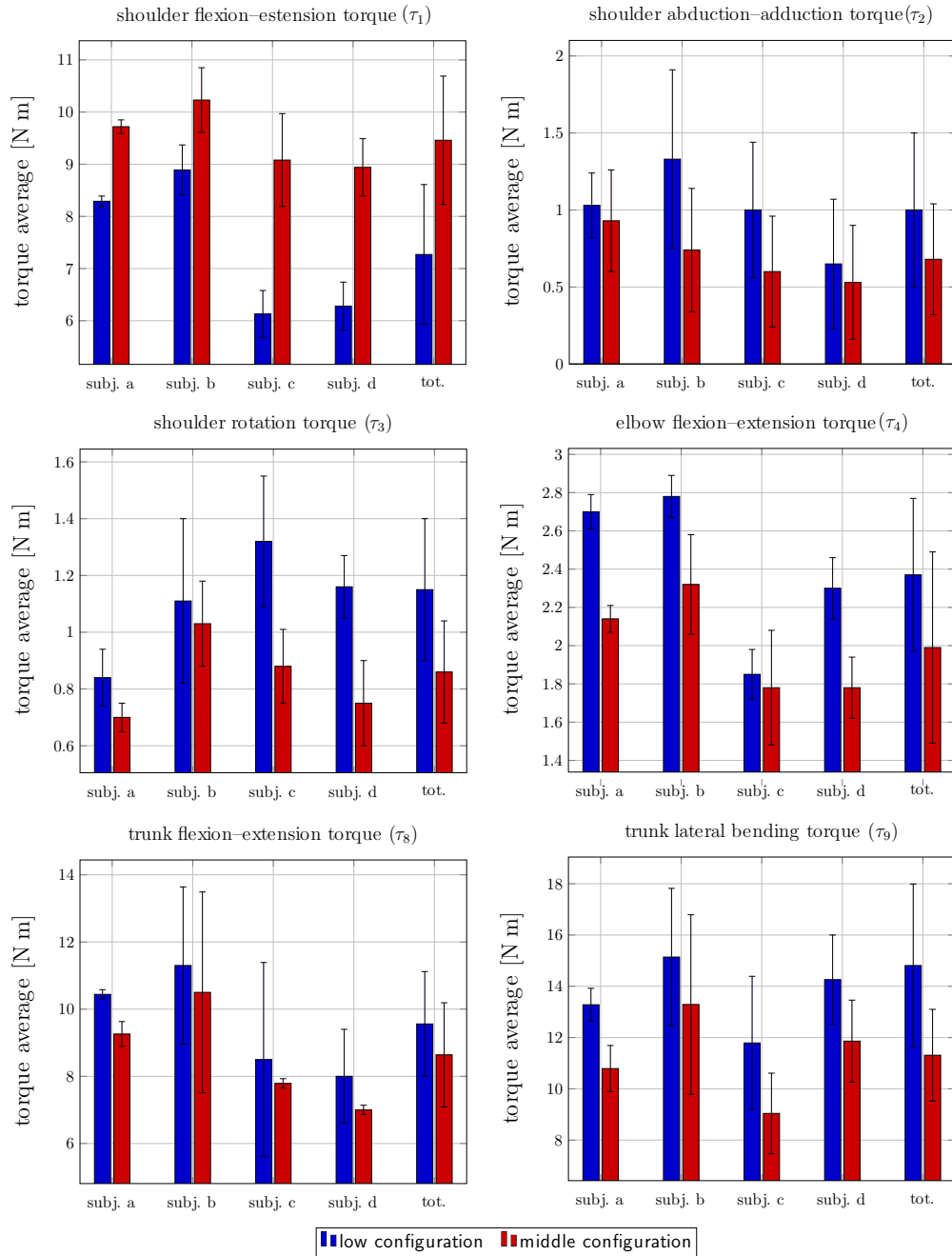


Figure 2.11: Average values of the joint torques for the four subjects (subj. a; subj. b; subj. c and subj. d) in two different configurations.

2.3.5 Muscle activities

The biomechanical analysis presented in this paper uses root mean square (*RMS*) of normalized muscle activation as metric for muscle activities. The results of the muscle activations are used to define the most activated muscle in the two different working height configurations.

RMS of normalized muscle activations The root mean square (RMS) values of the normalized muscle activations (NMA), for all subjects in the two different configurations, are reported in Fig. 2.12. The decrease and increase of the extensor carpi radialis longus (*EC*) and medial deltoid (*MD*) are not statistically significant. Moreover, the figure shows that the most activated muscles in *low configurations* are: anterior deltoid (*AD*) for subject a; biceps brachii (*BB*) for subject b and d; erector spinae at level L3 (*L3*) for subject c. The most activated muscles in *middle configurations* are: anterior deltoid (*AD*) for subject a, c and d; upper trapezium (*UT*) for subject b. As matter of the fact, we can notice:

- a significant increase, with a very large effect, of the anterior deltoid *AD* muscle activation of 0.14 ($p = 0.005$; $ES = 0.862$);
- a significant increase, with a very large effect, of the upper trapezium *UT* muscle activation of 0.14 ($p = 0.004$; $ES = 0.873$);
- a significant decrease, with a large effect, of the biceps brachii *BB* muscle activation of 0.10 ($p = 0.032$; $ES = 0.638$);
- a significant decrease, with a huge effect, of the long head of the triceps brachii *TB* muscle activation of 0.14 ($p < 0.001$; $ES = 1.635$);
- a significant decrease, with a large effect, of the erector spinae muscle activation at level *L3* of 0.09 ($p = 0.033$; $ES = 0.631$).
- a significant decrease, with a large effect, of the erector spinae muscle activation at level *T9* of 0.07 ($p = 0.035$; $ES = 0.627$).

2.4 Discussion

In this section we present an extensive discussion of the results. We compare the results with respect to standard approaches for ergonomic assessment currently used in industry and comparing works. Then, we present possible exploitation of the results from the industrial perspective. Finally, we conclude the section by presenting the limitations of the work.

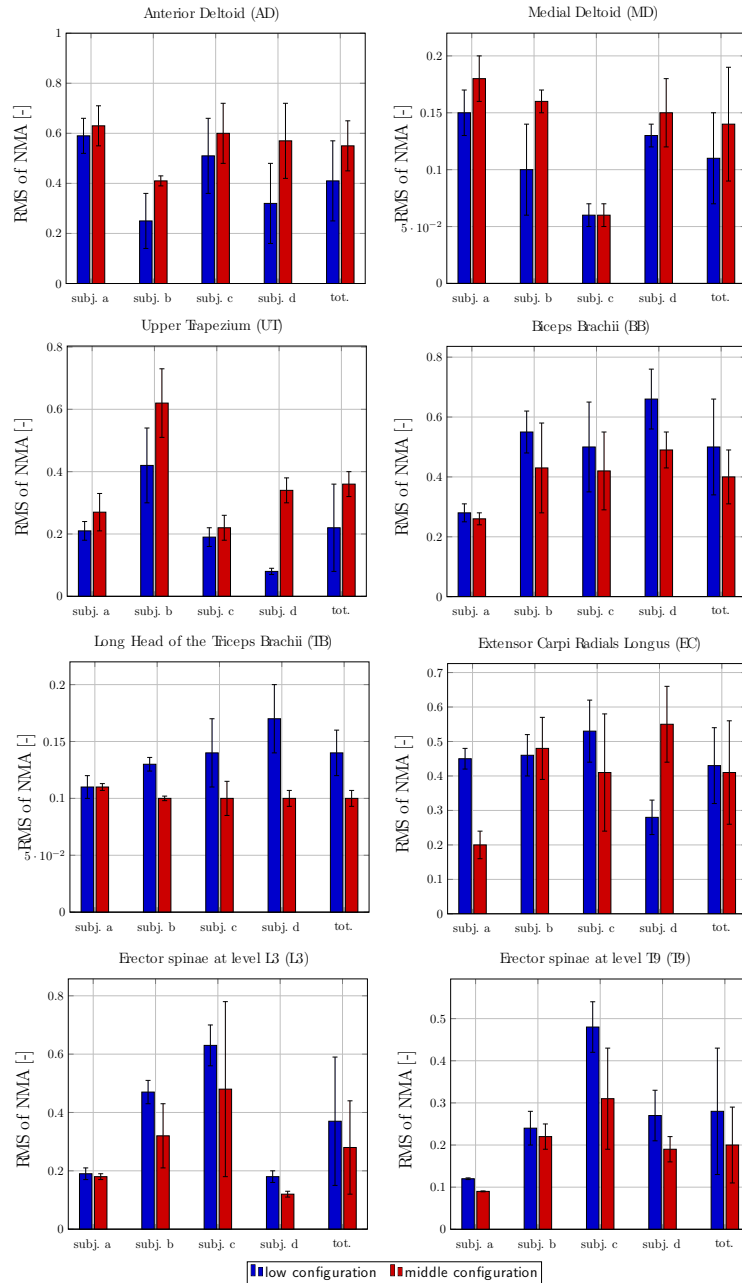


Figure 2.12: Root Mean Square (RMS) of the normalized muscle activation (NMA) values for the four subjects (subj. a; subj. b; subj. c and subj. d) in two different configurations.

2.4.1 Overall discussion of the results

Task performance

The reduction of movement duration in the *middle configuration* suggests that this configuration of the workstation increases the productivity of drilling overhead tasks (see Fig. 2.7). High productivity reduces costs for companies and can generate well-being among workers due to an average decrease in the workload of the individual worker.

Kinematic movements

The human joint trajectories are highly affected by the different configurations of the workstation: indeed, as we can see from the pairwise comparison of joint angles (Fig. 2.9 and Fig. 2.10), passing from *low configuration* to *middle configuration*, the average values of trunk joints (ι and κ), elbow joint (δ), shoulder joints (β and γ) have a significant decrease while the shoulder flexion–extension angle (α) has a significant increase. Moreover, the angles of the shoulder and elbow in the sagittal plane (α and δ) and the trunk angles on the three anatomical planes (θ , ι and κ) have a major correlation on the selected task. In summary, by only using kinematic metrics we are not able to distinguish which configuration is the most comfortable from the ergonomic point of view.

Dynamic loads

The analysis of human joint torques (Fig. 2.11) underlines that the most loaded joints in overhead drilling tasks are: shoulder and trunk joints (τ_1 , τ_8 and τ_9). There exists a common trend of the torques relative to the shoulder, elbow and trunk angles. In particular, the increase of shoulder flexion–extension torque (τ_1) and the decrease of elbow flexion–extension (τ_4), trunk flexion–extension and lateral bending (τ_8 and τ_9) are due to an increase and decrease of the relative human joint angles α , δ , θ and ι respectively (see Fig 2.8, Fig. 2.9 and Fig. 2.10). Again, using only dynamic metrics, we can individuate the most loaded joint but, it is difficult to discriminate the optimal configuration of the workstation. Moreover, the same results are obtained by using the most adopted ergonomic method in industry (i.e. RULA method) and they are also shown in the previous works presented in the literature (see Sec. 2.3.1).

Muscle activities

There exists a common trend of the muscle activations relative to the shoulder, elbow and trunk torques. In particular, the increase of anterior deltoid (*AD*) and medial deltoid (*MD*) and the decrease of biceps brachii (*BB*), long head of the triceps brachii (*TB*), erector spinae at level L3 and T9 (*L3* and *T9*) are due to increase and decrease of the relative human joint torques τ_1 , τ_4 , τ_8 and τ_9 (see Fig. 2.11). The normalized muscle activations of upper trapezius (*UT*) have

a significant increase passing from the *low configuration* to the *middle configuration*. This trend cannot be caused by an increase neck torques since, for the selected task, they are very small. For this reason, this trend could be caused by an isometric contraction of the muscle during the execution of the activity. The same results are also shown in the previous studies present in the literature (see Sec. 2.4.2). We can conclude that the RMS values of normalized muscle activations (Fig. 2.12 and Tab. 2.2) indicate that: shoulder/neck body muscles, arm/hand body muscles and trunk/lower back body muscles are the most activated in the *low configuration*; indeed, in the *middle configuration*, the most activated muscles refer only to shoulder/neck body muscles. Thus, from the muscle activities point of view, the *middle configuration* seems the best working configuration for workers. The latter configuration causes the isolation of the most activated muscles in a single muscle areas, and therefore it is possible to selectively act in this area to reduce worker muscle activities (see Sec. 2.4.3).

2.4.2 Comparison comparing works

The biomechanical analysis considered in this work has been compared with the RULA ergonomic assessment method and with comparing works.

The previous studies presented in the literature to estimate the loads and muscle activities of the worker during the execution of overhead drilling task in the same working height configuration highlight the equal difficulties encountered in this work [19, 84]. In particular, the first study [84] shows the effect of the working heights on shoulder torque and muscle activations. The authors propose to perform a static two-dimensional analysis to estimate the joint torque of the shoulder and the EMG analysis of three different muscles (anterior deltoid *AD*, biceps brachii *BB* and long head of the triceps brachii *TB*) during the execution of the task. The RMS of EMG signal and average values of torque are used as performance metrics. Passing from lower configuration to higher configuration, the results show a significant increase of shoulder torque of 6.04 Nm, a significant increase of muscle activations of anterior deltoid (*AD*) of 10.8% and a significant decrease of biceps brachii (*BB*) of 21.7%. The trend of results are in agreement with the results presented in this work, increasing the working height the shoulder muscles overload; the difference between the values of joint torque and muscle activations, could be due to the different weight of the drill used for the experiments. The second study [19], instead, illustrates the effect of working heights on shoulder muscle activities. The authors propose to perform EMG analysis of the muscles in the shoulder region. In particular, the EMG signal of anterior deltoid (*AD*), medial deltoid (*MD*) and upper trapezium (*UT*) muscles were acquired during a simulated overhead drilling task in different heights and the performance metric selected is maximum voluntary contraction. The results presented in this study [19] do not allow to notify a significant effects of working height on EMG-based muscle activities. The discrepancy between these results and the results presented in the present work may be due to the different se-

lected metrics. The metric selected for the present study is RMS of NMA and it calculates the area under the curve taking into consideration the evolution over time of the NMA. The metric selected in [19], instead, is the maximum of NMA and it takes into account only the maximum value of the muscle activation. It is important to underline that both previous studies focus on the static shoulder torque and upper arm muscle activities, not considering the effect of height on the trunk muscle activities which, as shown in this study, decrease passing from *low configuration* to *middle configuration*.

In summary: (i) our study considers a complete biomechanical analysis involving the analysis of joint kinematics and dynamics as well as muscle activities; (ii) our study includes joint angles, torques and muscles of the whole upper body; (iii) our results suggest that different working heights have an impact not only on the joints and muscles of the upper-limb, but also on the joints and muscles of the trunk.

2.4.3 Possible exploitation of the results

The results of these works can be exploited at different levels, with increasing complexity. Indeed, the proposed analysis can be used for multiple applications: (i) biomechanical analysis of existing industrial workstations; (ii) developing synthetic biomechanical indices [85, 86] for user-centered ergonomic evaluation of industrial tasks [87]; (iii) providing guidelines for the design of novel human-oriented industrial workstations [88]; (iv) providing guidelines for design of novel human- and task-oriented assistive devices [40].

In particular, the results of this study suggest that the *middle configuration* reduces the joint angles/torques of the trunk and elbow. However, this configuration implicates an increase of shoulder flexion-extension angle and torque. This seems a problem, but the important aspect is that in the *middle configuration* the most activated muscles are concentrated in a specific part of the body (shoulder/neck body muscles), differently from the *low configuration* where it is not possible to find this discrepancy and thus isolate the source of WMSD. This results is important since it allows to state that, for overhead tasks, the best configuration is the *middle configuration*, with the possibility to provide selective assistance in this anatomical area with wearable robots reducing the risks associated to the WMSD [47, 89].

Chapter 3

Functional requirements of soft wearable robot

In this chapter the functional requirements of a soft exoskeleton to assist human workers in performing overhead tasks is derived. These requirements are derived by analysing the biomechanical behaviour of human workers during the execution of such tasks in laboratory settings and from state-of-the-art considerations. A summary of the results obtained through biomechanical analysis are reported in Sec. 3.1; the requirements of soft wearable robots for industrial overhead tasks, instead, are reported in Sec. 3.2.

The basic flowchart of the adopted methodology is illustrated in Fig. 3.1, which underlines the idea of developing user-centered wearable systems from understanding the human motor control [47]. In particular, the first step is to select the industrial tasks, i.e. overhead manufacturing tasks, then the functional requirements, i.e. degrees of freedom of soft wearable robot, range of motion, torques required to support the human activities and the muscles to be supported, are defined using biomechanical analysis of the worker during the execution of the industrial tasks. The materials of the exoskeleton, the anthropometry, the mass and the contact pressure between robot and user are evaluated studying the literature. Finally, the functional requirements defined can be used to design soft exoskeleton for overhead industrial tasks.

3.1 Summary of the biomechanical results

The results of joint angles and torques of drilling, leveraging and cabling tasks are reported in Tab. 3.1. In particular, the tables shows the results of *middle configuration* defined and discussed in Ch. 2; the evolution of the joint angles and torques are reported in App. B.1. The table and plots report that the most loaded joints, for all tasks, are shoulder and elbow flexion-extension (τ_1 and τ_4). The results of root mean square (RMS) of normalized muscle activations (NMA) of drilling, leveraging and cabling tasks are reported in Tab. 3.2. Moreover, the evolution of the NMA for each task are reported in App. B.2. The results show

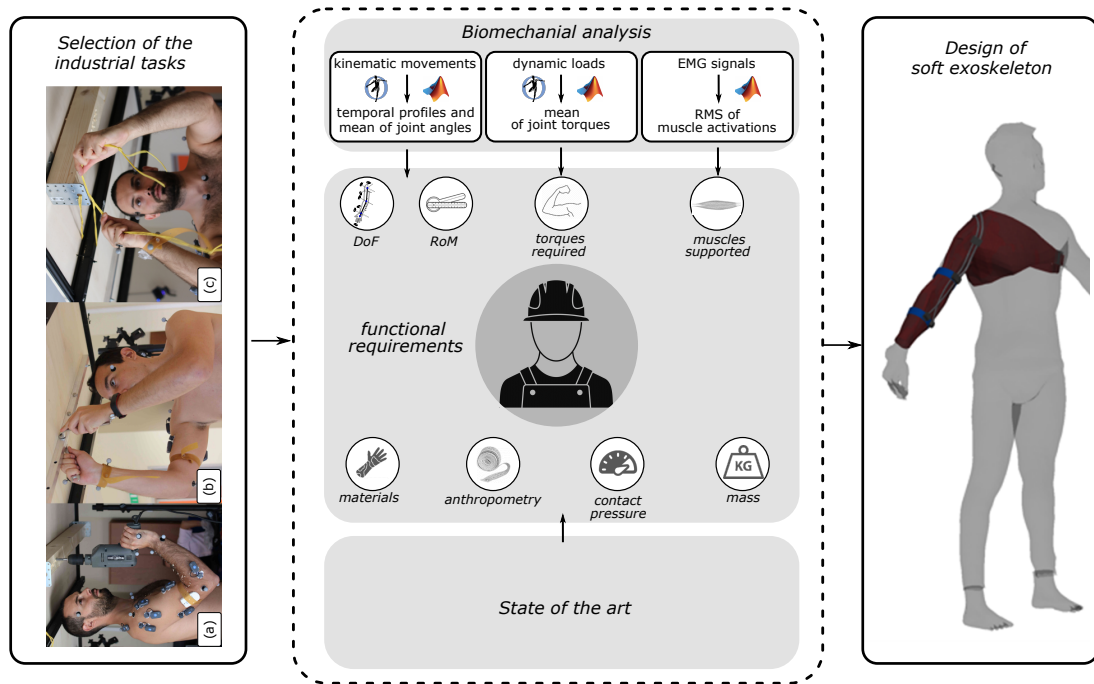


Figure 3.1: The proposed biomechanical-based process to derive the functional requirements of a soft industrial exoskeleton.

that the most activated muscles, for the three selected tasks, are anterior deltoid (*AD*) for shoulder muscles and biceps brachii (*BB*) for elbow muscles.

3.2 Functional requirements

The results of the biomechanical analysis of the workers while performing industrial overhead tasks, illustrated in Sec. 3.1, are used here to derive the functional requirements of the soft exoskeleton for industrial overhead tasks.

Movements and muscles supported The most activated muscles, as reported in Tab. 3.2, are: anterior deltoid for shoulder movements and biceps brachii for elbow movements. Therefore, the soft exoskeleton should be able to support the shoulder and elbow flexion–extension, thus reducing fatigue to anterior deltoid and biceps brachii.

Kinematics and dynamics The kinematic and dynamic results, reported in Tab. 3.1, are used to estimate the required forces and lengths of ideal actuators able to support the arm during the task execution. To do this, we use the kinematic model, reported in Fig. 3.2 and, the equations which link the human joint angles and torques with actuator lengths and forces as derived in [16]. In particular, the required shoulder force f_{sh} is:

Table 3.1: Mean values \pm standard deviation of joint angles and torques for the selected tasks. DT: drilling task; LT: leveraging task; CT: cabling task.

	joint angles [deg]			joint torques [Nm]		
	DT	LT	CT	DT	LT	CT
shoulder flexion–extension	54.9 (± 4.0)	120.4 (± 2.5)	107.7 (± 11.5)	9.5 (± 0.3)	7.54 (± 0.5)	7.2 (± 0.8)
shoulder abduction–adduction	20.1 (± 1.9)	10.5 (± 1.2)	14.9 (± 3.5)	0.7 (± 0.1)	0.5 (± 0.1)	0.4 (± 0.3)
shoulder rotation	7.9 (± 1.2)	36.2 (± 4.7)	37.4 (± 10.6)	1.1 (± 0.1)	0.8 (± 0.2)	1.0 (± 0.4)
elbow flexion–extension	89.1 (± 3.5)	57.0 (± 3.6)	61.5 (± 6.3)	2.0 (± 0.1)	1.32 (± 0.1)	1.21 (± 0.2)

Table 3.2: Mean values \pm standard deviation of root mean square (RMS) of the normalized muscle activation (NMA) for the selected tasks. DT: drilling task; LT: leveraging task; CT: cabling task.

	RMS of NMA [-]		
	DT	LT	CT
anterior deltoid	0.53 (± 0.13)	0.16 (± 0.01)	0.14 (± 0.02)
medial deltoid	0.17 (± 0.04)	0.09 (± 0.01)	0.08 (± 0.01)
upper trapezium	0.33 (± 0.07)	0.14 (± 0.01)	0.12 (± 0.04)
biceps brachii	0.48 (± 0.15)	0.18 (± 0.01)	0.13 (± 0.07)
triceps brachii	0.13 (± 0.04)	0.10 (± 0.04)	0.11 (± 0.02)

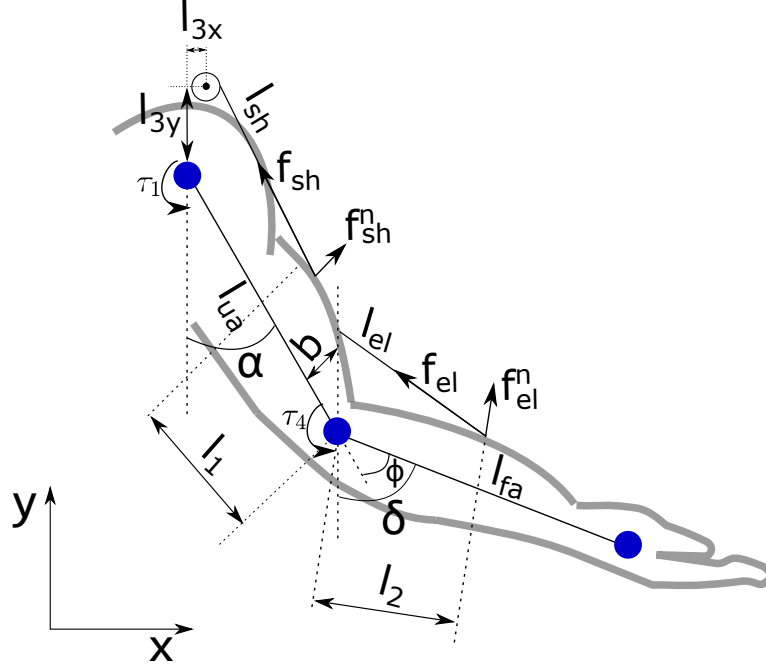


Figure 3.2: Kinematic model with two DoF, shoulder and elbow movement in the sagittal plane, of the human arm.

$$f_{sh} = \frac{f_{sh}^n}{\sin(\phi_{sh})} \quad (3.1)$$

where ϕ_{sh} is the angle between the shoulder force f_{sh} and its tangential force f_{sh}^t and it is:

$$\phi_{sh} = \tan^{-1} \frac{l_{ua} \cos(\alpha) + l_{3x}}{l_{ua} \sin(\alpha) - l_{3y}} + \alpha - \frac{\pi}{2} \quad (3.2)$$

The normal shoulder force f_{sh}^n is:

$$f_{sh}^n = \frac{\tau_1}{l_{ua} - l_1} \quad (3.3)$$

where τ_1 is the shoulder flexion–extension torque reported in Tab. 3.1. The definition of l_{ua} and l_1 are reported in Tab. 3.3.

The lengths of the shoulder actuator l_{sh} is:

$$l_{sh} = \sqrt{l_{shx}^2 + l_{shy}^2} \quad (3.4)$$

where:

$$l_{shx} = l_{3y} - (l_{ua} - l_1) \sin(\alpha) - b \cos(\alpha) \quad (3.5)$$

Table 3.3: Anthropometric data and measures for the involved subjects in the experiments, as obtained by using the model in [16]

Variable	Description	Length [mm]
l_{ua}	length of upper arm	366
l_{fa}	length of forearm	460
l_1	distance from the elbow joint to anchor point of upper arm ($l_1 = 0.27l_{ua}$)	98.82
l_2	distance from the elbow joint to anchor point of forearm ($l_2 = 0.21l_{fa}$)	96.6
l_{3x}, l_{3y}	origin position at the shoulder joint	100
b	distance between anchor point and the center of the upper arm	80

$$l_{shy} = -l_{3x} - (l_{ua} - l_1) \cos(\alpha) + b \sin(\alpha) \quad (3.6)$$

α is shoulder flexion–extension reported in Tab. 3.1; the definition of l_{3y} , l_{ua} , l_1 and b are reported in Tab. 3.3.

For elbow joint the same approach is followed. In particular, the required elbow force f_{el} is:

$$f_{el} = \frac{f_{el}^n}{\sin(\phi_{el})} \quad (3.7)$$

where ϕ_{el} is the angle between the elbow force f_{el} and its tangential force f_{el}^t and it is:

$$\phi_{el} = \frac{\pi}{2} - \delta \quad (3.8)$$

The normal elbow force f_{el}^n is:

$$f_{el}^n = \frac{\tau_4}{l_2} \quad (3.9)$$

where τ_4 is the elbow flexion–extension torque reported in Tab. 3.1. The definition of l_2 is reported in Tab. 3.3.

The lengths of the elbow actuator l_{el} is:

$$l_{el} = \sqrt{l_1^2 + l_2^2 - 2l_1l_2 \cos(\delta)} \quad (3.10)$$

δ is elbow flexion–extension reported in Tab. 3.1; the definition of l_1 and l_2 are reported in Tab. 3.3.

An example of the evolution of the joint angles, torques, required lengths and forces are shown in Fig. 3.3. The results for the most critical conditions are reported in the following: (i) for the shoulder, the maximum length occurs when the shoulder flexion–extension angle is equal to 0 degree ($l_{sh,max}(\alpha = 0) = 350$ mm),

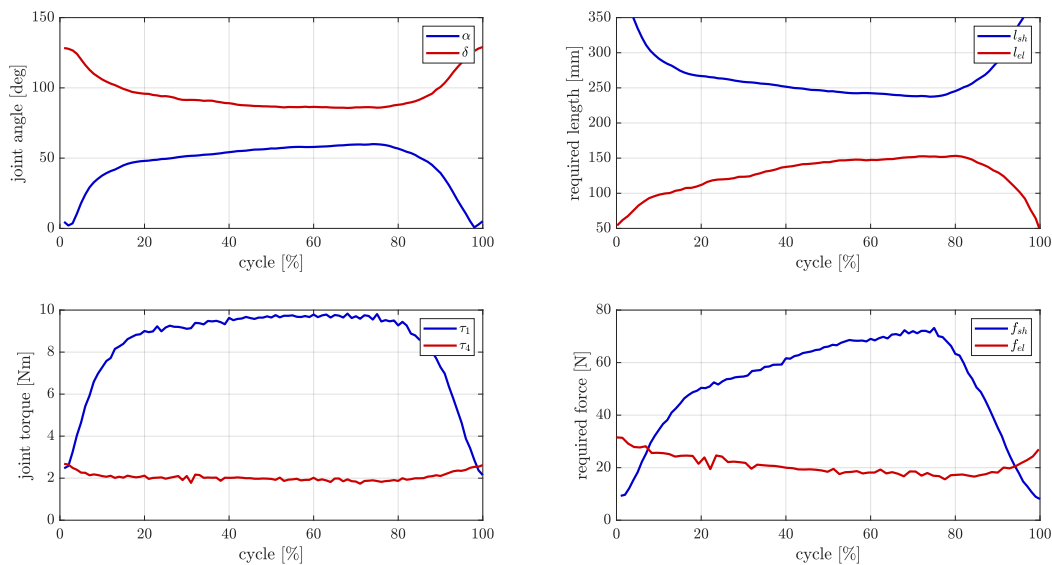


Figure 3.3: Evolution of the joint angles, torques, required lengths and forces for drilling overhead tasks. α and τ_1 : shoulder flexion–extension angle and torque; δ and τ_2 : elbow flexion–extension angle and torque; l_{sh} and l_{el} : shoulder and elbow required lengths; f_{sh} and f_{el} : shoulder and elbow required forces.

the minimum length occurs when the shoulder flexion–extension angle is equal to the maximum range of motion reported in Tab. 3.1 ($l_{sh,min}(\alpha = 120.4) = 185.8$ mm), the maximum force occurs when the shoulder flexion–extension torque is equal to the maximum joint torque reported in Tab. 3.1 ($f_{sh,max}(\tau_1 = 9.5) = 75.0$ N); (ii) following the same approach for the elbow, we obtain $l_{el,max}(\delta = 0) = 197.21$ mm, $l_{el,min}(\delta = 89.1) = 152.6$ mm, $f_{el,max}(\tau_2 = 2.0) = 20.05$ N. Two ideal soft actuators (one for the shoulder and one for the elbow) should ensure the lengths and forces illustrated above to fully support the shoulder and elbow joints while performing industrial overhead tasks.

Anthropometry In order to realize a custom solution tailored for each worker, the exoskeleton suit should be designed on the external morphology of the worker. Furthermore, the parameters in Tab. 3.3 should be derived from real measurements taken on the worker’s body, in particular for the anchor points for the actuators, whose position is decisive for the overall comfort of the worker and for obtaining the maximum force transmission between actuators and human joints. To develop custom and tailor made solutions, suitable 3D body scanners able to reconstruct the 3D body model and to extrapolate selective anthropometric characteristics should be used, as the INBODY – Instant Body Scan™ [41] from BeyondShape. An example of a custom and tailor made design of soft exoskeleton, developed on the real 3D body anatomy, is reported in Fig. 3.1.

In the following, indications from the literature are used to define the mass, materials and contact pressure of the soft wearable robot.

Mass and materials The current rigid exoskeletons used in industry define the mass limit, which is equal to 3.5 kg [23]. Soft systems are expected to weigh less, for instance pneumatic actuators are very light and the weight of the worn system can be estimated equal to 214 g [18]. The materials must be skin contact and stiff in order to guarantee the transfer of the forces due to the contraction of the actuator entirely to the arm. To do that, the exosuit composed by neoprene material, with thickness ≥ 1 mm (up to a maximum of 1.5 mm), can be an appropriate solution. Moreover, the anchor point can be reinforced using flexible plate as proposed in [90].

Contact pressure The limit of the contact pressure, defined as the pressure between the actuator and skin, is defined in such a way that it will not affect blood circulation. The literature sets the threshold value of the contact pressure to be equal to 10 kPa [91].

Chapter 4

Concept design of the two soft wearable robots

In the present chapter, the proposed soft suit of wearable robots is illustrated in Sec. 4.1 and the two concepts of the soft wearable robots are presented. In particular, the concepts use different actuation method: (i) soft exoskeletons using tendon-driven system, see Sec. 4.2; (ii) soft exoskeletons using pneumatic actuators, see Sec. 4.3. The proposed concept of the soft suit and tendon-driven soft wearable robot are an Italian patent pending technology [28].

In particular, the tendon-drive exoskeleton implements a single electric motor (under-actuated system) to support the shoulder and elbow flexion. Usually, in tendon-driven exoskeleton, the actuation source is worn by the user and for this reason the weight of the system is very important. In the present concept an under-actuation system is proposed in order to reduce the weight worn by the user during the execution of the tasks. The pneumatic exoskeleton, instead, uses McKibben artificial muscles (or pneumatic artificial muscles, PAM) to generate the forces to support the shoulder and elbow flexion movements.

4.1 Soft suit

The soft suit allows to correctly place the anchor points of the actuators and / or transmission systems.

The main components of the suit are reported in Fig. 4.1; they are: shoulder brace (t1), two arm braces (t2) and (t3); wrist brace (t4), bands (n) and elastic band (n2). The material of the braces (t1, t2, t3 and t4) is Neoprene, since it allows to adapt to the shapes of the human body and, at the same time, allows an adequate stiffness to transfer the forces from the robotic system (exoskeleton) to the anatomical joints.

The soft suit worn by the user is shown in Fig. 4.2. The proposed soft suit can be worn by the user alone without the help of another person and can be worn in less than 2 minutes.



Figure 4.1: Main components of soft suit: shoulder brace (t1), two arm braces (t2) and (t3); wrist brace (t4), bands (n) and elastic band (n2)

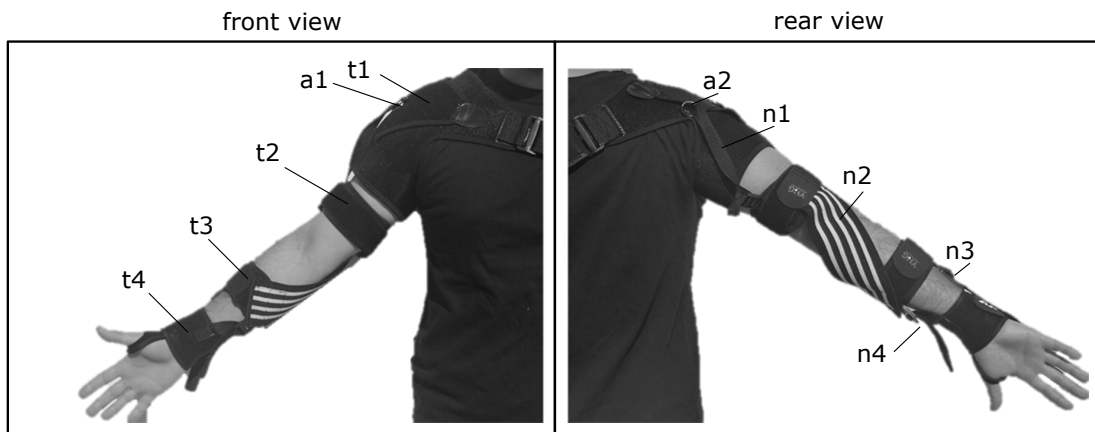


Figure 4.2: Soft suit of the soft wearable robot worn by the user. Shoulder brace (t1), two arm braces (t2) and (t3); wrist brace (t4), bands (n) and elastic band (n2)

In particular, the shoulder brace (t1) is positioned on the shoulder with closure around the chest; the band of the shoulder brace has a Velcro closure, this solution allows to adapt the brace for the different types of subjects with different anthropometric characteristics. The two arm braces (t2 and t3) are positioned one on the biceps (t2) and one on the forearm (t3), respectively. They also have a Velcro closure, for the same reasons mentioned above. Finally, the wrist brace (t4) is positioned on the wrist, its conformation allows to wrap the thumb both on the palm of the hand and on the upper part.

The anchor points of the cables or actuators are positioned on the shoulder brace (t1) and on the arm braces (t2 and t3). During the operation of the exoskeleton the cables or the actuators tend to slide the anchor points and consequently the arm braces (t2 and t3) both upwards and downwards. To avoid these problems Nylon bands are used (n1, n2, n3 and n4, see Fig. 4.2). In particular, two bands (n3 and n4) are sewn between forearm brace (t3) and wrist brace (t4), these bands prevent the forearm brace (t3) from sliding upwards. A plastic buckle is inserted for each band (n3 and n4), in this way the bands can be adjusted according to the anthropometric characteristics of the subject.

The same Nylon band (n1) is sewn between shoulder brace (t1) and biceps brace (t2). In this case, the direct connection, as proposed previously, was not possible to implement it since, during the flexion of the shoulder, the stitching point on the shoulder brace (t1) and the stitching point on the biceps brace (t2) approach and the Nylon bands do not remain in tension. To avoid this problem, the Nylon band (n1) follows the behaviour of the anatomical shoulder joint. In particular, the Nylon band (n1) has a first stitch on the biceps brace (t2 - front view), then the band (n1) passes inside two rings (a1 and a2) positioned on the shoulder brace (t1) and ends closing with a plastic buckle on the sewn onto the biceps brace (t2 - rear view). The proposed solution allows to follow the flexion and extension movement of the shoulder and the Nylon band (n1) is always under tension.

Finally, an elastic band (n2) is sewn between biceps brace (t2) and forearm brace (t3). Also in this case, the direct connection, as proposed for forearm brace (t2) and wrist brace (t3) is not possible for the same reason illustrated above. To avoid this problem, an elastic band (n2) is used which is sewn on the biceps brace (t2) and by wrapping the anatomical joint of the elbow it is fixed to the forearm brace (t3) using a Velcro solution. In particular, the Velcro allows to adapt this solution to the different anthropometric characteristics of the subjects.

4.2 Concept 1: Tendon-driven wearable robot

The concept of the tendon-driven wearable robot is designed as an exoskeleton which allows to assist the upper-limb movement during the execution of manufacturing tasks, i.e. overhead industrial tasks. Moreover, the exoskeleton is defined under-actuated since it allows to assist two degrees of freedom, i.e. shoulder and elbow flexion, using a single electric motor.

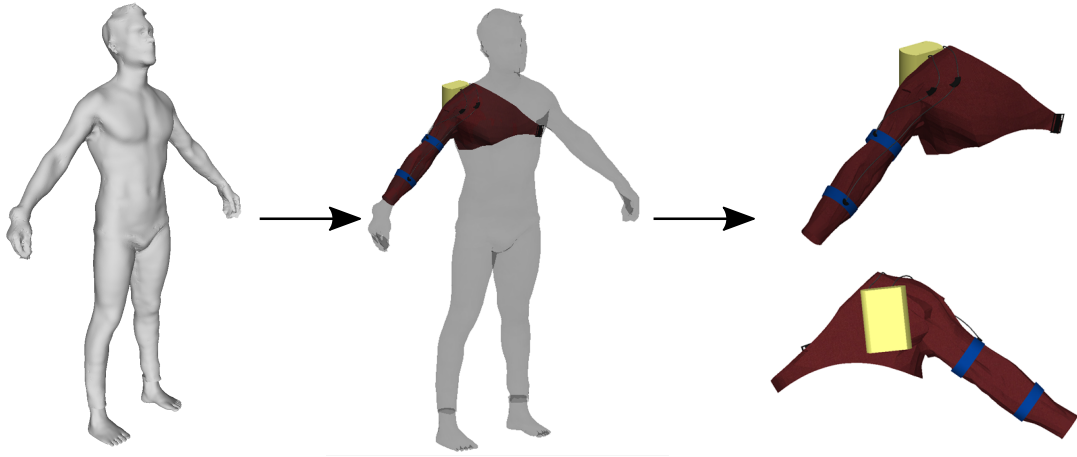


Figure 4.3: CAD model of tendon-driven exoskeleton under-actuated for assisting shoulder and elbow flexion.

A CAD (computer aided design) example of the concept is reported in Fig. 4.3. In particular, the figure reports a full body model of the human shape acquired and reconstructed using INBODY – Instant Body Scan™ [41] from BeyondShape; the human model was used to design the tendon-driven exoskeleton on the human shape through surface modelling using Solidworks software ¹.

Section 4.2.1 illustrates the transmission system of the exoskeleton, i.e. positions of the anchor points and cable paths; Sec. 4.2.2 describes the under-actuation system; Sec 4.2.3 presents the theoretical operating principle of the cable-driven exoskeleton.

4.2.1 Transmission system

The transmission system of the forces is made up of cables (or tendons), i.e. Bowden cables. In particular, two Bowden cables are used to transmit the forces from exoskeleton to user; one cable to assist the shoulder flexion and one cable to assist the elbow flexion. Moreover, the cable paths are defined following the concept introduced in [13] and defined as *tension line*. The concept of *tension line* is linked to bio-design techniques, techniques where the design of the systems, i.e. wearable robots (or exoskeletons), is inspired by nature. The *tension lines* are lines which link the starting and ending point of the joints affected by the muscle. In this way, the cables (or tendons) work in parallel with the human muscles in order to assist and reduce the muscle activations of the user during the execution of industrial tasks. For the industrial overhead tasks, the exoskeleton should assist the shoulder and elbow flexion and the most activated muscles for these movements are anterior deltoid and biceps brachii, as obtained in Sec. 3.2. To do that, the cables follow the *tension lines* of the anterior deltoid to support

¹<https://www.solidworks.com/>

the shoulder flexion and biceps brachii to support the elbow flexion. Finally, the cables are fixed on the human body using anchor points; two anchor points for the cable which assists the shoulder movement (shoulder cable) and two anchor points for the cable which assists the elbow movement (elbow cable). In particular, the anchor points for shoulder cable are positioned on the chest and biceps; the anchor points for elbow cable, instead, are positioned on the chest and forearm as illustrated in Fig. 4.3.

4.2.2 Actuation system

The actuation system and gears is illustrated in Fig. 4.4, the figure does not include the case of the actuation system to facilitate the view of all the components. The actuation system is composed by the following components: absolute encoder (a); electric motor (b); planetary reducer (c); a transmission shaft defined as principal transmission shaft (d) in which two principal gear wheels are positioned, defined respectively: principal gear wheel for assisting the shoulder flexion (f) and principal gear wheel for assisting elbow flexion (e).

Moreover, the principal gear wheel (f) is connected in parallel to another gear wheel defined secondary for assisting the shoulder flexion (i). The secondary gear wheel (i) is keyed onto a secondary transmission shaft (l), defined as secondary transmission shaft for shoulder assistance, in which there is a coil (m) which allows the cable (or tendon) to be wound during the movement of shoulder flexion. The principal gear wheel (f) and secondary gear wheel (i) for shoulder assistance have a transmission ration < 1 , this allows to multiply the torque generated by the electric motor (b) and supply the required torques to the shoulder, more details are illustrated in Sec. 5.1.1. This transmission ration is necessary since the shoulder flexion (τ_1) requires more torque than elbow flexion (τ_4), see Sec. 3.1.

In the same way, the principal gear wheel (e) is connected in parallel to another gear wheel defined secondary for assisting the elbow flexion (n). The secondary gear wheel (n) is keyed onto a secondary transmission shaft (o), defined as secondary transmission shaft for elbow assistance, in which there is a coil (p) which allows the cable (or tendon) to be wound during the movement of elbow flexion. The principal gear wheel (e) and secondary gear wheel (n) for elbow assistance have a 1:1 transmission ration, this allows to ideally transfer the entire torque generated by the electric motor (b).

The two principal gear wheels (f) and (e) have three different operating configurations: (1) simultaneous rotation of the gear wheels for shoulder and elbow assistance; (2) rotation of the single gear wheel for shoulder assistance; (3) rotation of the single gear wheel for elbow assistance. The transition from one operating configuration to another is guaranteed by the use of a mechanical pin (g) free to slide on a shaft slot; the mechanical pin (g) has a length equal to the distance between the two main gear wheels (e) and (f) plus their thickness. In particular, the pin can have three different positions defined in Fig. 4.4 as:

- position 0: the mechanical pin (g) is located in the center of both principal

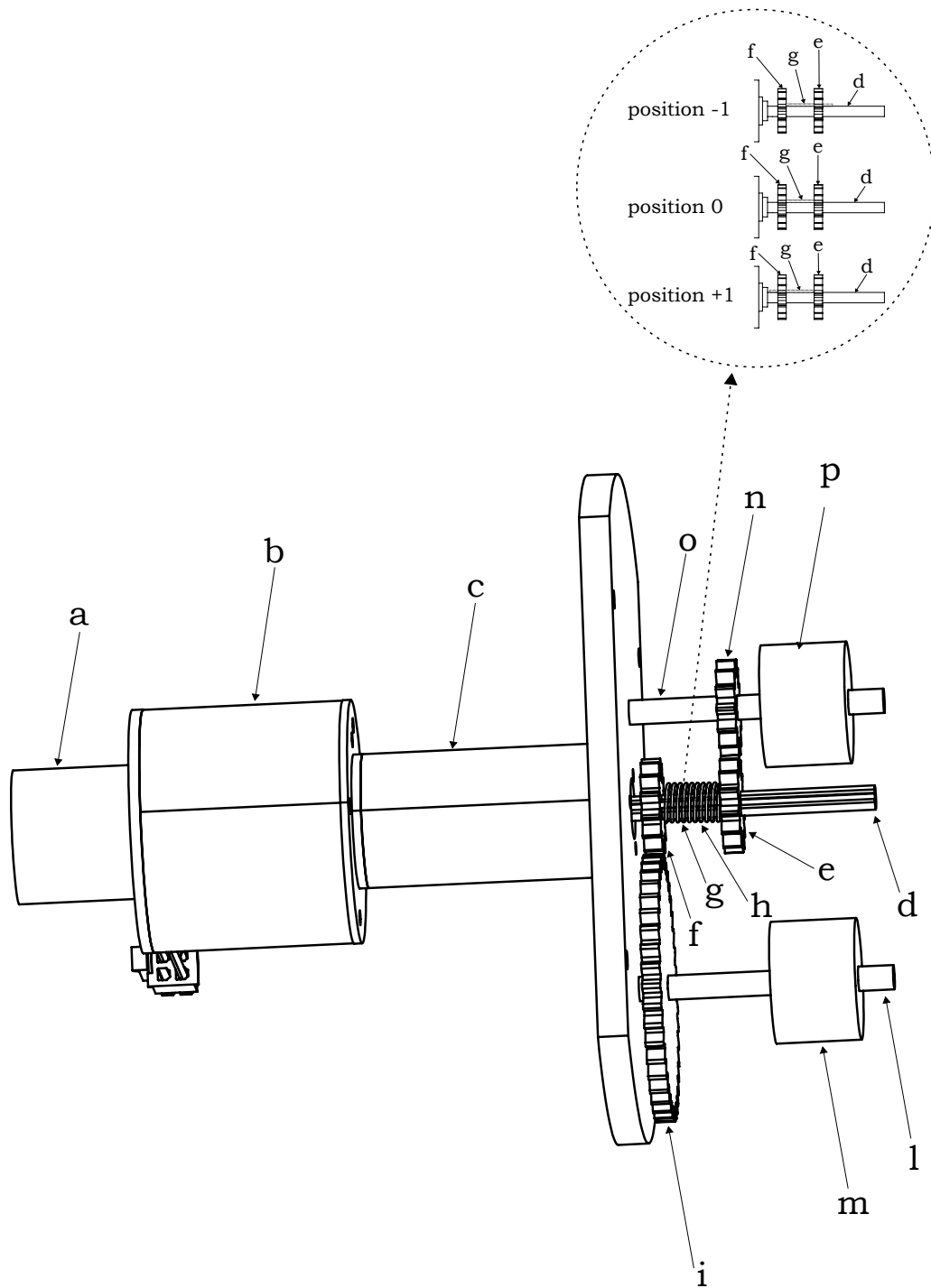


Figure 4.4: Actuation system of the tendon-driven exoskeleton. The main components of the wearable robot are: absolute encoder (a); electric motor (b); planetary reducer (c); principal transmission shaft (d); two principal gear wheels (f) and (e), solenoid (h); mechanical pin (g); two secondary transmission shafts (o) and (l), two secondary gear wheels (i) and (n); two coils (m) and (p).

gear wheels (e) and (f), in this way both gear wheels (e) and (f) mesh with the rotation of the principal transmission shaft (d) and transfer the motion to the two secondary gear wheels to assist the shoulder (i) and elbow (n). In the configuration defined as position 0, the exoskeleton is able to support both shoulder and elbow flexion.

- position +1: the mechanical pin (g) is displaced beyond the principal gear wheel (f), in this case only the gear (f) is capable of meshing with the rotation of the principal transmission shaft (d) and therefore the rotation motion of the principal transmission shaft (d) is transferred only to the secondary gear wheel for shoulder assistance (i). In the configuration defined as position +1, the exoskeleton is able to support only the shoulder flexion.
- position -1: the mechanical pin (g) is displaced beyond the principal gear wheel (e), in this case only the gear (e) is capable of meshing with the rotation of the principal transmission shaft (d) and therefore the rotation motion of the principal transmission shaft (d) is transferred only to the secondary gear wheel for elbow assistance (n). In the configuration defined as position -1, the exoskeleton is able to support only the elbow flexion.

The system described above needs to automatically move the mechanical pin (g); to do that an electromagnetic solution was chosen using a solenoid (h). The electromagnetic solution allows to generate a magnetic field, with a certain module, by passing current through the solenoid. In this case, the magnetic field allows to translate the mechanical pin (g), ferromagnetic component, beyond the principal gear wheel (f) or beyond the principal gear wheel (e). In the first case, the system is in the configuration defined as position +1; in the second case, instead, the system is in the configuration defined as position -1. More in detail, a power source allows the current to circulate inside the solenoid generating the translation of the mechanical pin (g) in one direction; the polarity inverter, instead, allows to invert the polarity of the system by making the mechanical pin (g) translate in the opposite direction compared to the previous one.

4.2.3 Working principle

The exoskeleton illustrated in Fig. 4.3 is composed by: (i) soft suit which allows to position the anchor points and actuation systems, it is described in detailed in Sec. 4.1; (ii) transmission system composed by two Bowden cables and four anchor points; two anchor points for shoulder cable placed in parallel to *tension line* of anterior deltoid and two anchor points for elbow cable placed in parallel to *tension line* of biceps brachii, see Sec. 4.2.1; (iii) actuation system placed on the upper part of the back of the subject which also includes a battery and a controller, Sec. 4.2.2; (iv) finally, the exoskeleton includes three inertial measurement units (IMU), they are not reported in Fig. 4.3, which allow to monitor the human activities, i.e. human joint angles. In particular, one IMU is placed on the chest

of the subject, one IMU is placed on the biceps and one IMU is placed on the forearm.

The actuation and gear system allows to provide assistance to the shoulder and the elbow in a combined and/or separate way. In particular, three different assistance modes are illustrated:

- assistance for simultaneous shoulder and elbow flexion: when the IMU sensors register an increasing flexion angle of the shoulder and elbow, the electric motor (b) generates a torque proportional to the torque required for the elbow flexion (τ_4). Then the torque of the electric motor (b) is tripled on the secondary transmission shaft (l) for shoulder assistance through the gear ratio between the gear wheels (f) and (i) of 3:1, while the torque on the secondary transmission shaft (o) for elbow assistance is proportional to torque generated by the electric motor (b) since the gear ratio between the gear wheels (e) and (n) is 1:1. In this case, the mechanical pin (g) is between the gear wheels (f) and (e), see position 0 in Fig 4.4 and, no current flows inside the solenoid (h).
- assistance for shoulder flexion: when the IMU sensors register an increasing flexion angle of the shoulder, the electric motor (b) generate a torque equal to about 1/3 of the torque required for shoulder flexion (τ_1). The torque delivered is then tripled on the secondary shaft to assist the shoulder (l) through the gear ratio between the gear wheels (f) and (i) of 3:1. At the same time, the controller sends current to the solenoid (h) allowing to generate an electromagnetic force capable of translating the mechanical pin (g) beyond the primary gear wheel (f) (defined as position +1, see Fig 4.4). In this way, the rotation of the principal transmission shaft (d) is transferred to the secondary transmission shaft (l) for assisting the shoulder flexion.
- assistance for elbow flexion: when the IMU sensors register an increasing flexion angle of the elbow, the electric motor (b) generate a torque proportional to the torque required for elbow flexion (τ_4). The torque delivered is transferred on the secondary shaft to assist the elbow (o) through the gear ratio between the gear wheels (e) and (n) of 1:1. At the same time, the controller sends current to the solenoid (h) that using the polarity inverter allowing to generate an electromagnetic force capable of translating the mechanical pin (g) beyond the primary gear wheel (e) (defined as position -1, see Fig 4.4). In this way, the rotation of the principal transmission shaft (d) is transferred to the secondary transmission shaft (o) for assisting the shoulder flexion.

4.3 Concept 2: Pneumatic wearable robot

The concept of the pneumatic wearable robot is designed as an exoskeleton which allows to assist the upper-limb movement during the execution of manufacturing

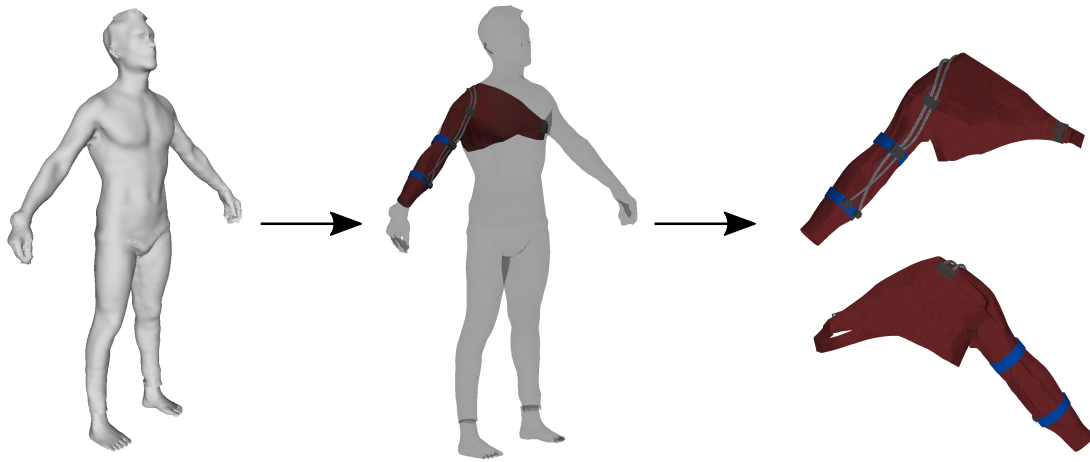


Figure 4.5: CAD model of pneumatic exoskeleton for assisting shoulder and elbow flexion.

tasks, i.e. overhead industrial tasks. The exoskeletons implements pneumatic artificial muscles to support the shoulder and elbow flexion. The PAM are usually use since their behaviour is similar to behaviour of human muscle.

A CAD (computer aided design) example of the concept is reported in Fig. 4.5. In particular, the figure reports a full body model of the human shape acquired and reconstructed using INBODY – Instant Body Scan™ [41] from BeyondShape; the human model was used to design the pneumatic exoskeleton on the human shape through surface modelling using Solidworks software ².

Section 4.3.1 illustrates the transmission and actuators implemented, i.e. positions of the anchor points and PAM; Sec. 4.3.2 describes the control board unit; Sec 4.3.3 presents the theoretical operating principle of the pneumatic exoskeleton.

4.3.1 Transmission system and actuators

The forces are generated using McKibben artificial muscles (or pneumatic artificial muscles, PAM). The muscles consist of an inflatable inner tube/bladder inside a braided mesh, clamped at the ends. When the inner bladder is pressurized and expands, the geometry of the mesh acts like a scissor linkage and translates this radial expansion into linear contraction and their behaviour is similar to human muscles. The PAM could work in parallel with the human muscles in order to support the most activated muscles during the execution of manufacturing tasks. For the industrial overhead tasks, the most activated muscles are anterior deltoid and biceps brachii, as obtained in Sec. 3.2, in order to reduce the shoulder and elbow flexion torques. In the present concept, two PAM are implemented to support the shoulder flexion and two PAM are used to support the elbow flexion, see

²<https://www.solidworks.com/>

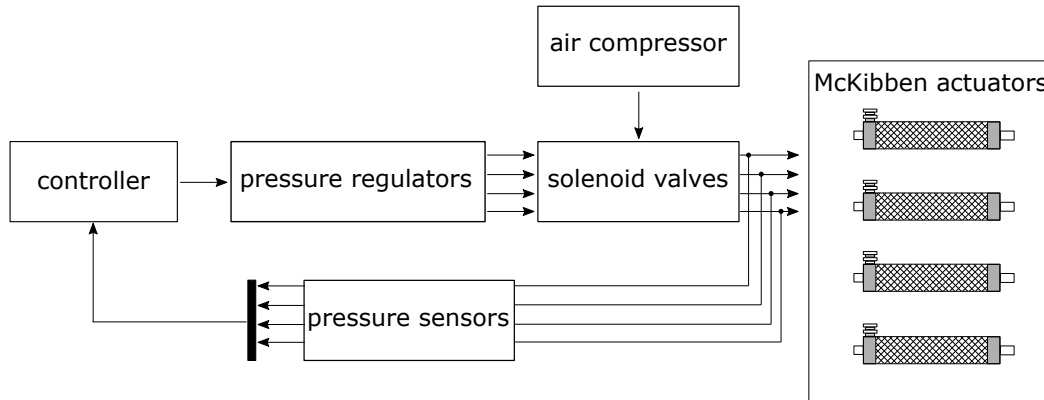


Figure 4.6: Architecture of pneumatic control board.

Fig. 4.5. The path of the actuators for shoulder assist is similar to the concept introduced for tendon-driven wearable robot and defined *tension lines* and, in the same way the anchor points are on the upper back and on upper arm. The path of the actuators for elbow assist, instead, is not follow the concept of *tension lines* since it was preferred to optimize the contraction ratio of the actuators by creating a solution in which the two actuators are in an x-shaped configuration. In this case, the anchor points of the actuators are on the upper arm and forearm.

4.3.2 Control board system

The control board system allows to actuate and control the pneumatic wearable robot, the proposed architecture is illustrated in Fig. 4.6. The architecture includes one pressure regulator, solenoid valve and pressure sensor for each McKibben muscles; the pneumatic wearable robot includes four artificial muscles, two for shoulder assist and two for elbow assist as indicated in Sec. 4.3.1. Overall the control board is composed by: (i) one controller; (ii) four pressure regulators, (iii) four solenoid valves; (iv) four pressure sensor; (v) air compressor. The pressure regulator allows to control the pressure of the fluid and allows to send the fluid at the desired pressure to the solenoid valves, it is an electromechanically operated valve; finally, the pressure sensor allows to estimate the flow loss in the circuit.

4.3.3 Working principle

The pneumatic wearable robot illustrated in Fig. 4.5 is composed by: (i) soft suit illustrated in Sec. 4.1; (ii) four McKibben artificial muscles as actuators in order to assist the shoulder and elbow flexion during the execution of industrial overhead tasks, see Sec. 4.3.1; (iii) fluid control board which allows to actuate and control the four McKibben actuators, see Sec.4.3.2; (iv) finally, the exoskeleton includes three inertial measurement units (IMU), they are not reported in 4.5, which allow to monitor the human activities, i.e. human joint angles. In particular, one

IMU is placed on the chest of the subject, one IMU is placed on the biceps and one IMU is placed on the forearm.

The pneumatic control board and PAM allow to provide assistance to the shoulder and the elbow movements. In particular, three different assistance modes are illustrated:

- assistance for simultaneous shoulder and elbow flexion: when the IMU sensors register an increasing flexion angle of the shoulder and elbow, the control board generates: (i) a pressure proportional to the torque required for the shoulder flexion (τ_1) for the two McKibben muscles which support shoulder assist; (ii) a pressure proportional to the torque required for the elbow flexion (τ_4) for the two McKibben muscles which support elbow assist.
- assistance for shoulder flexion: when the IMU sensors register an increasing flexion angle of the shoulder, the control board: (i) generates a pressure proportional to the torque required for the shoulder flexion (τ_1) for the two McKibben muscles which support shoulder assist; (ii) closes the solenoid valves which provide fluid to the McKibben actuators for elbow assist.
- assistance for elbow flexion: when the IMU sensors register an increasing flexion angle of elbow, the control board: (i) closes the solenoid valves which provide fluid to the McKibben actuators for shoulder assist; (ii) generates a pressure proportional to the torque required for the elbow flexion (τ_4) for the two McKibben muscles which support elbow assist.

4.4 Contributions of the proposed soft wearable robots

This section presents a brief summary and discussion of the most important contributions of the proposed concepts.

Soft suit The soft suit, presented in Sec. 4.1, allows to place the anchor points of the transmission and actuation systems in order to correctly transfer the forces from robot (or exoskeleton) to user. In particular, the innovativeness of the suit is to ensure the correct positioning of the anchor points during the operation of the exoskeleton, using braces connected with bands which follow the course of the anatomical joint of the shoulder and elbow braces, without the use of rigid components [28], i.e. rigid braces or rigid links, as proposed in previous works [6, 16].

Tendon-driven wearable robot The tendon-driven wearable robot, presented in Sec. 4.2, is an under-actuated system since allows to support two degrees of freedom, i.e. should and elbow flexion, using a single electric motor. The implementation of under-actuated system allows to reduce the weight

of the exoskeleton worn by the user and also allows to support the two DOF, i.e. shoulder and elbow flexion, independently or combined [28]. The implementation in an independent or combined way of DOF represents the innovativeness of the system since the current soft exoskeletons under-actuated presented in the literature actuate several DOF but not independently of each other [16].

Pneumatic wearable robot The pneumatic wearable robot, presented in Sec. 4.3, uses four McKibben artificial muscles, two artificial muscles to support the shoulder flexion and two artificial muscles to support the elbow flexion, to assist the worker during the execution of industrial overhead tasks. The pneumatic exoskeleton, differently from the tendon-driven exoskeleton, uses an actuation source, i.e. compressed air, already available in factory environments and for this reason the actuation source and the control system may not be worn by the user. This allows to reduce the overall weight worn by the worker.

Chapter 5

Technological insights in concept development

In this chapter dimensional and geometric characteristics of soft wearable robots, presented in Ch. 4, are defined. In particular, the characteristics of the electric motor and gear systems of tendon-driven wearable robot are presented in Sec. 5.1; the geometric characteristics of the McKibben artificial muscles of pneumatic wearable robot, instead, are defined in Sec. 5.2.

5.1 Tendon-driven wearable robot

The aim of present section is to define the characteristics of the motor, i.e. electric motor, and of the gear system in order to support the shoulder and elbow flexion, see Sec. 5.1.1. Finally, the electronic components of the actuation system are reported in Sec. 5.1.2.

5.1.1 Modeling of transmission and actuation systems

The tendon-driven wearable robot, presented in Sec. 4.2.2, is defined as under-actuated system since it uses a single electric motor to support two DoF, i.e. shoulder and elbow flexion. In particular, the actuation source is composed by a gear system which allows to transfer the correct torques to the two secondary transmission shafts to support the shoulder flexion and elbow flexion. The secondary transmission shaft for elbow movement, indicated with (o) in Fig. 4.4, transmits the torque generated by the electric motor since the gear wheels, denoted with (e) and (n) in Fig. 4.4, have the same transmission ratio. The secondary transmission shaft for shoulder movements, defined as (l) in Fig. 4.4, multiply the torque generated by the electric motor since the gear wheels, denoted with (f) and (i) in Fig. 4.4, have a transmission ratio less than 1.

The present section illustrates the procedure to calculate the torque and power required by the electric motor and the procedure to calculate the transmission ratio between gear wheels. To do that, the section is divided in: (i) definition of

the torque and power of the electric motor based on force required by the elbow cable; (ii) definition of the transmission ration between gear wheels, defined as (f) and (i) in Fig. 4.4, to multiply the torque generated by the motor in order to support the shoulder movements.

The first step, as indicated above, is to define the required power by the electric motor in order to support the elbow flexion torque. To do that, the tendon-driven transmission model presented in [20] is used to model the friction phenomena. The model imposes two assumptions:

- the model assumes that the greatest losses due to the friction effect occur between the inner cable and the outer sheet;
- the model also assumes that friction losses can be modeled as the sliding of a cable on a fixed cylinder.

After these assumptions, the force transmission efficiency can be written as:

$$\frac{f_{ideal}}{f_{real}} = e^{-\mu_f \phi_{act}} \quad (5.1)$$

where:

- μ_f : friction coefficient between the cable and outer sheet, the static friction coefficient of the teflon–steel is equal to 0.4 ($\mu_f = 0.4$) as indicated in [20];
- ϕ_{act} : total wrap angle of the outer sheath of the Bowden cable, the actuator is carried out in a backpack and the total wrap angle is equal to π ($\phi_{act} = \pi$);
- f_{ideal} : cable force before transmission;
- f_{real} : cable force after transmission.

For the elbow joint the Eq. 5.1 becomes:

$$\frac{f_{el}}{f_{el,real}} = e^{-\mu_f \phi_{act}} \quad (5.2)$$

where the f_{el} is the ideal force required by the elbow cable defined and calculated in Sec. 3.2. Finally, combining the Eq. 3.7 and Eq. 5.2 the force of the elbow cable after the transmission $f_{el,real}$ can be written as following:

$$f_{el,real} = \frac{\tau_4}{l_2 \sin(\frac{\pi}{2} - \delta)} / e^{-\mu_f \phi_{act}} \quad (5.3)$$

Finally, the torque required by the electric motor τ_{em} can be calculated using the principle of conversion of energy:

$$\tau_{em} = \frac{\partial h_{el}^T}{\partial \delta}(\delta) f_{el,real} \quad (5.4)$$

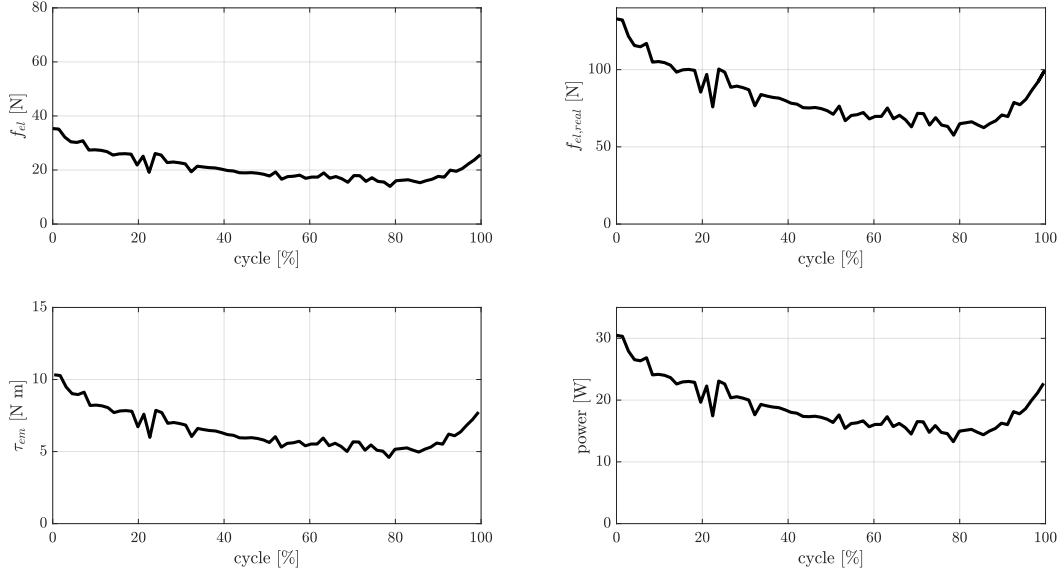


Figure 5.2: Forces, torque and power required by the electric motor to support the elbow flexion. f_{el} : cable force before transmission; $f_{el,real}$ cable force after transmission; τ_{em} torque required by the electric motor; $power$ the power required by the electric motor.

electric motor to assist the elbow flexion τ_{em} evaluated using the Eq. 5.6; the motor power of the electric motor.

The second step, as indicated above, is to define the transmission ration of the gear wheels to multiply the torque generated by the electric motor in order to support the shoulder flexion. The gear system is a multiplier system since the shoulder flexion torque τ_1 is bigger than the elbow flexion torque τ_4 .

The transmission ration can be defined as following:

$$\frac{\omega_2}{\omega_1} = \frac{r_1}{r_2} \quad (5.7)$$

where:

- ω_1 : angular velocity of the driving wheel indicated with (f) in Fig. 4.4;
- ω_2 : angular velocity of the driven wheel indicated with (i) in Fig. 4.4;
- r_1 : radius of the pitch circumference of the driving wheel indicated with (f) in Fig. 4.4;
- r_2 : radius of the pitch circumference of the driven wheel indicated with (i) in Fig. 4.4.

The torque of the driving wheel M_1 is:

$$M_1 = F_t r_1 \quad (5.8)$$

the torque of the driven wheel M_2 , instead, is:

$$M_2 = F_t r_2 \quad (5.9)$$

where the F_t is the tangential force exchanged between the two gear wheels. In the same way, the Eq. 5.8 and Eq. 5.9 can be written:

$$\frac{r_2}{r_1} = \frac{M_2}{M_1} \quad (5.10)$$

Setting the maximum values of the shoulder and elbow torques defined in Sec. 3.2 ($M_1 = \tau_{4,max} = 2 \text{ Nm}$, $M_2 = \tau_{1,max} = 9.5 \text{ Nm}$), it is possible to calculate the transmission ratio between the gear wheels using Eq. 5.7 and, it is equal to 0.21 ($r_1/r_2 = 0.21$).

5.1.2 Choice of the components

The tendon-driven actuation system is reported in Fig. 4.3. In particular, it includes: absolute encoder (a); electric motor (b); planetary reducer (c); principal transmission shaft (d); two principal gear wheels (f) and (e), solenoid (h); mechanical pin (g); two secondary transmission shafts (o) and (l), two secondary gear wheels (i) and (n); two coils (m) and (p). The electric motor (b) could be a brushless electric motor which guarantees the torques and powers defined in Sec. 5.1.1, i.e. Maxon, EC-i 40, 50 W ¹. The absolute encoder (a) could be an incremental encoder, i.e. Scancon, 2RMHF, 5000, pulses/rev ². The gear wheels, instead, could be chosen using the standard tables so as to guarantee the transmission ratio defined in Sec. 5.1.1. Finally, the FlexSEA ³ could be the controller to use to control the wearable robot.

5.2 Pneumatic wearable robot

In this section, the McKibben muscle model is proposed to define the geometric characteristics of the actuators. In particular, McKibben artificial muscle model is presented in Sec. 5.2.1 and then, it is used to define the diameter, thickness of latex tube of soft actuators and the operating pressure of the actuators in order to exert the desired forces defined in Sec. 3.2. Moreover, electronic and pneumatic components of pneumatic control board are illustrated in Sec. 5.2.3.

5.2.1 Modeling of McKibben artificial muscle

The invention of McKibben artificial muscles is generally attributed to Richard H Gaylord (1958) then Joseph L McKibben (1960) introduced their use in orthotic

¹<https://www.maxongroup.com/>

²<https://www.scancon.dk/>

³<https://flexsea.media.mit.edu///>

applications [21]. The modeling of the McKibben muscle is proposed for the first time in [92], then different approaches have been presented in order to obtain simulation results as close to reality as possible [21]. In this section, a static model of McKibben artificial muscle, reported in [21], is followed to define the geometric and working characteristics of McKibben artificial muscles, i.e. diameter and thickness of latex tube and pressure.

Static model of McKibben artificial muscle

The geometric and working characteristics of the McKibben artificial muscle are evaluated using the model presented in [21]. To do that, the model applies: (i) a simple virtual work analysis of an ideal cylindrical muscle; (ii) studies the actuator as an ideal cylinder (ideal McKibben muscle); (iii) finally, studies the actuator as a rubber inner tube (real McKibben muscle).

Ideal cylindrical muscle As a first approximation, the McKibben artificial muscle is defined as a cylinder. The ideal cylinder, when pressurized, reduces its length l and increases its radius according to a predefined positive function $f(\epsilon_{PAM})$, such as:

$$\frac{r}{r_0} = f(\epsilon_{PAM}) \quad (5.11)$$

$$\epsilon_{PAM} = \frac{l_0 - l}{l_0} \quad (5.12)$$

where:

- r_0 and r = initial and final muscle radius;
- ϵ_{PAM} = contraction ratio of artificial muscle;
- l_0 and l = initial and final muscle length.

The muscle contraction force $F(\epsilon_{PAM})$ can be calculated applying a simple virtual work analysis. In particular, assuming that the cylindrical artificial muscle is fixed at one side and that its free side is put in equilibrium by the positive force F as reported in Fig. 5.3, the virtual work theorem can be written as:

$$2\pi r l P \delta r + \pi r^2 P \delta l + F \delta l = 0 \quad (5.13)$$

and

$$\delta r = -\left(\frac{r_0}{l_0}\right) \dot{f}(\epsilon_{PAM}) \delta l \quad (5.14)$$

From the Eq. 5.11 and 5.12, $F(\epsilon)$ is equal to:

$$F(\epsilon_{PAM}) = (\pi r_0^2) P [2(1 - \epsilon_{PAM}) f(\epsilon_{PAM}) \dot{f}(\epsilon_{PAM}) - f^2(\epsilon_{PAM})] \quad (5.15)$$

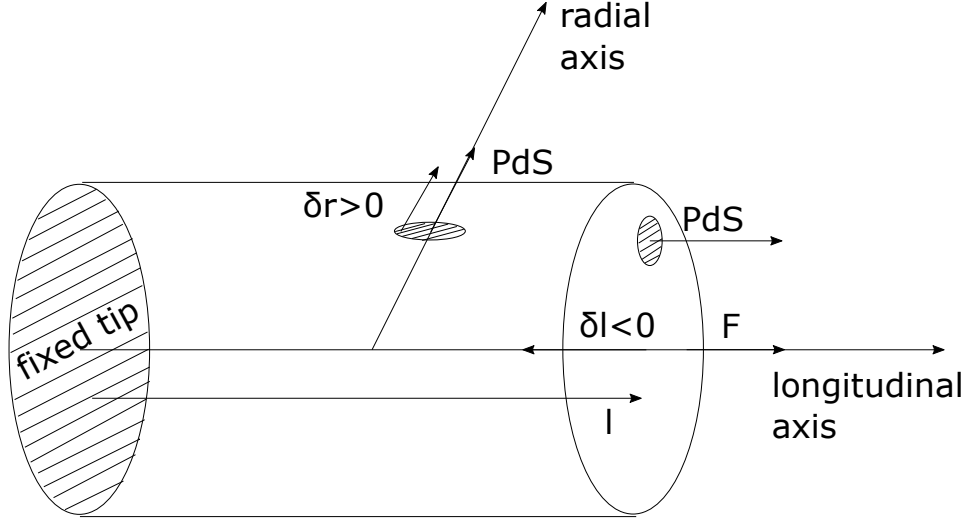


Figure 5.3: Virtual work theorem applied to ideal cylindrical artificial muscle [21].

$F(\epsilon_{PAM})$ can be also write as:

$$F(\epsilon_{PAM}) = \frac{1}{l_0} \frac{dV}{d\epsilon_{PAM}} P \quad (5.16)$$

or

$$F(l) = -\frac{dV}{dl} P \quad (5.17)$$

where $V = \pi r^2 l = \pi r_0^2 l_0 [(1 - \epsilon_{PAM}) f^2]$ is the muscle volume.

Ideal McKibben muscle The assumptions underlying ideal McKibben muscle are:

- the model considers a planar network of jointed identical pantographs, see Fig. 5.4. It is composed by m columns and n rows. The envelope created is a rectangle; its initial length is l_0 , its initial width is L_0 and, the angle of each pantograph is defined as $\alpha_{PAM,0}$. When pressurized the angle α_{PAM} increases ($\alpha_{PAM,0} < \alpha_{PAM}$), the width L increases ($L_0 < L$) and the length decreases ($l_0 > l$).
- The model assumes that the cylinder has an initial radius r_0 , that is $L_0 = 2\pi r_0$; and the current radius r , that is $L = 2\pi r$.
- Finally, the model assumes that the side of each pantograph remains constant.

From the hypotheses introduced, the following equations can be written:

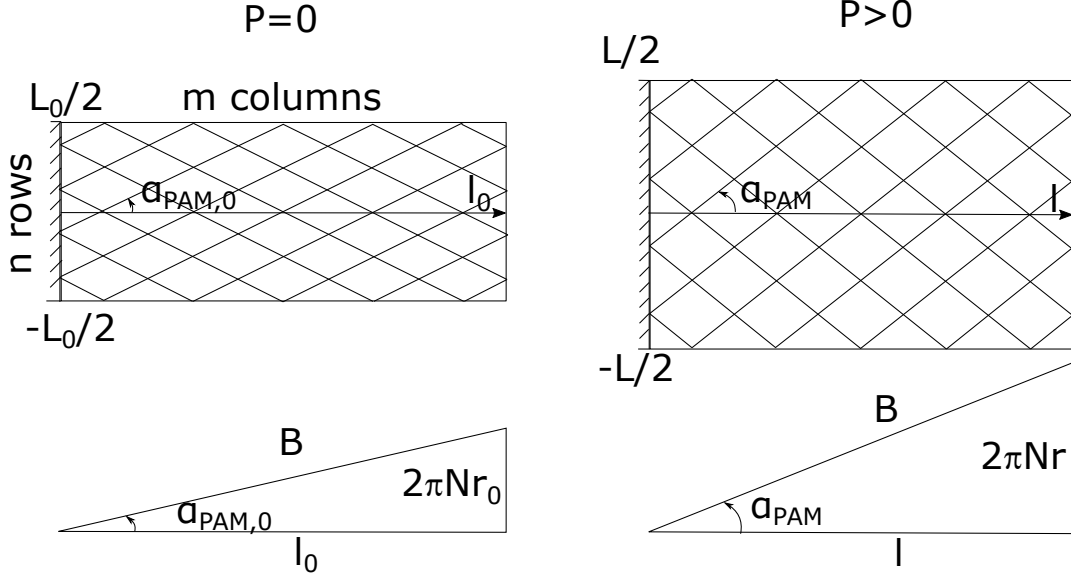


Figure 5.4: Geometrical characterization of the planar jointed identical pantographs of McKibben muscle [21].

$$\frac{r}{r_0} = \frac{\sin(\alpha_{PAM})}{\sin(\alpha_{PAM,0})} \quad (5.18)$$

and

$$\frac{l}{l_0} = \frac{\cos(\alpha_{PAM})}{\cos(\alpha_{PAM,0})} \quad (5.19)$$

From the Eq. 5.11, 5.18 and 5.19 the $f(\epsilon_{PAM})$ can be written as:

$$f(\epsilon_{PAM}) = \frac{1}{\sin(\alpha_{PAM,0})} \sqrt{1 - \cos^2(\alpha_{PAM,0})(1 - \epsilon_{PAM})^2} \quad (5.20)$$

Finally, the ideal force of McKibben muscle $F_{ic}(\epsilon_{PAM})$ can be obtained by combining the Eq. 5.15 and Eq. 5.20:

$$F_{ic}(\epsilon_{PAM}) = (\pi r_0^2) P [a(1 - \epsilon_{PAM})^2 - b], \quad 0 \leq \epsilon_{PAM} \leq \epsilon_{PAM,max} \quad (5.21)$$

with $a = 3/\tan^2(\alpha_{PAM,0})$ and $b = 1/\sin^2(\alpha_{PAM,0})$.

Figure 5.5 reports the relationship between ratio force and contraction ratio of the ideal McKibben muscle. In particular, the figure illustrates this relationship for two ideal McKibben muscle, the first uses an angle $\alpha_{PAM,0}$ equal to 20 deg ($\alpha_{PAM,0} = 20 \text{ deg}$); the second, instead, uses an angle $\alpha_{PAM,0}$ equal to 30 deg ($\alpha_{PAM,0} = 30 \text{ deg}$). The figure denotes that increasing the angle $\alpha_{PAM,0}$ the ratio force decreases.

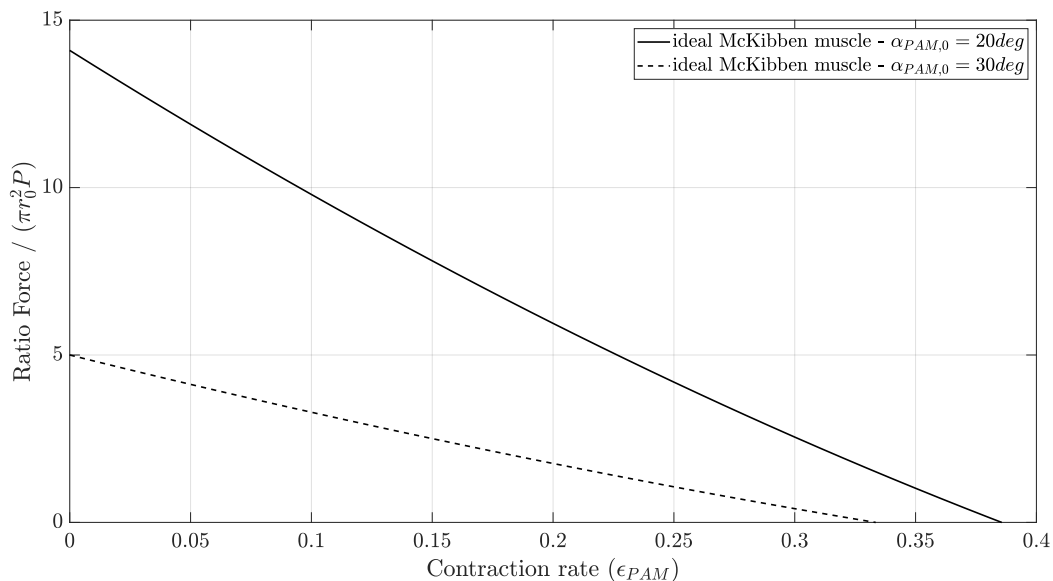


Figure 5.5: Plot of the static force of the ideal McKibben muscle.

Real McKibben muscle The model presented before does not study and explain how the braided sheath make the transmission of pressurized force possible. To do that, the model considers a rubber inner tube with: r_{i0} and r_0 : internal and external initial radius; r_i and r : internal and external radius of the current state; t_0 and t_i : initial and current tube thicknesses.

The hypothesis of the real McKibben model are:

- the model assumes that the pressure is sufficient in order to transfer of pressure forces to the braided sheath. A schematic situation is reported in Fig. 5.6; the figure reports that the rubber inner tube is surrounded by a network of identical pantographs in the form of a matrix $n \times m$, as reported in Fig. 5.4.
- the model assumes that full pantograph network remains in contact with the exterior surface of the rubber tube in each contraction state of the muscle.

From the aforementioned hypotheses, the following equations can be written:

$$l = 2ms \cos(\alpha_{PAM}) \quad (5.22)$$

and

$$2\pi r = 2ns \sin(\alpha_{PAM}) \quad (5.23)$$

The Eq. 5.22 and Eq. 5.23 report that for any angle α_{PAM} , each pantograph maintains its side of value constant s .

Moreover, applying the virtual-work theorem:

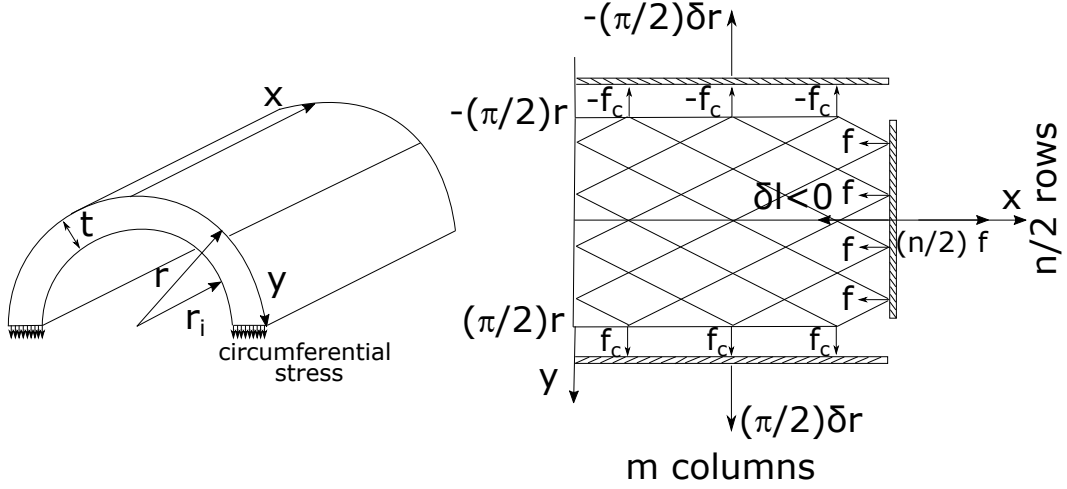


Figure 5.6: Analysis of the forces in the real McKibben artificial muscle [21].

$$2mf_c\left(\frac{\pi}{2}\right)\delta r + \frac{n}{2}f\delta l = 0 \quad (5.24)$$

$$f = \frac{\cos(\alpha_{PAM})}{\sin(\alpha_{PAM})}f_c \quad (5.25)$$

Where:

- f is the positive contraction force in the x (longitudinal) direction, it is produced by each row of the network;
- f_c is the positive force in the y (circumferential) direction, it is produced by each column of the network.

The total circumferential force is equal to $r_i l P$; the elementary force f_c , instead, is: $f_c = r_i l P / m$. By using the Eq. 5.22 and Eq. 5.22, the force generated by the braid sheath f_{cb} is:

$$f_{cb} = 2nf = 2\pi r_i r \frac{\cos^2(\alpha_{PAM})}{\sin^2(\alpha_{PAM})} P \quad (5.26)$$

Taking in to account the pressure force and free extremity of McKibben artificial muscle, an expression of the force generated by the real cylindrical McKibben muscle is obtained:

$$f_{rc} = \left(2\pi r_i r \frac{\cos^2(\alpha_{PAM})}{\sin^2(\alpha_{PAM})} - \pi r_i^2\right) P \quad (5.27)$$

The Eq. 5.27 simulates the behaviour of the real artificial muscle, however it does not take into account any possible friction or elastic effects.

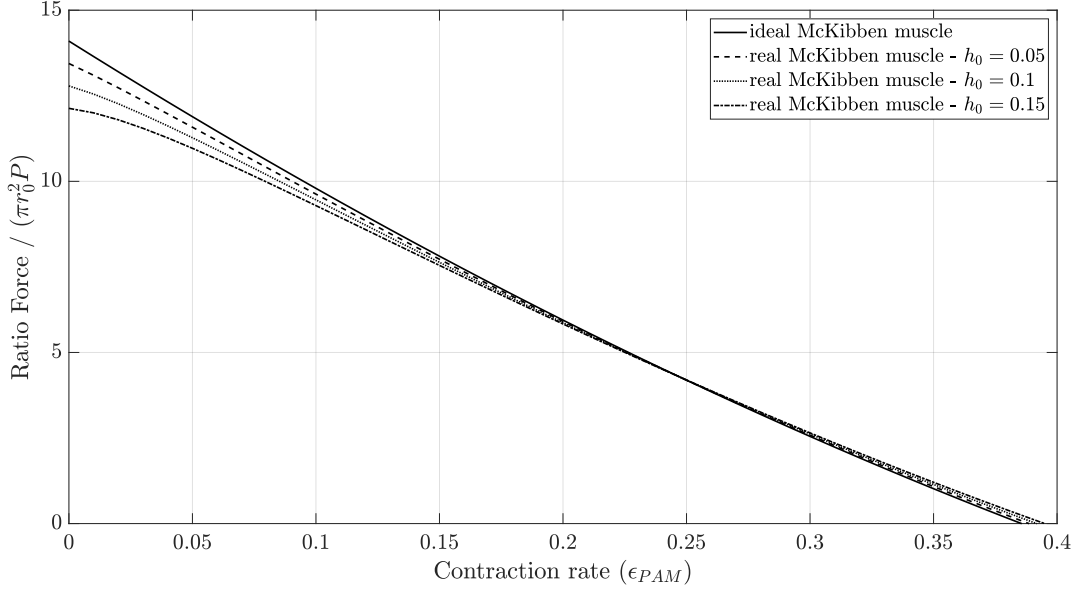


Figure 5.7: Plot of the static force of the real McKibben muscle.

Finally, for a specific case denoted as thin-walled rubber inner tube; the assumption of incompressibility is: $(r_i/r_{i0})(l/l_0)(t/t_0) = 1$. Disregarding t^2 with respect to r^2 , the force generated by the real McKibben muscle is:

$$F_{rc} = F_{ic} - (\pi r_0^2 P) \times \left[2h_0 \frac{(2 \cos^2(\alpha_{PAM,0})(1 - \epsilon_{PAM})^2 - 1)}{(1 - \epsilon_{PAM})(1 - \cos^2(\alpha_{PAM,0})(1 - \epsilon_{PAM})^2)} \right] \quad (5.28)$$

where $h_0 = t_0/r_0$. Figure 5.7 reports the ration force of the McKibben muscle with respect to contraction rate ϵ_{PAM} using the ideal and real McKibben muscle model. In particular, different values of the h_0 are studied, i.e. $h_0 = 0.05; h_0 = 0.10; h_0 = 0.15$. The figure shows that the explicable force decreases with increasing h_0 .

5.2.2 Definition of McKibben requirements

The pneumatic wearable robot has four McKibben artificial muscles to support the shoulder and elbow flexion. In this section, the geometric and operating characteristics of the artificial muscles are defined.

The McKibben actuators, as defined in Sec. 5.2.1, are characterized by: (i) initial angle of the pantograph $\alpha_{PAM,0}$; (ii) initial internal and external diameter of the latex tube d_{i0} and d_0 ; (iii) pressure at which the air is blown into the actuators (operating pressure) P . In particular:

- the angle $\alpha_{PAM,0}$ influences the contraction rate ϵ_{PAM} of the artificial McKibben muscle; as the alpha angle increases the contraction rate decreases ϵ_{PAM} , see Fig. 5.5.

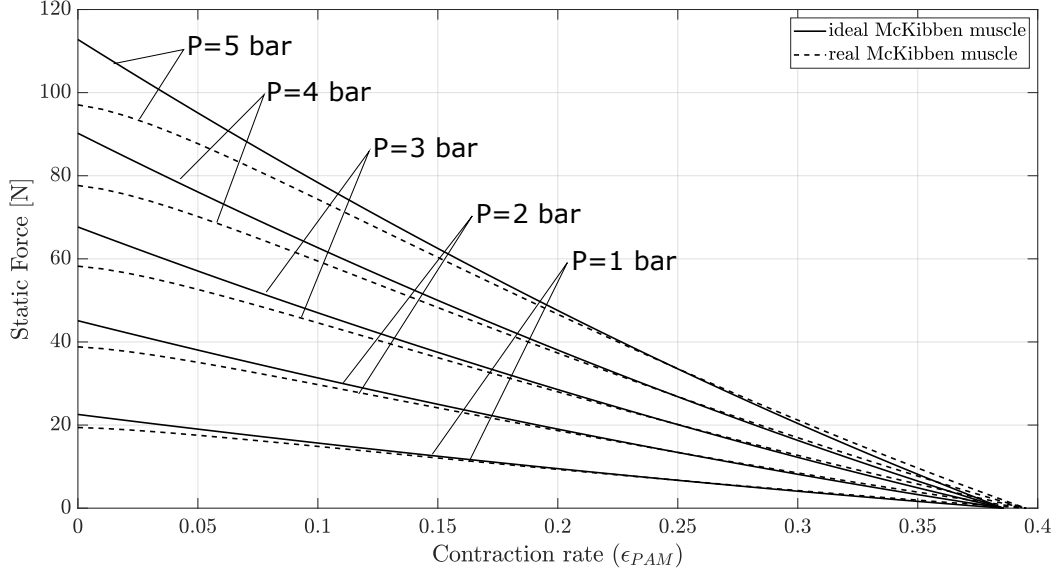


Figure 5.8: Plot of static force of ideal and real McKibben artificial muscle. The imposed values are: $\alpha_{PAM} = 20$ deg and $h_0 = 0.15$.

- The initial diameters d_{i0} , d_0 and the operating pressure of the McKibben artificial muscle influence the force that can be exerted by the actuators. Figure 5.7 shows that as h_0 ($h_0 = \frac{r_0 - r_{i0}}{r_0}$) increases, the maximum force F_{rc} tends to decrease. Moreover, the Fig. 5.8 reports that as the operating pressure increases P the McKibben muscle force that can be exerted by the actuator F_{rc} increases.

The Sec. 3.2 reports the maximum forces required to support the shoulder and elbow movements: (i) the maximum force to support shoulder flexion is equal to 75 N ($f_{sh,max} = 75.0$ N); (ii) the maximum force to support the elbow flexion is equal to 20.05 N ($f_{el,max} = 20.05$ N). The Fig. 5.8 shows that the required forces can be generated by McKibben artificial muscles having an angle α_{PAM} equal to 20 deg, an internal initial radius of rubber inner tube r_{i0} equal to 6 mm and a thickness t_0 equal to 0.9 mm. In particular, a single McKibben artificial muscle, with the geometric characteristics defined previously and the operating pressure P equal to 4 bar, generates a force f_{rc} equal to 77 N. Moreover, a single McKibben artificial muscle, with the geometric characteristics defined previously and an operating pressure P equal to 1 bar, generates a force f_{rc} equal to 20 N.

Finally, the components to fabricate a McKibben artificial muscle are reported in Tab. 5.1.

5.2.3 Pneumatic control board

The pneumatic control board that could be used to control the wearable robot is presented in [93]. In particular, the main electronic and pneumatic components

Table 5.1: Main components of fabric-based artificial muscle.

Component	Quantity
expandable polyester sleeving	1
soft latex rubber tubing	1
tight-seal plastic barbed tube fittings for air	1
easy-view plastic barbed tube fittings for Air	1
pinch clamps for tube	2

Table 5.2: Components of control board system

Component	Quantity
Electronic components	
Arduino Mega as controller	1
switch module with 4 Mosfet channels	1
power supply	1
potentiometer	1
jumpers	-
voltage regulator	1
Pneumatic components	
air compressor	1
solenoid valves	4
polyurethane tubes	5
manifold series SY100	4
pressure sensors	4

of the control board are reported in Tab. 5.2. The potentiometer is connected to the Arduino board via Analog port and to a 5 V power supply that is supplied by the microcontroller itself. The same power supply is supplied to the Mosfet which however requires a connection to Arduino via a Digital port. This last component acts as a bridge between the voltage generator (24 V) and the valve itself. Voltage generator and air compressor are both connected to a voltage of 220 V. The compressor generates a pressure of no more than 5 bar for the correct functioning of the actuator and this pressure, through connections with the polyurethane pipes, is detected by a pressure sensor. The latter is connected to Arduino via an Analog port and powered with a voltage of 5 V directly from Arduino. The main action performed by the board is to activate and deactivate the MOSFET based on the voltage value that is detected at the input by the potentiometer. A schematic architecture of the pneumatic control board is reported in Fig. 5.9.

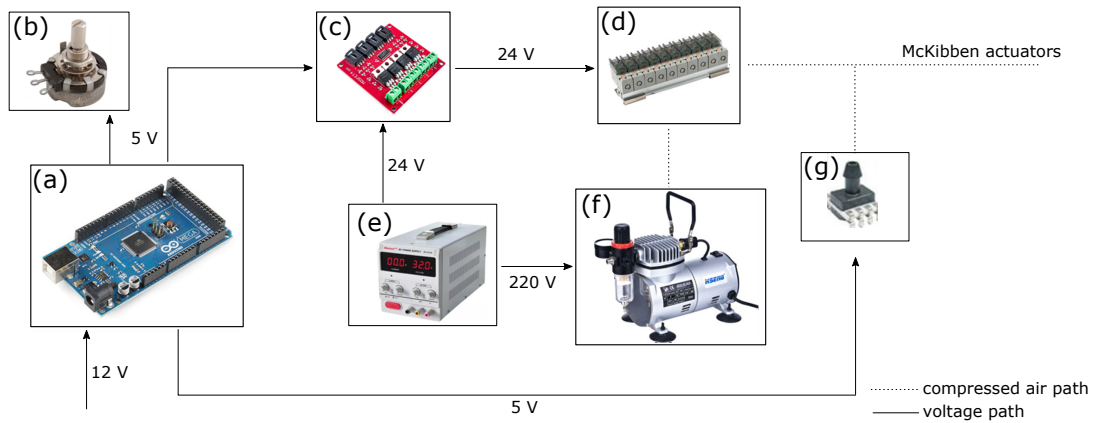


Figure 5.9: Pneumatic control board. (a) Arduino Mega; (b) potentiometer; (c) switch module with 4 Mosfet channels; (d) solenoid valves; (e) power supply; (f) air compressor.

Chapter 6

Comparison of the two concepts based on group decision making

The comparison of the two proposed concepts, i.e. tendon-driven and pneumatic wearable robots, are carried out using a multi-criteria decision making (MCDM) method, see Sec. 6.1. The results of the MCDM method using ELIGERE web platform are presented in Sec. 6.2; finally, the Sec. 6.3 illustrates the discussion.

6.1 Multi-criteria decision making

The optimal alternative selection from a set of alternatives according to the preferences provided by a group of experts is a problem defined group decision making (GDM). In case different criteria are taken into consideration, the problem is defined multi-criteria decision making (MCDM) [94]. The MCDM method allows to identify the most important factors to make the decision and allows to perform a comparison of the design or concept alternatives.

Over the last decade, different methods have been presented in the literature; an exhaustive list is illustrated in [95]. The review reports that the most approached used are: (i) the analytic hierarchy process (AHP), a panel of experts are used to estimate the relative magnitudes of factors through a pairwise comparisons; each of the respondents compares the relative importance each pair of items using a custom questionnaire; (ii) the technique for order of preference by similarity to ideal solution (TOPSIS), it is a method of compensatory aggregation that compares a set of alternatives by identifying weights for each criterion, normalising scores for each criterion and calculating the geometric distance between each alternative and the ideal alternative, which is the best score in each criterion. Finally, when the fuzzy theory is introduced to uniquely identify linguistic variables, the literature refers to the fuzzy MCDM (FMCDM), fuzzy AHP (FAHP) and fuzzy TOPSIS (FTOPSIS).

ELIGERE platform ELIGERE is a fuzzy AHP web platform for group decision making [96]. More details about the ELIGERE framework are reported in

App. C.

Definition of the concept alternatives The alternatives are the two concepts presented in Ch. 4: (i) tendon-driven wearable robot; (ii) pneumatic wearable robot. The description of the alternatives, or concepts, provided to the workers and researchers before to carry out the questionnaires are reported in App. C.

Definition of the criteria An initial brainstorming is carried out to define the target groups of the questionnaire and the related criteria. In particular, the target groups of the questionnaire are three and they are: (i) workers since they are the user of the soft exoskeleton in manufacturing environment; (ii) managers of the companies since they are the potential customers of the device; (iii) researchers since they are the designer and developers of the soft exoskeletons. In particular, the results of the questionnaire for workers and managers allow to define the operational requirements from a user and customers point of view; the results of the questionnaire for researchers, instead, allow to compare the concepts from a technical point of view. Then, for each target group, a list of possible criteria is defined to compare the two proposed concepts.

The three worker's criteria selected are:

- weight (W): weight of the soft wearable robot worn by the use;
- invasiveness (I): invasiveness of the device in terms of freedom of movement of the worker;
- operating space (OS): freedom of movement of the worker throughout the factory space.

The three manager's criteria selected are:

- innovativeness (IN): how innovative the proposed concept is compared to the state of the art and compared to the solutions already available on the market;
- safety (S): ability to not harm the worker and / or surrounding objects during the execution of the task. Ability, also, to support the worker during the execution of the industrial task in order to reduce the risks associated with musculoskeletal disorders deriving from biomechanical overloads;
- robustness (R): ability to continue to work even in the event of system failure.

The three researcher's criteria selected are:

- response speed (RS): ability of the soft wearable robot to quickly adapt to different task configurations;

- full-assisted (FA): ability of soft wearable robot to exert the full torques required by the anatomical joints;
- maintainability (M): ability of the transmission systems and actuators to be maintained quickly and easily.

The criteria chosen for the workers are highly subjective criteria and can only be evaluated from the user's point of view. In particular, the operating space of the exoskeleton represents a very important criterion since it will allow to understand whether to orient the choice exclusively towards one specific concept, i.e. tendon - driven wearable robot, or understand that both concepts, i.e. tendon-driven and pneumatic wearable robots, could be implemented in real factory environments. The criteria chosen for the researchers, instead, are technical criteria which allow to define the global characteristics of the wearable robots presented using the opinion of a group of experts who working in this specific scientific sector.

6.2 Results

To carry out the comparison between the proposed concepts the questionnaire was provided to nine workers which work in the mechanical field for at least five years. In particular, the workers involved refer to Italian car mechanic shops which use the car lift bridge on a daily basis. The results of the multiple criteria decision-making, evaluated using ELIGERE platform, are reported in Fig. 6.1. In the same way, to compare the proposed concepts the questionnaire was provided to seven managers that work in Italian manufacturing companies. The results of the ELIGERE questionnaire are reported in Fig. 6.2. Finally, to compare the proposed concepts the questionnaire was provided to nine researcher experts in the field. In particular, two researchers from Istituto Italiano di Tecnologia (IIT), five from University of Naples Federico II (UNINA), one from Chemnitz University of Technology (TUC) and one from Fraunhofer Institutes (IWS). The results of the multiple criteria decision-making, evaluated using ELIGERE platform, are reported in Fig. 6.3. The figures report: (i) the score of the criteria for each target group selected, i.e. worker and researchers; (ii) the ranking of the criteria; (iii) the ranking of alternatives, i.e. tendon-driven wearable robot and pneumatic wearable robot.

In particular the results are in the following summarized:

- The results of the comparison of the criteria, reported on the top-left in the Fig. 6.1, reports that the weight and invasiveness were defined as the most important criteria for the selection of the concept. Moreover, the ranking of alternatives, reported on the top-right of the Fig. 6.1, reports the final ranking of the alternatives; it is equal to 42% for tendon-driven concept and equal to 58% for pneumatic concept.

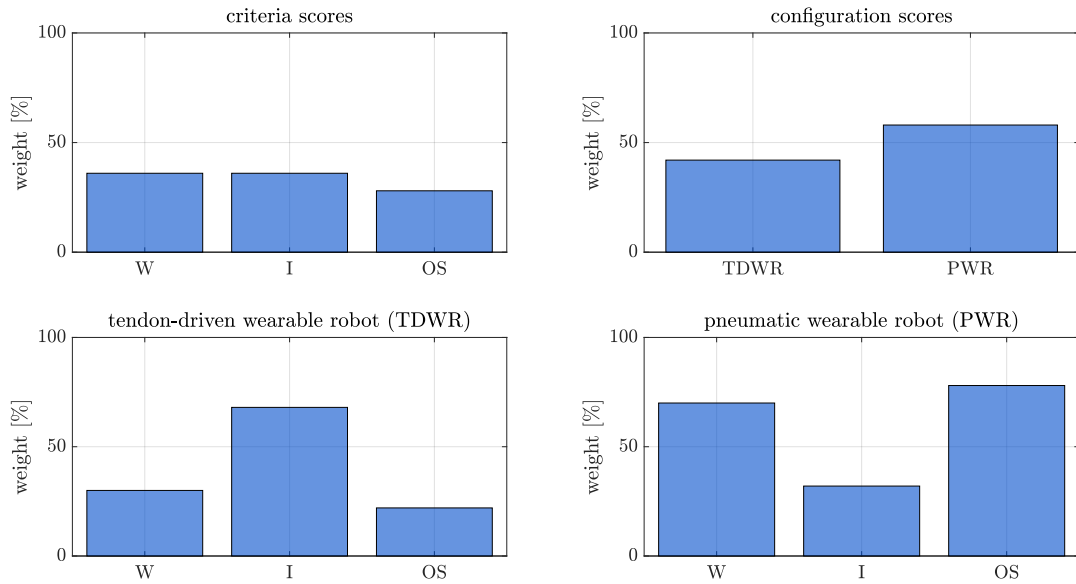


Figure 6.1: Eligere questionnaire results of the workers:(top-left) the score of the criteria; (top-right) the final ranking of the configurations; (bottom-left) the score of the tendon-driven configuration w.r.t criteria separately; (bottom-right) the score of the pneumatic configuration w.r.t. criteria separately. W: weight; I: invasiveness; OS: operating space.

- The results of the comparison of the criteria, reported on the top-left in the Fig. 6.2, reports that the innovativeness and safety were defined as the most important criteria for the selection of the concept. Moreover, the ranking of alternatives, reported on the top-right of the Fig. 6.2, reports the final ranking of the alternatives; it is equal to 23% for tendon-driven concept and equal to 77% for pneumatic concept.
- The results of the comparison of the criteria, reported on the top-left in the Fig. 6.3, reports that the response speed and full-assisted were defined as the most important criteria for the selection of the concept. Moreover, the ranking of alternatives, reported on the top-right of the Fig. 6.3, reports the final ranking of the alternatives; it is equal to 43% for tendon-driven concept and equal to 57% for pneumatic concept.

6.3 Discussion

The results of the ELIGERE questionnaire aimed at workers show that the operative space criterion is evaluated as not real relevant since the wearable robot is used only during the execution of the task in the workspace areas. In these areas, the soft wearable robots proposed are the same ability and characteristics. Moreover, the results of the ELIGERE questionnaire for the managers and researchers

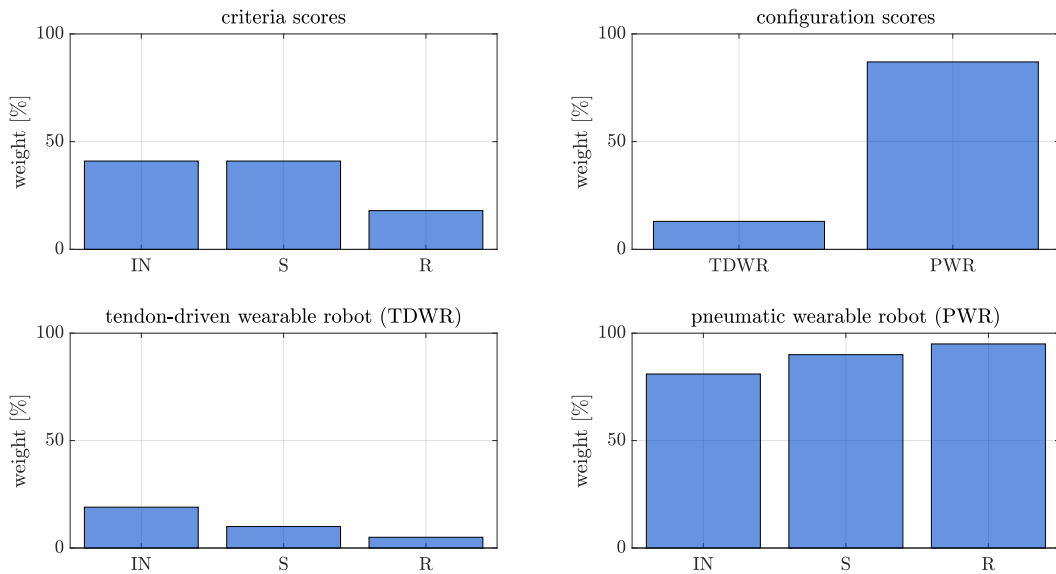


Figure 6.2: Eligere questionnaire results of the managers: (top-left) the score of the criteria; (top-right) the final ranking of the configurations; (bottom-left) the score of the tendon-driven configuration w.r.t criteria separately; (bottom-right) the score of the pneumatic configuration w.r.t. criteria separately. IN: innovativeness; S: safety; R: robustness.

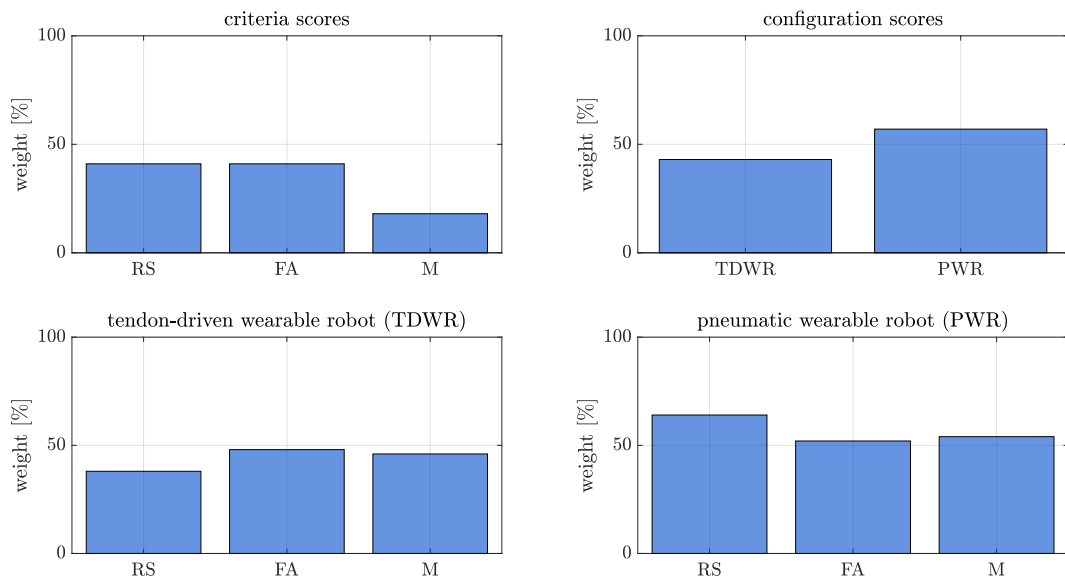


Figure 6.3: Eligere questionnaire results of the researchers: (top-left) the score of the criteria; (top-right) the final ranking of the configurations; (bottom-left) the score of the tendon-driven configuration w.r.t criteria separately; (bottom-right) the score of the pneumatic configuration w.r.t. criteria separately. RS: response speed; FA: full-assisted; M: maintainability.

notice that the maintainability and robustness are less relevant compared to the other criteria.

For the three group of experts selected, the pneumatic wearable robot is the optimal solution to implement in manufacturing environments to support the shoulder and elbow flexion movements during the execution of industrial overhead tasks. However, only for the results of the managers' questionnaire there is a difference between the two concepts, in the other two cases, the scores are not very different. For this reason it could be convenient to develop both devices and choose the best solution based on the comparison of the kinematic and physiological parameters of the worker evaluated with tendon-driven and pneumatic wearable robots during the execution of the industrial tasks.

Conclusion

In this thesis, the design of two different wearable robots, i.e. tendon-driven and pneumatic wearable robots, for industrial overhead tasks was presented. In particular, the design includes the soft suit, transmission system and power unit.

At first, three different overhead tasks, i.e. drilling, leveraging and cabling tasks, were performed at two different working heights at laboratory environment. The results in terms of joint angles, joint torques and muscle activations show that, for a specific working configuration defined as *middle configuration*, there is a concentration of the worker's efforts in the upper-limb joints. These results suggest that the wearable robots should assist the shoulder and elbow flexion during task performance in that specific configuration defined as *middle configuration*.

Then, the results of the biomechanical analysis are used to define the range of motion and the torques required by the human joints. In particular, a two degrees of freedom model of the upper-limb, which include the shoulder and elbow joints, were used to define the functional requirements of the soft exoskeletons, i.e. ideal lengths and forces of actuators or transmission system in order to support the joint torques required during the execution of the industrial tasks.

Subsequently, the concept of soft suit and the soft wearable robots were presented. The main contributions are:

- design of a soft suit that allows to avoid slipping phenomena of the anchor points of the transmission system, i.e. cables or actuators. To do that, Nylon bands are included between the shoulder, elbow and wrist braces; their paths follow the behaviour of the anatomical shoulder and elbow joint [28].
- the design of the two soft wearable robots for industrial overhead tasks: (i) tendon-driven wearable robot, an under-actuated system which allows the shoulder and elbow joint to be supported independently or combined using a single electric motor [28]; (ii) pneumatic wearable robot, system which uses two McKibben artificial muscles to support the shoulder movement and two McKibben artificial muscles to support the elbow movement;

The detailed design phase is carried out using the model of tendon-driven unit and McKibben artificial muscle. These models and the functional requirements based on biomechanical analysis of the overhead tasks were used: (i) to define the characteristics of the electric motor and gears system of tendon-driven system;

Conclusion

(ii) to define the geometric characteristics of the McKibben artificial muscles to exercise the required forces.

Finally, the comparison of the concepts proposed was carried out using multi-criteria decision making submitted to three different group of experts: (i) workers who are the potential future users of the devices; (ii) managers who are the potential customers of the devices; (iii) researchers who are the potential developers of soft wearable robots. For the both group of experts, the pneumatic wearable robot is the preferred solution for industrial applications.

Further work

Future developments could be:

- development of the soft wearable robot based on the results obtained in the present thesis;
- definition and implementation of a control strategy so that the support of the exoskeleton is perceived as natural by the user;
- assessment of the soft wearable robot in laboratory and industrial environments in order to define the physiological and kinematic effects on worker movements.

Appendix A

Modeling

In this appendix the procedures for inverse kinematic and inverse dynamic computation starting from the motion capture and ground reaction forces data, are reviewed.

A.1 Inverse kinematics

The inverse kinematics aims at computing the evolution over time of the joint angles. Here, the problem is to minimize the weighted squared error between the motion capture data and the virtual model [49], as

$$\min_q = \sum_{i=1}^o \omega_i (\mathbf{x}_{i,s} - \mathbf{x}_{i,m})^2 + \sum_{j=1}^n \omega_j (\mathbf{q}_{j,s} - \mathbf{q}_{j,m})^2 \quad (\text{A.1})$$

where:

- ω_i and ω_j : weight coefficients for markers and joint angles, respectively;
- $\mathbf{x}_{i,s}$ and $\mathbf{x}_{i,m}$: three dimensional positional vectors of the i^{th} marker, respectively for the subject and the model ($x \in \mathbb{R}^n$);
- $\mathbf{q}_{j,s}$ and $\mathbf{q}_{j,m}$: three dimensional vectors of generalized coordinates (unknowns) of the j^{th} joint angle, respectively for the subject and the model ($q \in \mathbb{R}^n$);
- n, o : respectively, degrees-of-freedom (DoF) of the model (i.e. number of considered joint angles) and number of markers.

A.2 Inverse dynamics

The inverse dynamics aims at computing the evolution over time of the joint torques, starting from the joint angles and the measured ground reaction forces.

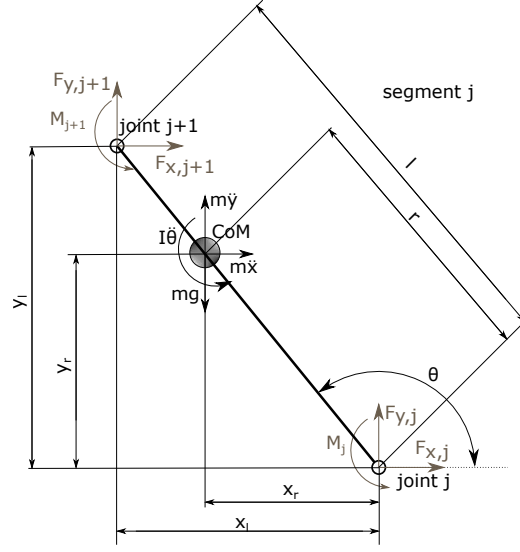


Figure A.1: Schematic model of the generic body segment between two human joints.

By neglecting the viscous and friction effects, the dynamic model takes the classic Lagrangian form:

$$\mathbf{M}(\mathbf{q})\ddot{\mathbf{q}} + \mathbf{c}(\mathbf{q}, \dot{\mathbf{q}}) + \mathbf{g}(\mathbf{q}) = \boldsymbol{\tau} \quad (\text{A.2})$$

where:

- $\mathbf{q}, \dot{\mathbf{q}}, \ddot{\mathbf{q}}$: position, velocity, and acceleration of the generalized coordinates ($\mathbf{q} \in \mathbb{R}^n$);
- \mathbf{M} : mass matrix ($\mathbf{M} \in \mathbb{R}^{n \times n}$);
- \mathbf{c} : vector of Coriolis and centrifugal forces ($\mathbf{c} \in \mathbb{R}^n$);
- \mathbf{g} : vector of gravitational forces ($\mathbf{g} \in \mathbb{R}^n$);
- $\boldsymbol{\tau}$: vector of unknown generalized forces ($\boldsymbol{\tau} \in \mathbb{R}^n$);

The dynamic model (A.2) can be also written in Newton–Euler formulation as:

$$\begin{aligned} \mathbf{x}, \dot{\mathbf{x}}, \ddot{\mathbf{x}} &\rightarrow \sum \mathbf{F}_x = m\ddot{\mathbf{x}} \\ \mathbf{y}, \dot{\mathbf{y}}, \ddot{\mathbf{y}} &\rightarrow \sum \mathbf{F}_y = m\ddot{\mathbf{y}} \\ \boldsymbol{\theta}, \dot{\boldsymbol{\theta}}, \ddot{\boldsymbol{\theta}} &\rightarrow \sum \mathbf{M} = I\ddot{\boldsymbol{\theta}} \end{aligned} \quad (\text{A.3})$$

where:

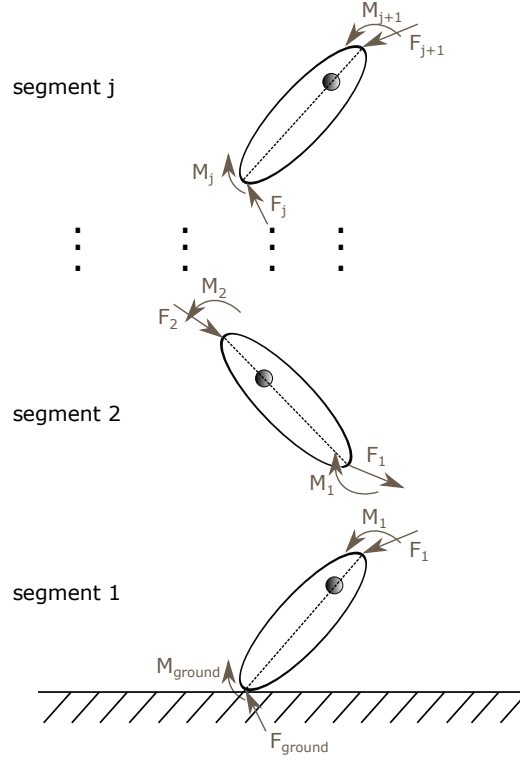


Figure A.2: Graphical model of the inverse dynamics calculation of joint forces and torques for each segment

- F_x : forces along x;
- m : mass of the human segment;
- \ddot{x} : linear acceleration along x;
- F_y : forces along y;
- \ddot{y} : linear acceleration along y;
- M : moment;
- I : mass moment of inertia;
- $\ddot{\theta}$: angular acceleration

By considering a generic body segment (segment j) which links two consecutive human joints (joint j and joint $j + 1$) and, by considering the nomenclature in Fig. A.1, we can re-write the dynamic model (A.3) in two different ways:

$$\begin{aligned}
 F_{x,j+1} &= m\ddot{x} - F_{x,j} \\
 F_{y,j+1} &= m\ddot{y} - mg - F_{y,j} \\
 M_{j+1} &= I\ddot{\theta}_j - M_j - F_{x,j+1}(y_l - y_r) + F_{y,j+1}(x_l - x_r) + \\
 &\quad + F_{y,j}y_r - F_{x,j}x_r
 \end{aligned} \tag{A.4}$$

$$\begin{aligned}
F_{x,j+1} &= m\ddot{x} - F_{x,j} \\
F_{y,j+1} &= m\ddot{y} - mg - F_{y,j} \\
M_{j+1} &= I\ddot{\theta}_j - M_j - F_{x,j+1}(l-r)S(\theta) + F_{y,j+1}(l-r)C(\theta) + \\
&\quad + F_{y,j}rC(\theta) - F_{x,j}rS(\theta)
\end{aligned} \tag{A.5}$$

In (A.4) and (A.5), the forces due to the acceleration of the mass along x and y axes (i.e., $m\ddot{x}$ and $m\ddot{y}$), as well as the weight force mg are applied in the center of mass (CoM) of the considered body segment. The moment of inertia $I\ddot{\theta}$ is also considered about the CoM. Instead, the internal generalised forces (i.e., forces F_j and F_{j+1} ; torques M_j and M_{j+1}), are applied at the joints location (joint j and $j + 1$).

Equation A.4 depends on the distances between the CoM and the joints along x and y axes (y_r and y_l ; x_r and x_l); instead, Eq. A.5 depends on the joint angle θ . Starting from the segment 1, where the ground reaction forces are known, it is possible to reconstruct the forces and torques applied at each human joint (see Fig. A.2 for a graphical interpretation).

Appendix B

Biomechanical analysis results

B.1 Joint angle and torque results

The evolution of the joint angles, i.e. shoulder flexion-extension α , shoulder abduction-adduction β , shoulder rotation γ and elbow flexion-extension δ , during the execution of drilling task are reported in Fig. B.1. The evolution of the joint angles during the execution of leveraging task are reported in Fig. B.2. The joint torque results during the execution of the drilling task are reported in Fig. B.3.

B.2 Muscle activation results

The normalized muscle activation results are reported in Fig. B.4 for drilling task, in Fig. B.5 for leveraging task and in Fig. B.6 for cabling task.

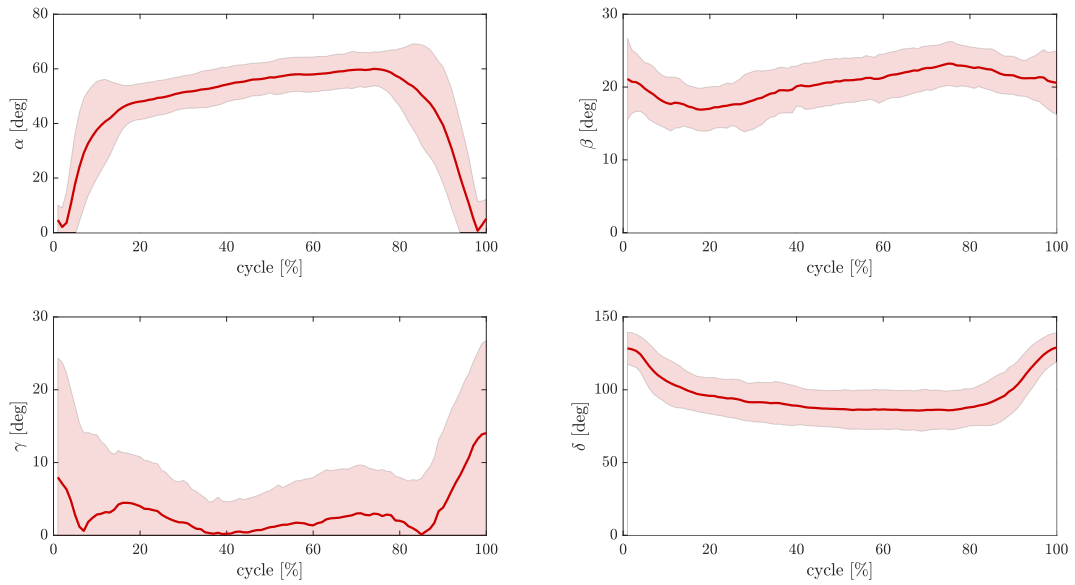


Figure B.1: The evolution of joint angles, during the execution of drilling task, presented as mean \pm standard deviation for *middle configuration*. The joint angles represented in the figure are: α : shoulder flexion-extension; β : shoulder abduction-adduction; γ : shoulder rotation; δ : elbow flexion-extension.

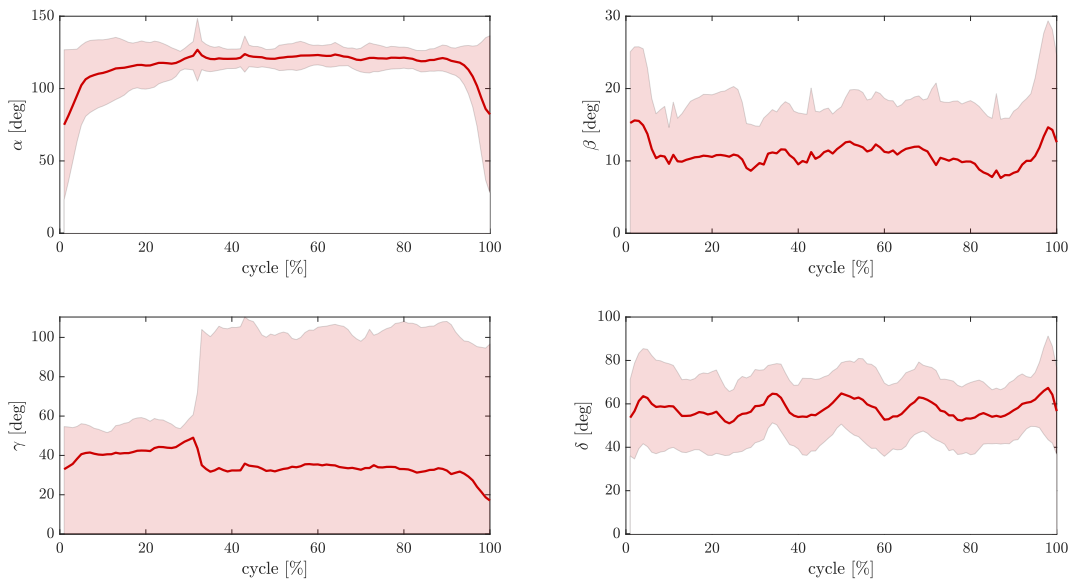


Figure B.2: The evolution of joint angles, during the execution of leveraging task, presented as mean \pm standard deviation for *middle configuration*. The joint angles represented in the figure are: α : shoulder flexion-extension; β : shoulder abduction-adduction; γ : shoulder rotation; δ : elbow flexion-extension.

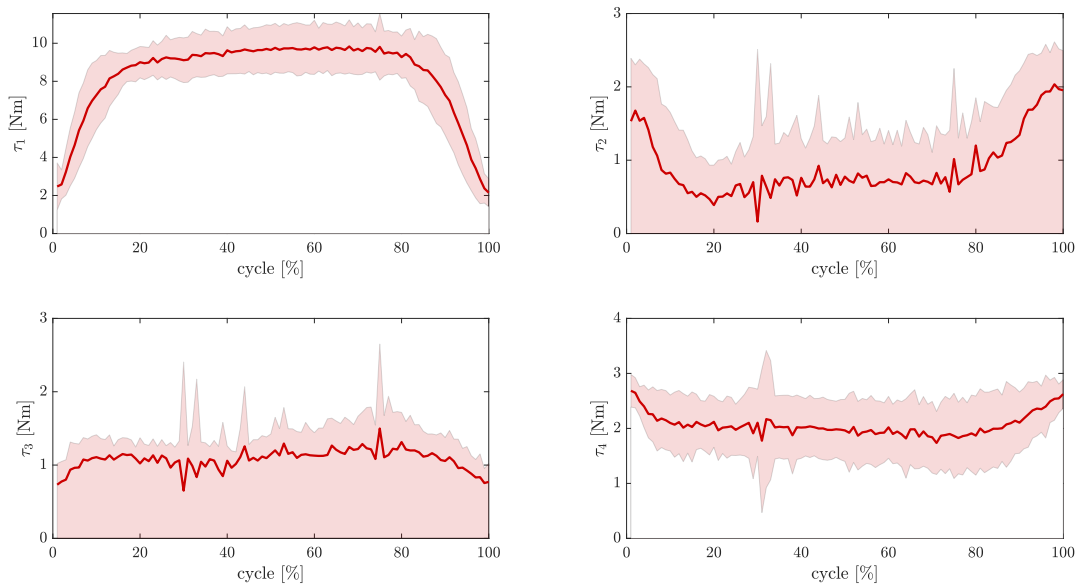


Figure B.3: The evolution of joint torques, during the execution of drilling task, presented as mean \pm standard deviation for *middle configuration*. The joint torques represented in the figure are: τ_1 : shoulder flexion-extension torque; τ_2 : shoulder abduction-adduction torque; τ_3 : shoulder rotation torque; τ_4 : elbow flexion-extension torque.

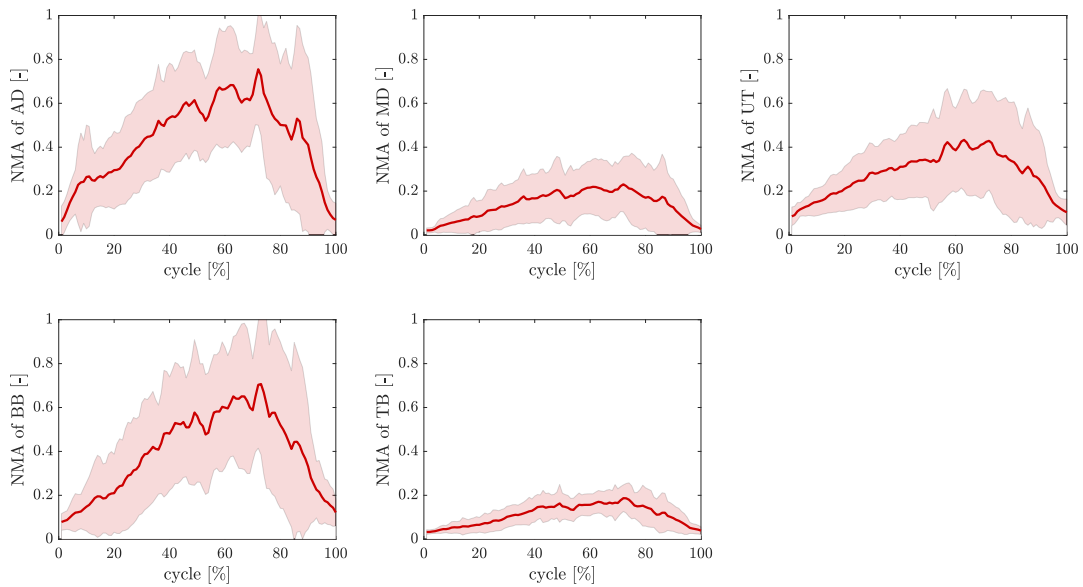


Figure B.4: The evolution of normalized muscle activations (NMA), during the execution of drilling task, presented as mean \pm standard deviation for *middle configuration*. The muscles represented in the figure are: *AD*: anterior deltoid; *MD*: medial deltoid; *UT*: upper trapezium; *BB*: biceps brachii; *TB*: triceps brachii.

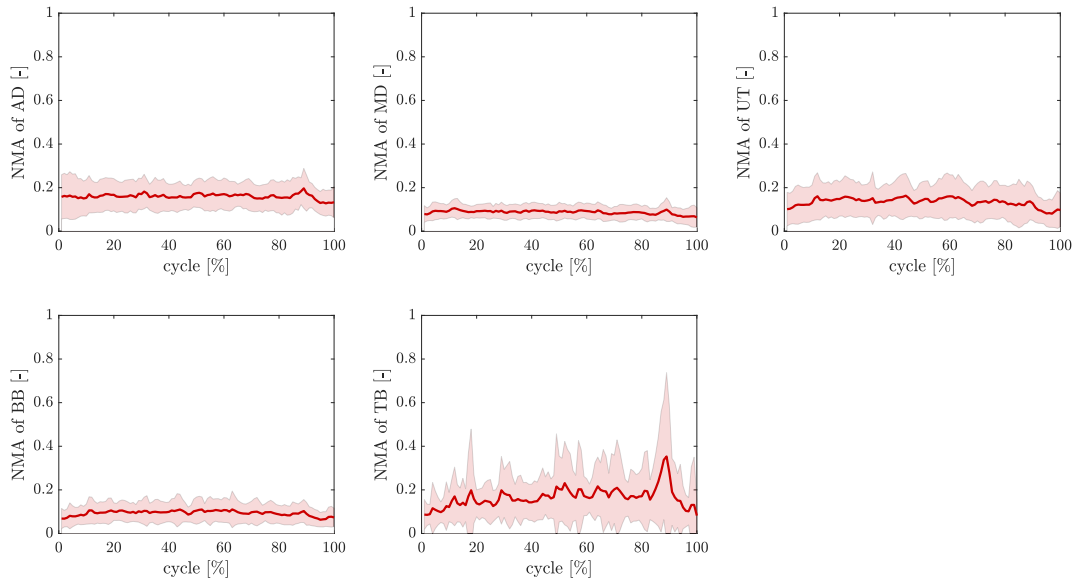


Figure B.5: The evolution of normalized muscle activations (NMA), during the execution of leveraging task, presented as mean \pm standard deviation for *middle configuration*. The muscles represented in the figure are: *AD*: anterior deltoid; *MD*: medial deltoid; *UT*: upper trapezium; *BB*: biceps brachii; *TB*: triceps brachii.

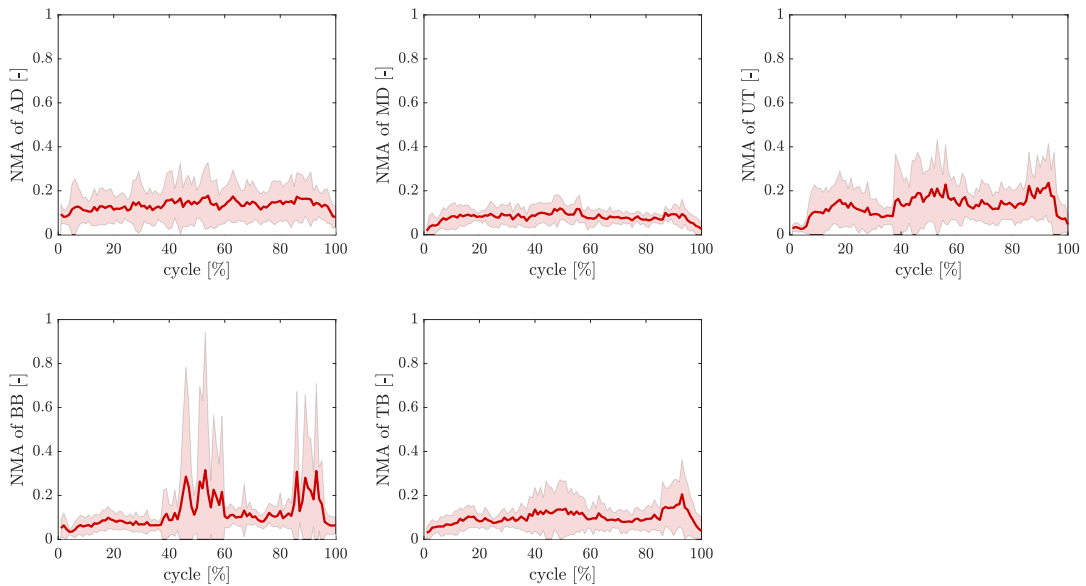


Figure B.6: The evolution over time of normalized muscle activations (NMA), during the execution of cabling task, presented as mean \pm standard deviation for *middle configuration*. The muscles represented in the figure are: *AD*: anterior deltoid; *MD*: medial deltoid; *UT*: upper trapezium; *BB*: biceps brachii; *TB*: triceps brachii.

Appendix C

ELIGERE questionnaire

The platform is based on the analysis of the questionnaires submitted to a panel of experts. The experts is asked to answer the questionnaire and it is divided in two main parts: (i) comparison, in pairwise manner, of the criteria defined; (i) comparison, in pairwise manner, of the alternatives involved for that specific study with respect to each criterion separately. The results of the first part is the ranking of the criteria; the results of the second part, instead, is the ranking of the configurations (or alternatives) according to the FAHP method. The fuzzy conversion scale used is reported in Tab. C.1.

C.1 Description of the alternatives

The description of the alternatives, or concepts, provided to the workers, managers and researchers are:

Tendon-driven wearable robot The system uses a single electric motor to support the shoulder and elbow flexion (under-actuated system), see Fig. 4.3. The transmission system of the forces is made up of cables (or tendons), i.e. Bowden cables. In particular, two Bowden cables are used to transmit the forces from exoskeleton to user; one cable to assist the shoulder flexion and one cable to assist the elbow flexion. Moreover, the cable paths is defined following the

Table C.1: Fuzzy conversion scale used in Eligere platform.

Absolutely more important	+ + +
More important	+ +
Weakly more important	+
Equally important	=
Weakly less important	-
Less important	- -
Absolutely less important	- - -

concept defined as tension line. The concept of tension line is linked to bio-design techniques, techniques where the design of the systems, i.e. wearable robots, is inspired by nature. The tension lines are lines which link the starting and ending point of the joints affected by the muscle, in this way, the cables (or tendons) work in parallel with the human muscles in order to assist and reduce the muscle activations of the user during the execution of industrial tasks. The actuation is electric, i.e. electric motor. In particular, the actuation system is positioned in the upper back of the workers (yellow component in Fig. 4.3), this allows to make the tendon—driven wearable robot independent from an external actuation source. Moreover, the system is defined under-actuated since it uses one electric motor to support two degrees of freedom, i.e. shoulder and elbow flexion. The system allows to assist only one movement, i.e. shoulder flexion or elbow flexion, or both movements simultaneously. The switch from one operating configuration to another configuration takes place automatically by translating a pin using an electromagnetic solution. Finally, a gear system allows to apply the desired torque by the two different joints.

Pneumatic wearable robot The system uses four McKibben artificial muscles to support the shoulder and elbow flexion, see Fig. 4.5. The pneumatic wearable robot assists the worker activities using McKibben artificial muscles (or pneumatic artificial muscles, PAM). The PAM consist of an inflatable inner tube/bladder inside a braided mesh, clamped at the ends. When the inner bladder is pressurized and expands, the geometry of the mesh acts like a scissor linkage and translates this radial expansion into linear contraction and their behaviour is similar to human muscles. The PAM could work in parallel with the human muscles in order to support the most activated muscles during the execution of manufacturing tasks. For the present soft wearable robots four McKibben actuators are used, in particular, two actuators to support the shoulder flexion and two actuators to support the elbow flexion. The pneumatic wearable robot is actuated and controlled using pneumatic control board. It includes: (i) one controller; (ii) four pressure regulators, (iii) four solenoid valves; (iv) four pressure sensor; (v) air compressor. The pressure regulator allows to control the pressure of the fluid and to send the fluid at the desired pressure to the solenoid valves; finally, the pressure sensor estimates the flow loss in the circuit. The pneumatic control board, which includes air compressor, is not worn by the user, for this reason to work it must be connected to a compressed air hose (usually placed in the immediate vicinity of the workstations).

C.2 Questionnaires

Questionnaire for workers The questionnaire submitted to the workers is reported in Fig. C.1 and Fig. C.2.

The screenshot shows the ELIGERE web application interface. At the top, the logo 'ELIGERE' is displayed in large blue letters. Below the logo, there is a navigation bar with links for 'Home', 'Sign in', 'Registration', 'Logout', a clock icon showing '2021-09-26 11:08:42', a user profile icon with 'welcome eligere@gmail.com', and an 'Info' icon.

The main content area is titled 'Section 1: "Preferences"' and includes a sub-header 'Criteria Fuzzy conversion scale'. Below this, there is an introductory text: 'In the first section the user is asked to express a preference about the given evaluation criteria. Each question asks to compare two criteria simultaneously (i.e. pairwise comparison) according to the fuzzy conversion scale.'

The questionnaire consists of three rows of questions, each with a 'Tag' and a 'Question'. The questions are:

- Tag: C1390C2391, Question: How important is the **weight** when it is compared to **invasiveness**?
- Tag: C1391C2392, Question: How important is the **invasiveness** when it is compared to **operating space**?
- Tag: C1390C2392, Question: How important is the **weight** when it is compared to **operating space**?

 Each question has a set of radio buttons corresponding to the fuzzy conversion scale: '+++', '++', '+', '=', '-', '--', and '---'. The '+++' and '++' options are highlighted in green in the first row.

At the bottom of the questionnaire, there is a blue button labeled 'Next Section'. Below the questionnaire, there is a footer with the text: 'Copyright © 2017 ELIGERE. All rights reserved.'

Figure C.1: Comparison of the worker's criteria.

Questionnaire for managers The questionnaire submitted to the managers is reported in Fig. C.3 and Fig. C.4.

Questionnaire for researchers The questionnaire submitted to the workers is reported in Fig. C.5 and Fig. C.6.

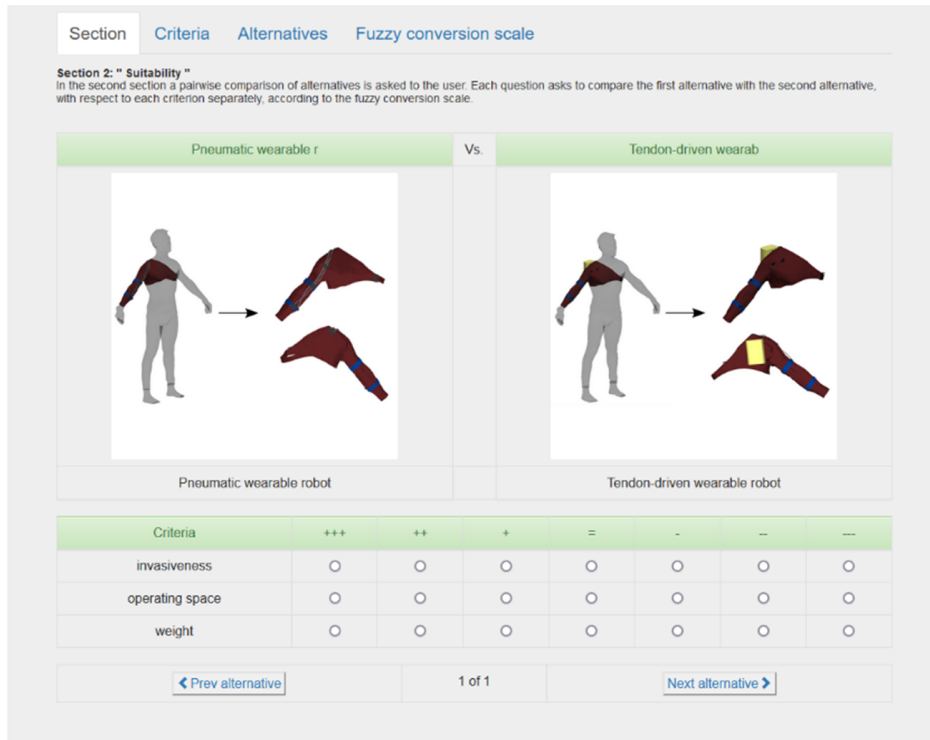


Figure C.2: Comparison of the alternatives based on the worker’s criteria.

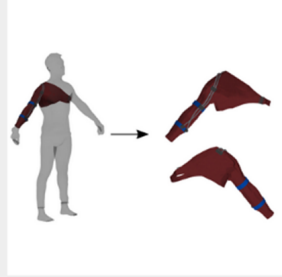


Figure C.3: Comparison of the manager’s criteria.

Section **Criteria** Alternatives Fuzzy conversion scale

Section 2: "Suitability"
 In the second section a pairwise comparison of alternatives is asked to the user. Each question asks to compare the first alternative with the second alternative, with respect to each criterion separately, according to the fuzzy conversion scale.

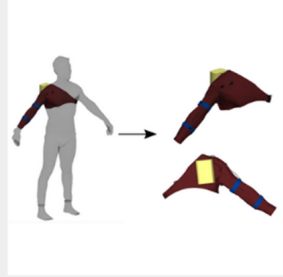
Pneumatic wearable r



Pneumatic wearable robot

Vs.

Tendon-driven wearab



Tendon-driven wearable robot

Criteria	+++	++	+	=	-	--	---
Innovativeness	<input type="radio"/>	<input type="radio"/>	<input type="radio"/>	<input type="radio"/>	<input type="radio"/>	<input type="radio"/>	<input type="radio"/>
Robustness	<input type="radio"/>	<input type="radio"/>	<input type="radio"/>	<input type="radio"/>	<input type="radio"/>	<input type="radio"/>	<input type="radio"/>
Safety	<input type="radio"/>	<input type="radio"/>	<input type="radio"/>	<input type="radio"/>	<input type="radio"/>	<input type="radio"/>	<input type="radio"/>

[← Prev alternative](#) 1 of 1 [Next alternative →](#)

Figure C.4: Comparison of the alternatives based on the manager’s criteria.

ELIGERE

[Home](#) [Sign in](#) [Registration](#) [Logout](#) 2021-09-22 14:28:26 [welcome.eligere@gmail.com](#) [Info](#)

Section **Criteria** Fuzzy conversion scale

Section 1: "Preferences"
 In the first section the user is asked to express a preference about the given evaluation criteria. Each question asks to compare two criteria simultaneously (i.e. pairwise comparison) according to the fuzzy conversion scale.

Tag	Question	+++	++	+	=	-	--	---
C1387C2388	How important is the Response speed when it is compared to Full-assisted ?	<input type="radio"/>	<input type="radio"/>	<input type="radio"/>	<input type="radio"/>	<input type="radio"/>	<input type="radio"/>	<input type="radio"/>
C1388C2389	How important is the Full-assisted when it is compared to Maintainability ?	<input type="radio"/>	<input type="radio"/>	<input type="radio"/>	<input type="radio"/>	<input type="radio"/>	<input type="radio"/>	<input type="radio"/>
C1387C2389	How important is the Response speed when it is compared to Maintainability ?	<input type="radio"/>	<input type="radio"/>	<input type="radio"/>	<input type="radio"/>	<input type="radio"/>	<input type="radio"/>	<input type="radio"/>

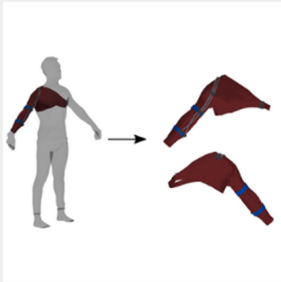
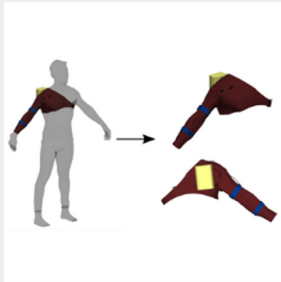
Next Section

Copyright © 2017 ELIGERE. All rights reserved.

Figure C.5: Comparison of the researcher’s criteria.

Section Criteria Alternatives Fuzzy conversion scale

Section 2: "Suitability"
 In the second section a pairwise comparison of alternatives is asked to the user. Each question asks to compare the first alternative with the second alternative, with respect to each criterion separately, according to the fuzzy conversion scale.

Pneumatic wearable r	Vs.	Tendon-driven wearab
		
Pneumatic wearable robot		Tendon-driven wearable robot

Criteria	+++	++	+	=	-	--	---
Full-assisted	<input type="radio"/>	<input type="radio"/>	<input type="radio"/>	<input type="radio"/>	<input type="radio"/>	<input type="radio"/>	<input type="radio"/>
Maintainability	<input type="radio"/>	<input type="radio"/>	<input type="radio"/>	<input type="radio"/>	<input type="radio"/>	<input type="radio"/>	<input type="radio"/>
Response speed	<input type="radio"/>	<input type="radio"/>	<input type="radio"/>	<input type="radio"/>	<input type="radio"/>	<input type="radio"/>	<input type="radio"/>

[◀ Prev alternative](#)
1 of 1
[Next alternative ▶](#)

Figure C.6: Comparison of the alternatives based on the researcher's criteria.

Bibliography

- [1] D. Park and K.-J. Cho, “Development and evaluation of a soft wearable weight support device for reducing muscle fatigue on shoulder,” *PLoS one*, vol. 12, no. 3, 2017.
- [2] R. Natividad and C.-H. Yeow, “Development of a soft robotic shoulder assistive device for shoulder abduction,” in *2016 6th IEEE International Conference on Biomedical Robotics and Biomechanics (BioRob)*, pp. 989–993, IEEE, 2016.
- [3] C. Simpson, B. Huerta, S. Sketch, M. Lansberg, E. Hawkes, and A. Okamura, “Upper extremity exomuscle for shoulder abduction support,” *bioRxiv*, 2020.
- [4] C. O’Neill, T. Proietti, K. Nuckols, M. E. Clarke, C. J. Hohimer, A. Cloutier, D. J. Lin, and C. J. Walsh, “Inflatable soft wearable robot for reducing therapist fatigue during upper extremity rehabilitation in severe stroke,” *IEEE Robotics and Automation Letters*, vol. 5, no. 3, pp. 3899–3906, 2020.
- [5] N. Thompson, A. Sinha, and G. Krishnan, “Characterizing architectures of soft pneumatic actuators for a cable-driven shoulder exoskeleton,” in *2019 International Conference on Robotics and Automation (ICRA)*, pp. 570–576, IEEE, 2019.
- [6] M. Xiloyannis, D. Chiaradia, A. Frisoli, and L. Masia, “Physiological and kinematic effects of a soft exosuit on arm movements,” *Journal of neuro-engineering and rehabilitation*, vol. 16, no. 1, p. 29, 2019.
- [7] L. Lu, Q. Wu, X. Chen, Z. Shao, B. Chen, and H. Wu, “Development of a semg-based torque estimation control strategy for a soft elbow exoskeleton,” *Robotics and Autonomous Systems*, vol. 111, pp. 88–98, 2019.
- [8] T. H. Koh, N. Cheng, H. K. Yap, and C.-H. Yeow, “Design of a soft robotic elbow sleeve with passive and intent-controlled actuation,” *Frontiers in neuroscience*, vol. 11, p. 597, 2017.
- [9] C. M. Thalman, Q. P. Lam, P. H. Nguyen, S. Sridar, and P. Polygerinos, “A novel soft elbow exosuit to supplement bicep lifting capacity,” in *2018 IEEE/RSJ International Conference on Intelligent Robots and Systems (IROS)*, pp. 6965–6971, IEEE, 2018.

- [10] S. J. Park and C. H. Park, “suit-type wearable robot powered by shape-memory-alloy-based fabric muscle,” *Scientific reports*, vol. 9, no. 1, pp. 1–8, 2019.
- [11] S.-H. Park, J. Yi, D. Kim, Y. Lee, H. S. Koo, and Y.-L. Park, “A lightweight, soft wearable sleeve for rehabilitation of forearm pronation and supination,” in *2019 2nd IEEE International Conference on Soft Robotics (RoboSoft)*, pp. 636–641, IEEE, 2019.
- [12] J. Realmuto and T. Sanger, “A robotic forearm orthosis using soft fabric-based helical actuators,” in *2019 2nd IEEE International Conference on Soft Robotics (RoboSoft)*, pp. 591–596, IEEE, 2019.
- [13] N. Li, T. Yang, P. Yu, J. Chang, L. Zhao, X. Zhao, I. H. Elhajj, N. Xi, and L. Liu, “Bio-inspired upper limb soft exoskeleton to reduce stroke-induced complications,” *Bioinspiration & biomimetics*, vol. 13, no. 6, p. 066001, 2018.
- [14] S. Lessard, P. Pansodtee, A. Robbins, J. M. Trombadore, S. Kurniawan, and M. Teodorescu, “A soft exosuit for flexible upper-extremity rehabilitation,” *IEEE Transactions on Neural Systems and Rehabilitation Engineering*, vol. 26, no. 8, pp. 1604–1617, 2018.
- [15] Y. G. Kim, M. Xiloyannis, D. Accoto, and L. Masia, “Development of a soft exosuit for industrial applications,” in *2018 7th IEEE International Conference on Biomedical Robotics and Biomechatronics (Biorob)*, pp. 324–329, IEEE, 2018.
- [16] Y. G. Kim, K. Little, B. Noronha, M. Xiloyannis, L. Masia, and D. Accoto, “A voice activated bi-articular exosuit for upper limb assistance during lifting tasks,” *Robotics and Computer-Integrated Manufacturing*, vol. 66, p. 101995, 2020.
- [17] G. Belforte, G. Eula, A. Ivanov, T. Raparelli, and S. Sirolli, “Presentation of textile pneumatic muscle prototypes applied in an upper limb active suit experimental model,” *The Journal of The Textile Institute*, vol. 109, no. 6, pp. 757–766, 2018.
- [18] S. Das and Y. Kurita, “Forcearm: A wearable pneumatic gel muscle (pgm)-based assistive suit for the upper limb,” *IEEE Transactions on Medical Robotics and Bionics*, vol. 2, no. 2, pp. 269–281, 2020.
- [19] D. Sood, M. A. Nussbaum, and K. Hager, “Fatigue during prolonged intermittent overhead work: reliability of measures and effects of working height,” *Ergonomics*, vol. 50, no. 4, pp. 497–513, 2007.
- [20] M. Xiloyannis, K. Dhin, L. Cappello, C. Antuvan, and L. Masia, “A soft wearable elbow exosuit: design considerations,” *Wearable Technology in Medicine and Health Care*, p. 193, 2018.

- [21] B. Tondu, “Modelling of the mckibben artificial muscle: A review,” *Journal of Intelligent Material Systems and Structures*, vol. 23, no. 3, pp. 225–253, 2012.
- [22] M. Hayes, D. Cockrell, and D. Smith, “A systematic review of musculoskeletal disorders among dental professionals,” *International journal of dental hygiene*, vol. 7, no. 3, pp. 159–165, 2009.
- [23] M. P. De Looze, T. Bosch, F. Krause, K. S. Stadler, and L. W. O’Sullivan, “Exoskeletons for industrial application and their potential effects on physical work load,” *Ergonomics*, vol. 59, no. 5, pp. 671–681, 2016.
- [24] B. Tondu, “Estimating shoulder-complex mobility,” *Applied Bionics and Biomechanics*, vol. 4, no. 1, pp. 19–29, 2007.
- [25] E. Pennestri, R. Stefanelli, P. Valentini, and L. Vita, “Virtual musculoskeletal model for the biomechanical analysis of the upper limb,” *Journal of biomechanics*, vol. 40, no. 6, pp. 1350–1361, 2007.
- [26] J. Li, Z. Zhang, C. Tao, and R. Ji, “A number synthesis method of the self-adapting upper-limb rehabilitation exoskeletons,” *International Journal of Advanced Robotic Systems*, vol. 14, no. 3, p. 1729881417710796, 2017.
- [27] C. Thalman and P. Artemiadis, “A review of soft wearable robots that provide active assistance: Trends, common actuation methods, fabrication, and applications,” *Wearable Technologies*, vol. 1, 2020.
- [28] S. Grazioso, D. Panariello, T. Caporaso, A. Palomba, A. Grazioso, M. Caporaso, G. Di Gironimo, and A. Lanzotti, “Esoscheletro soft sotto-attuato con sistema di attuazione a cavi per l’assistenza degli arti superiori,” IT Patent pending - application number 102021000022091, Sept. 2021.
- [29] V. Sanchez, C. J. Walsh, and R. J. Wood, “Textile technology for soft robotic and autonomous garments,” *Advanced Functional Materials*, vol. 31, no. 6, p. 2008278, 2021.
- [30] M. Xiloyannis, R. Alicea, A.-M. Georgarakis, F. L. Haufe, P. Wolf, L. Masia, and R. Riener, “Soft robotic suits: State of the art, core technologies, and open challenges,” *IEEE Transactions on Robotics*, 2021.
- [31] D. Panariello, S. Grazioso, T. Caporaso, G. D. Gironimo, and A. Lanzotti, “A detailed analysis of the most promising concepts of soft wearable robots for upper-limb,” in *International Conference on Design, Simulation, Manufacturing: The Innovation Exchange*, pp. 71–81, Springer, 2021.
- [32] N. Lotti, M. Xiloyannis, G. Durandau, E. Galofaro, V. Sanguineti, L. Masia, and M. Sartori, “Adaptive model-based myoelectric control for a soft wearable arm exosuit: A new generation of wearable robot control,” *IEEE Robotics & Automation Magazine*, vol. 27, no. 1, pp. 43–53, 2020.

- [33] P. H. Nguyen and W. Zhang, “Design and computational modeling of fabric soft pneumatic actuators for wearable assistive devices,” *Scientific reports*, vol. 10, no. 1, pp. 1–13, 2020.
- [34] S. Grazioso, G. Di Gironimo, and B. Siciliano, “A geometrically exact model for soft continuum robots: The finite element deformation space formulation,” *Soft robotics*, vol. 6, no. 6, pp. 790–811, 2019.
- [35] B. N. Fournier, E. D. Lemaire, A. J. Smith, and M. Doumit, “Modeling and simulation of a lower extremity powered exoskeleton,” *IEEE transactions on neural systems and rehabilitation engineering*, vol. 26, no. 8, pp. 1596–1603, 2018.
- [36] F. Ferrati, R. Bortoletto, and E. Pagello, “Virtual modelling of a real exoskeleton constrained to a human musculoskeletal model,” in *Conference on Biomimetic and Biohybrid Systems*, pp. 96–107, Springer, 2013.
- [37] C. M. Harbauer, M. Fleischer, C. E. Bandmann, and K. Bengler, “Optimizing force transfer in a soft exoskeleton using biomechanical modeling,” in *Congress of the International Ergonomics Association*, pp. 274–281, Springer, 2021.
- [38] V. Cacucciolo, J. Shintake, Y. Kuwajima, S. Maeda, D. Floreano, and H. Shea, “Stretchable pumps for soft machines,” *Nature*, vol. 572, no. 7770, pp. 516–519, 2019.
- [39] D. Panariello, S. Grazioso, T. Caporaso, A. Palomba, G. Di Gironimo, and A. Lanzotti, “Evaluation of human joint angles in industrial tasks using opensim,” in *2019 II Workshop on Metrology for Industry 4.0 and IoT (MetroInd4.0&IoT)*, pp. 78–83, IEEE, 2019.
- [40] D. Panariello, S. Grazioso, T. Caporaso, G. Di Gironimo, and A. Lanzotti, “Preliminary requirements of a soft upper-limb exoskeleton for industrial overhead tasks based on biomechanical analysis,” in *Congress of the International Ergonomics Association*, pp. 317–324, Springer, 2021.
- [41] S. Grazioso, M. Selvaggio, and G. Di Gironimo, “Design and development of a novel body scanning system for healthcare applications,” *International Journal on Interactive Design and Manufacturing (IJIDeM)*, vol. 12, no. 2, pp. 611–620, 2018.
- [42] S. Grazioso, M. Selvaggio, T. Caporaso, and G. Di Gironimo, “A digital photogrammetric method to enhance the fabrication of custom-made spinal orthoses,” *JPO: Journal of Prosthetics and Orthotics*, vol. 31, no. 2, pp. 133–139, 2019.
- [43] S. Grazioso, T. Caporaso, M. Selvaggio, D. Panariello, R. Ruggiero, and G. Di Gironimo, “Using photogrammetric 3d body reconstruction for the

- design of patient-tailored assistive devices,” in *2019 II Workshop on Metrology for Industry 4.0 and IoT (MetroInd4. 0&IoT)*, pp. 240–242, IEEE, 2019.
- [44] D. Kim, J. Kwon, S. Han, Y.-L. Park, and S. Jo, “Deep full-body motion network for a soft wearable motion sensing suit,” *IEEE/ASME Transactions on Mechatronics*, vol. 24, no. 1, pp. 56–66, 2018.
- [45] Y. M. Zhou, C. Hohimer, T. Proietti, C. T. O’Neill, and C. J. Walsh, “Kinematics-based control of an inflatable soft wearable robot for assisting the shoulder of industrial workers,” *IEEE Robotics and Automation Letters*, 2021.
- [46] S. Grazioso, T. Caporaso, A. Palomba, S. Nardella, B. Ostuni, D. Panariello, G. Di Gironimo, and A. Lanzotti, “Assessment of upper limb muscle synergies for industrial overhead tasks: a preliminary study,” in *2019 II Workshop on Metrology for Industry 4.0 and IoT (MetroInd4. 0&IoT)*, pp. 89–92, IEEE, 2019.
- [47] T. Caporaso, S. Grazioso, D. Panariello, G. Di Gironimo, and A. Lanzotti, “Understanding the human motor control for user-centered design of custom wearable systems: case studies in sports, industry, rehabilitation,” in *International Conference on Design, Simulation, Manufacturing: The Innovation Exchange*, pp. 753–764, Springer, 2019.
- [48] G. Averta, G. Valenza, V. Catrambone, F. Barontini, E. P. Scilingo, A. Bichi, and M. Bianchi, “On the time-invariance properties of upper limb synergies,” *IEEE Transactions on Neural Systems and Rehabilitation Engineering*, vol. 27, no. 7, pp. 1397–1406, 2019.
- [49] S. L. Delp, F. C. Anderson, A. S. Arnold, P. Loan, A. Habib, C. T. John, E. Guendelman, and D. G. Thelen, “Opensim: open-source software to create and analyze dynamic simulations of movement,” *IEEE transactions on biomedical engineering*, vol. 54, no. 11, pp. 1940–1950, 2007.
- [50] S. Spada, L. Ghibauda, S. Gilotta, L. Gastaldi, and M. P. Cavatorta, “Analysis of exoskeleton introduction in industrial reality: main issues and eaws risk assessment,” in *International Conference on Applied Human Factors and Ergonomics*, pp. 236–244, Springer, 2017.
- [51] P. Maurice, J. Čamernik, D. Gorjan, B. Schirrmeyer, J. Bornmann, L. Tagliapietra, C. Latella, D. Pucci, L. Fritzsche, S. Ivaldi, *et al.*, “Objective and subjective effects of a passive exoskeleton on overhead work,” *IEEE Transactions on Neural Systems and Rehabilitation Engineering*, 2019.
- [52] S. Alabdulkarim, M. A. Nussbaum, E. Rashedi, S. Kim, M. Agnew, and R. Gardner, “Impact of task design on task performance and injury risk: case study of a simulated drilling task,” *Ergonomics*, vol. 60, no. 6, pp. 851–866, 2017.

- [53] M. Peruzzini, M. Pellicciari, and M. Gadaleta, “A comparative study on computer-integrated set-ups to design human-centred manufacturing systems,” *Robotics and Computer-Integrated Manufacturing*, vol. 55, pp. 265–278, 2019.
- [54] N. Sylla, V. Bonnet, F. Colledani, and P. Fraisse, “Ergonomic contribution of able exoskeleton in automotive industry,” *International Journal of Industrial Ergonomics*, vol. 44, no. 4, pp. 475–481, 2014.
- [55] A.-M. Georgarakis, P. Wolf, and R. Riener, “Simplifying exosuits: Kinematic couplings in the upper extremity during daily living tasks,” in *2019 IEEE 16th International Conference on Rehabilitation Robotics (ICORR)*, pp. 423–428, IEEE, 2019.
- [56] W. Kim, J. Lee, L. Peternel, N. Tsagarakis, and A. Ajoudani, “Anticipatory robot assistance for the prevention of human static joint overloading in human–robot collaboration,” *IEEE robotics and automation letters*, vol. 3, no. 1, pp. 68–75, 2017.
- [57] W. Kim, M. Lorenzini, K. Kapıcioğlu, and A. Ajoudani, “Ergotac: A tactile feedback interface for improving human ergonomics in workplaces,” *IEEE Robotics and Automation Letters*, vol. 3, no. 4, pp. 4179–4186, 2018.
- [58] Y. Blache, L. Desmoulins, P. Allard, A. Plamondon, and M. Begon, “Effects of height and load weight on shoulder muscle work during overhead lifting task,” *Ergonomics*, vol. 58, no. 5, pp. 748–761, 2015.
- [59] J. M. Maciukiewicz, A. C. Cudlip, J. N. Chopp-Hurley, and C. R. Dickerson, “Effects of overhead work configuration on muscle activity during a simulated drilling task,” *Applied ergonomics*, vol. 53, pp. 10–16, 2016.
- [60] F. Bruno, L. Barbieri, and M. Muzzupappa, “A mixed reality system for the ergonomic assessment of industrial workstations,” *International Journal on Interactive Design and Manufacturing (IJIDeM)*, vol. 14, no. 3, pp. 805–812, 2020.
- [61] G. Di Gironimo, T. Caporaso, D. M. Del Giudice, A. Tarallo, and A. Lanzotti, “Development of a new experimental protocol for analysing the race-walking technique based on kinematic and dynamic parameters,” *Procedia engineering*, vol. 147, pp. 741–746, 2016.
- [62] I. Conforti, I. Mileti, D. Panariello, T. Caporaso, S. Grazioso, Z. Del Prete, A. Lanzotti, G. Di Gironimo, and E. Palermo, “Validation of a novel wearable solution for measuring l5/s1 load during manual material handling tasks,” in *2020 IEEE International Workshop on Metrology for Industry 4.0 & IoT*, pp. 501–506, IEEE, 2020.

- [63] A. Muro-De-La-Herran, B. Garcia-Zapirain, and A. Mendez-Zorrilla, “Gait analysis methods: An overview of wearable and non-wearable systems, highlighting clinical applications,” *Sensors*, vol. 14, no. 2, pp. 3362–3394, 2014.
- [64] D. Roetenberg, H. Luinge, and P. Slycke, “Xsens mvn: Full 6dof human motion tracking using miniature inertial sensors,” *Xsens Motion Technologies BV, Tech. Rep*, vol. 1, 2009.
- [65] H. M. Schepers, H. F. Koopman, and P. H. Veltink, “Ambulatory assessment of ankle and foot dynamics,” *IEEE Transactions on Biomedical Engineering*, vol. 54, no. 5, pp. 895–902, 2007.
- [66] E. Palermo, S. Rossi, F. Marini, F. Patanè, and P. Cappa, “Experimental evaluation of accuracy and repeatability of a novel body-to-sensor calibration procedure for inertial sensor-based gait analysis,” *Measurement*, vol. 52, pp. 145–155, 2014.
- [67] U. Raschke, “The jack human simulation tool,” *Working Postures and Movements—tools for evaluation and engineering*. Boca Raton: CRC Press LLC, pp. 431–437, 2004.
- [68] M. Damsgaard, J. Rasmussen, S. T. Christensen, E. Surma, and M. De Zee, “Analysis of musculoskeletal systems in the anybody modeling system,” *Simulation Modelling Practice and Theory*, vol. 14, no. 8, pp. 1100–1111, 2006.
- [69] P. Maurice, *Virtual ergonomics for the design of collaborative robots*. PhD thesis, 2015.
- [70] J. Chang, *The risk assessment of work-related musculoskeletal disorders based on opensim*. PhD thesis, 2018.
- [71] E. Cacciari, S. Milani, A. Balsamo, E. Spada, G. Bona, L. Cavallo, F. Cerutti, L. Gargantini, N. Greggio, G. Tonini, *et al.*, “Italian cross-sectional growth charts for height, weight and bmi (2 to 20 yr),” *Journal of endocrinological investigation*, vol. 29, no. 7, pp. 581–593, 2006.
- [72] S. Spada, R. Castellone, and M. P. Cavatorta, ““la fabbrica si misura”: An anthropometric study of workers at fca italian plants,” in *Congress of the International Ergonomics Association*, pp. 389–397, Springer, 2018.
- [73] V. M. Manghisi, A. E. Uva, M. Fiorentino, V. Bevilacqua, G. F. Trotta, and G. Monno, “Real time rula assessment using kinect v2 sensor,” *Applied ergonomics*, vol. 65, pp. 481–491, 2017.
- [74] S. van Sint Jan, *Color Atlas of Skeletal Landmark Definitions E-Book: Guidelines for Reproducible Manual and Virtual Palpations*. Elsevier Health Sciences, 2007.

- [75] A. Silder, B. Whittington, B. Heiderscheit, and D. G. Thelen, “Identification of passive elastic joint moment–angle relationships in the lower extremity,” *Journal of biomechanics*, vol. 40, no. 12, pp. 2628–2635, 2007.
- [76] K. Huysamen, T. Bosch, M. de Looze, K. S. Stadler, E. Graf, and L. W. O’Sullivan, “Evaluation of a passive exoskeleton for static upper limb activities,” *Applied ergonomics*, vol. 70, pp. 148–155, 2018.
- [77] A. Rajagopal, C. L. Dembia, M. S. DeMers, D. D. Delp, J. L. Hicks, and S. L. Delp, “Full-body musculoskeletal model for muscle-driven simulation of human gait,” *IEEE transactions on biomedical engineering*, vol. 63, no. 10, pp. 2068–2079, 2016.
- [78] J. D. Mortensen, A. N. Vasavada, and A. S. Merryweather, “The inclusion of hyoid muscles improve moment generating capacity and dynamic simulations in musculoskeletal models of the head and neck,” *PloS one*, vol. 13, no. 6, 2018.
- [79] J. Cohen, “Statistical power analysis for the social sciences,” 1988.
- [80] S. S. Sawilowsky, “New effect size rules of thumb,” *Journal of Modern Applied Statistical Methods*, vol. 8, no. 2, p. 26, 2009.
- [81] O. Karhu, P. Kansi, and I. Kuorinka, “Correcting working postures in industry: a practical method for analysis,” *Applied ergonomics*, vol. 8, no. 4, pp. 199–201, 1977.
- [82] L. McAtamney and E. N. Corlett, “Rula: a survey method for the investigation of work-related upper limb disorders,” *Applied ergonomics*, vol. 24, no. 2, pp. 91–99, 1993.
- [83] L. McAtamney and S. Hignett, “Rapid entire body assessment,” in *Handbook of Human Factors and Ergonomics Methods*, pp. 97–108, CRC press, 2004.
- [84] D. Anton, L. D. Shibley, N. B. Fethke, J. Hess, T. M. Cook, and J. Rosecrance, “The effect of overhead drilling position on shoulder moment and electromyography,” *Ergonomics*, vol. 44, no. 5, pp. 489–501, 2001.
- [85] T. Caporaso, A. Palomba, S. Grazioso, D. Panariello, G. Di Gironimo, F. Gimigliano, G. Iolascon, and A. Lanzotti, “Development of site-specific biomechanical indices for estimating injury risk in cycling,” in *2020 IEEE International Symposium on Medical Measurements and Applications (MeMeA)*, pp. 1–5, IEEE, 2020.
- [86] T. Caporaso, S. Grazioso, G. Di Gironimo, and A. Lanzotti, “Biomechanical indices represented on radar chart for assessment of performance and infringements in elite race-walkers,” *Sports Engineering*, vol. 23, no. 1, pp. 1–8, 2020.

- [87] A. Lanzotti, A. Vanacore, A. Tarallo, D. Nathan-Roberts, D. Coccorese, V. Minopoli, F. Carbone, R. d'Angelo, C. Grasso, G. Di Gironimo, *et al.*, “Interactive tools for safety 4.0: virtual ergonomics and serious games in real working contexts,” *Ergonomics*, vol. 63, no. 3, pp. 324–333, 2020.
- [88] D. Panariello, S. Grazioso, T. Caporaso, G. Di Gironimo, and A. Lanzotti, “User-centered approach for design and development of industrial workplace,” *International Journal on Interactive Design and Manufacturing (IJIDeM)*, pp. 1–3, 2020.
- [89] J. Wirekoh, L. Valle, N. Pol, and Y.-L. Park, “Sensorized, flat, pneumatic artificial muscle embedded with biomimetic microfluidic sensors for proprioceptive feedback,” *Soft robotics*, vol. 6, no. 6, pp. 768–777, 2019.
- [90] C. T. O’Neill, N. S. Phipps, L. Cappello, S. Paganoni, and C. J. Walsh, “A soft wearable robot for the shoulder: Design, characterization, and preliminary testing,” in *2017 International Conference on Rehabilitation Robotics (ICORR)*, pp. 1672–1678, IEEE, 2017.
- [91] K. Ogata and L. A. Whiteside, “Effects of external compression on blood flow to muscle and skin,” *Clinical Orthopaedics and Related Research*®, vol. 168, pp. 105–107, 1982.
- [92] C.-P. Chou and B. Hannaford, “Measurement and modeling of mckibben pneumatic artificial muscles,” *IEEE Transactions on robotics and automation*, vol. 12, no. 1, pp. 90–102, 1996.
- [93] D. P. Holland, E. J. Park, P. Polygerinos, G. J. Bennett, and C. J. Walsh, “The soft robotics toolkit: Shared resources for research and design,” *Soft Robotics*, vol. 1, no. 3, pp. 224–230, 2014.
- [94] H. Liao, Z. Xu, X.-J. Zeng, and J. M. Merigó, “Framework of group decision making with intuitionistic fuzzy preference information,” *IEEE Transactions on Fuzzy Systems*, vol. 23, no. 4, pp. 1211–1227, 2014.
- [95] A. Mardani, A. Jusoh, and E. K. Zavadskas, “Fuzzy multiple criteria decision-making techniques and applications—two decades review from 1994 to 2014,” *Expert systems with Applications*, vol. 42, no. 8, pp. 4126–4148, 2015.
- [96] S. Grazioso, M. Selvaggio, D. Marzullo, G. Di Gironimo, and M. Gospodarczyk, “Eligere: a fuzzy ahp distributed software platform for group decision making in engineering design,” in *2017 IEEE International Conference on Fuzzy Systems (FUZZ-IEEE)*, pp. 1–6, IEEE, 2017.